Session I

Monday, September 4 - afternoon

I1

MICROSTRUCTURE AND FUNCTIONALITY OF MATERIALS INTERFACES

J. Keckes

Department of Materials Physics, Montanuniversität Leoben and Erich Schmid Institute for Materials Science, Austrian Academy of Sciences, A-8700 Leoben, Austria
jozef.keckes@gmail.com

Although interfaces represent only a small volume fraction of biological and man-made materials, their influence on functional properties like fracture toughness, hardness and overall mechanical integrity is decisive. In this contribution, the relationship between microstructure and mechanical properties of interface-based materials like wood, multilayered thin films and ceramic nanocomposites is discussed on the bases of experimental data, obtained using synchrotron X-ray diffraction and transmission electron microscopy techniques. The results demonstrate that using clever microstructural and interface design it is possible to enhance mechanical properties of materials significantly.

First, the microstructure of a macroscopic branch-stem interface of Norway spruce is analysed using wide-angle X-ray diffraction and evaluated magnitudes of the microfibril angle are correlated with various protective mechanisms operating at different length scales . It is demonstrated that wood adjusts the cellulose fibre texture in order to protect both the stem and the branch from structural damage.

In order to understand the functionality of micro- and nano-scopic interfaces, cross-sectional synchrotron X-ray nanodiffraction experiments on thin films are performed at ID13 and P03 beamlines of ESRF and Petra III, respectively. By comparing cross-sectional distributions of phases, texture, crystallite size and strains, it is possible to understand the influence of distinct thin film regions on the overall and local mechanical response of the films. In-situ diffraction experiments combined with indentation are used to determine microstructural changes and stress concentrations accompanying various fracture modes .
Finally, a combinatorial refinement of microstructure, property and process conditions at graded TiAlN thin film cross-sections is performed using X-ray nanodiffraction in order to identify interface microstructures with the highest hardness. The micromechanical and X-ray diffraction experiments are performed iteratively in three steps and are applied as a basis to design novel types of coating materials.

1. U. Müller, W. Gindl-Altmutter, J. Konnerth, G.A. Maier, J. Keckes, *Sci. Rep.* **5** (2015) 14522.
2. J. Keckes, M. Bartosik, R. Daniel, C. Mitterer, G. Maier, W. Ecker, J. Vila-Comamala, C. David, S. Schoeder, M. Burghammer, *Scr. Mater.* **67** (2012) 748–751.
3. A. Zeilinger, J. Todt, C. Krywka, M. Müller, W. Ecker, B. Sartory, M. Meindlhumer, M. Stefenelli, R. Daniel, C. Mitterer, J. Keckes, *Sci. Rep.* **6** (2016) 22670.

C1

XRD VS. PHOTOLUMINESCENCE A NEW CLASS OF DEVICES TO CALIBRATE DEFORMATION POTENTIALS

D. Ziss[1], J. Martín-Sánchez[1], T. Lettner[1], R. Trotta[1], J. Stangl[1], A. Rastelli[1], G. Piredda[2], J. Edlinger[2], G. Trevisi[3]

[1]Institute of Semiconductor Physics, JKU, Altenbergerstr. 69, 4040 Linz, Austria
[2]Research Center for Microtechnology, FH Vorarlberg, 6850 Dornbirn, Austria
[3]IMEM - CNR Institute, Parco Area delle Scienze 37/a, 43124 Parma, Italy
dorian.ziss@jku.at

In the last several years many methods have been established to manipulate the optical properties of III-V semiconductors which are a very promising material class for non-classic quantum light sources [1]. One highly effective possibility to change their band structure (e.g. order of LH/HH bands), which defines the optical properties, is to get full control of the strain/stress tensor. The deformation potentials describe the changes in the band structure upon variation of the applied strain.

A versatile way to control the strain state is to bond a semiconductor membrane onto a piezoelectric carrier material. By applying an electrical field to the carrier and therefore, making use of the inverse piezoelectric effect, strain acts on the membrane. This approach has already

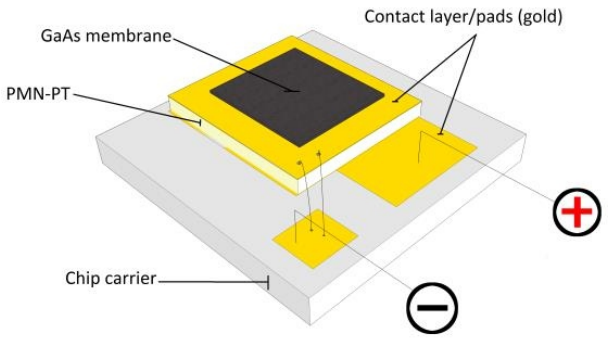

Figure 1. Schematic representation of the device for straining the GaAs membrane. The gold layers on the top and the bottom side of the piezoelectric carrier (PMN-PT) were used to apply a homogenous electric field.

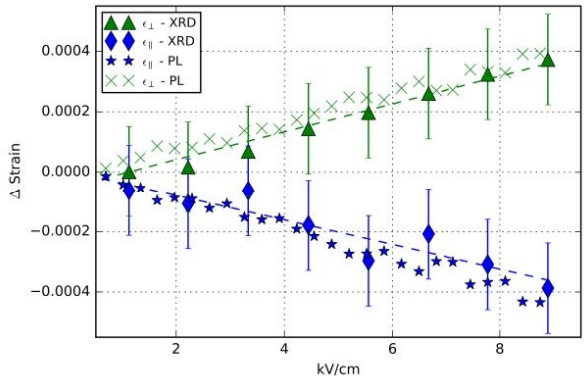

Figure 2. In-plane (♦,★) and out-of-plane (^,×) strain components of GaAs measured with XRD and calculated from PL line shifts (using a=-8.75eV). The pre-strain is set to 0. Thus the strain value at 0 kV/cm defines the offset for all following values.

been used to change the optical properties of GaAs and the embedded quantum dots on top of the carrier. Such devices (schematically shown in Fig. 1) have been fully characterized by the change in the photoluminescence (PL) spectra for a varying electrical field applied to the piezoelectric carrier [2]. Looking carefully at these PL changes, one is able to recalculate the strain tensor, yet these calculations sensitively depend on the accurate knowledge of the deformation potentials (*a* is the hydrostatic and *b, d* are called the shear potentials). The literature values for these deformation potentials vary in a rather wide range, depending on the applied calibration method (experimentally or theoretical calculation) [3]. To overcome the problem of uncertainties in the deformation potentials, we now investigated the strained GaAs in-situ by X-ray diffraction (XRD), while sweeping the electrical field. Information about the strain in the GaAs membrane, and the piezo carrier was acquired simultaneously. This allows a direct comparison of the strain tensor calculated from the PL shift and the physical strain induced in the material, see Fig. 2. Thus, by combining the results from both techniques we can finally re-define the deformation potentials.

The big advantage in using piezoelectric straining devices is the possibility to continuously tune the strain from a minimum value given by the pre-strain induced during processing of the device up to a strain of 1-2% with advanced geometries of the carrier material. Furthermore, this technique is not limited to GaAs, in principal strain can be applied in this way to every material.

We present first results on the relation of PL line-shifts with measured strain values from XRD comparing different device geometries and re-calculating the deformation potentials by comparing the results acquired by both methods.

1. I. J. Lemoore, R. Toro, O. Del Pozo-Zamudio, N. A. Wasley, E. A. Chekhovich, A. M. Sanchez, R. Beanland, A. M. Fox, M. S. Skolnick, H. Y. Liu, A. I. Tartakovskii, *Scientific Reports 3*, Article number: 1239 (2013).
2. J. D. Plumhof, R. Trotta, V. Křápek, E. Zallo, P. Atkinson, S. Kumar, A. Rastelli, and O. G. Schmidt, *PHYSICAL REVIEW B 87*, 075311 (2013) .
3. O. Madelung, U. Rössler, M. Schulz (ed.) in: *SpringerMaterials - Gallium arsenide (GaAs), deformation potentials, Landolt-Börnstein - Group III Condensed Matter* 41A1 (2002).

C2

X-RAY NANOBEAMS FOR NITRIDE WIRES

J. Eymery[1,2], A. Messanvi[1,2,3], C. Durand[1,2], M. Tchernycheva[3], F. Julien[3], M. Elzo Aizarna[1,2], G. Martinez-Criado[4], D. Salomon[4], M.-I. Richard[5,4], S. Labat[5], O. Thomas[5], T. Cornélius[5], O. Mandula[6], V. Favre-Nicolin[1,2,4]

[1]University Grenoble Alpes, CEA, INAC-SP2M, F-38000 Grenoble, France
[2]CEA-INAC, 17 rue des Martyrs, 38054 Grenoble Cedex, France
[3]IEF, UMR 8622 CNRS, Université Paris Sud, Orsay, France
[4]European Synchrotron Radiation Facility, BP 220, F-38043 Grenoble Cedex, France
[5]Aix Marseille University, CNRS, IM2NP UMR 7334, 13397 Marseille, France
[6]Fondation Nanoscience, 23 Rue des Martyrs, 38000 Grenoble, France
[7]Institut Universitaire de France, Paris, France
joel.eymery@cea.fr

One-dimensional nitride heterostructures demonstrated novel optical and electronic properties making use of quantum confinement effects and strain engineering. The emergence of disruptive functionalities is now related to the growth and technology controls [1], but also to the development of advanced characterization techniques having high spatial resolution. To complement the information provided by grazing incidence diffraction techniques, the use of focused micro/nano X-ray beams provides innovative solutions to analyse quantitatively the morphology, defects, strain and composition of these materials. This will be illustrated in this paper by recent breakthroughs obtained at the European synchrotron radiation facility (ESRF) with the study of nitride wires and their core-shell heterostructures grown by Metal Organic Vapour Phase Epitaxy.

First, it will be shown how the structure of single defects such as Inversion Domain Boundaries (IDB) inside n-doped GaN wires can be extracted from the *X-ray coherent diffraction imaging* with a monochromatic beam [2] with an unprecedented accuracy. The complex 3D IDB configuration inside a single wire can be measured without any slicing in contrast to electron microscopy and the lattice displacements along/across the wire length deduced from the analysis of the intensity of several Bragg peaks by *phase retrieval* methods (with pm resolution) will be shown to be in full agreement with electronic structure *ab initio* calculations [3].

Then, GaN/InGaN Multiple Quantum Well (MQW) core-shell heterostructure grown on the m-plane sidewalls of c-axis GaN wires [2,3] will be analysed by multimodal hard X-ray nanoprobe to perform *X-ray excited optical luminescence* (XEOL) and *X-ray Fluorescence* (XRF) [4]. The localized blue light emission can be measured in the spatiotemporal domain with 50 ps resolution to get the photoluminescence time decay (100 ps) that can be related the electron confinement/local composition in the wire [4]. These techniques will be also applied on connected wire-LED devices to evidence fluctuations of XEOL and X-ray Beam Induced Current (XBIC).

More generally, the interest of these statistical/fluctuation mappings in nitride optoelectronic devices with a nanometre beam will be presented, as well as new XANES spectroscopy results. This work will be extended to other heterostructures such as GaN/AlInN MQW tubes (*i.e.* etched wires) dedicated to UV emission.

1. R. Koester *et al.*, *Nano Lett.,* **11**, (2011), 4839. S. Salomon *et al.*, *Nanotechnology,* **25,** (2014), 375502-8. N. Guan *et al.*, *ACS Photonics,* **3** (2016) 597.
2. S. Labat et al., *ACS Nano,* **9**, (2015), 9210.
3. F. Lançon et al., to be submitted to *Phys. Rev. Lett.*
4. G. Martinez-Criado *et al., Adv. Mater.* **26** (2014), 7873-7879.

Acknowledgements to the French laboratory of excellence GaNEX (ANR-11-LABX-0014) and to the French ANR MECANIX (ANR-11-BS10-0014) and PLATOFIL (ANR-14-CE26-0020) projects.

C3

X-RAY DIFFRACTION STUDY OF STRAIN RELAXATION IN COALESCED GaN NANOWIRES

V. Kaganer, B. Jenichen, O. Brandt

Paul-Drude-Institut für Festkörperelektronik, Berlin, Germany
kaganer@pdi-berlin.de

GaN nanowires form spontaneously on various substrates without requiring a metal droplet to induce growth. A decisive advantage of this spontaneous formation is the possibility to synthesize abrupt axial heterojunctions. However, the spontaneous formation inevitably results in dense arrays, and thus in subsequent nanowire coalescence during growth [see Fig. 1(a)]. We have found that the process of coalescence is governed by nanowire bundling, which reduces the surface energy of the side facets at the expense of elastic bending energy [1]. In the present work, we study the strain state of GaN nanowire ensembles by laboratory X-ray diffractometry in conjunction with an analysis of the energetics of nanowire bundling. Our results demonstrate that the elastic bending of nanowires caused by their bundling gives rise to a large elastic strain, which is reduced plastically via the creation of dislocation walls at the joints.

The shape of the bundled nanowires in Fig. 1(b) and the elastic energy of bending are deduced in the framework of the elasticity of thin rods. Alternatively, dislocations at the joints form small angle boundaries, as shown in Fig. 1(c). This introduction of dislocations is found to significantly reduce the total energy of the bundle. The relative misorientation of the nanowires at the joint due to the small-angle boundary reduces the nanowire curvature by an order of magnitude and hence gives rise to narrower diffraction lines.

The X-ray diffraction intensity is produced by the whole volume of a nanowire ensemble, while the volume of the joints containing dislocations is only a small fraction of this volume. As a result, x-ray diffraction reveals mainly the residual bending of the nanowires due to their bundling, but is insensitive to details of plastic relaxation at the joints. Figure 2(a) compares the experimental X-ray diffraction profiles from a spontaneously formed GaN nanowire ensemble on Si(111) in successive reflection orders [2] with the calculated profiles. The calculation is performed with a Monte Carlo average over random lengths, diameters, and distances between nanowires, as well as random orientations of the bundled pairs. We also take into account the vertical divergence of the X-ray beam in a laboratory diffraction experiment, which gives rise to the asymmetry of the profiles [2] observed in Fig. 2(a). The shapes of the tails of the calculated diffraction profiles well agree with the observed ones, which confirms the inhomogeneous bending of the bundled nanowires as a main source of the x-ray scattering.

An agreement between calculated and observed diffraction profiles is obtained with a broad and asymmetric distribution of the lengths of bundled segments, as shown in Fig. 2(b). We describe this asymmetry by log-normal distributions with comparable mean value and standard deviation, which makes shorter segments more probable. Symmetric distributions, such as Gaussians, do not provide an agreement with the experiment. The effective distances between bundled nanowires in Fig. 2(d) are notably smaller than the real distances. Hence, a partial relaxation of the bending energy by dislocations at the joints takes place, which may be limited by the difficulty to introduce dislocations when atomically flat facets of the two nanowires merge. Our X-ray diffraction experiments show that a major part of the elastic bending energy of the nanowires is released by creation of dislocations at the coalescence joints.

1. V. M. Kaganer, S. Fernández-Garrido, P. Dogan, K. K. Sabelfeld, and O. Brandt, *Nano Lett.* (2016), DOI: 10.1021/acs.nanolett.6b01044.

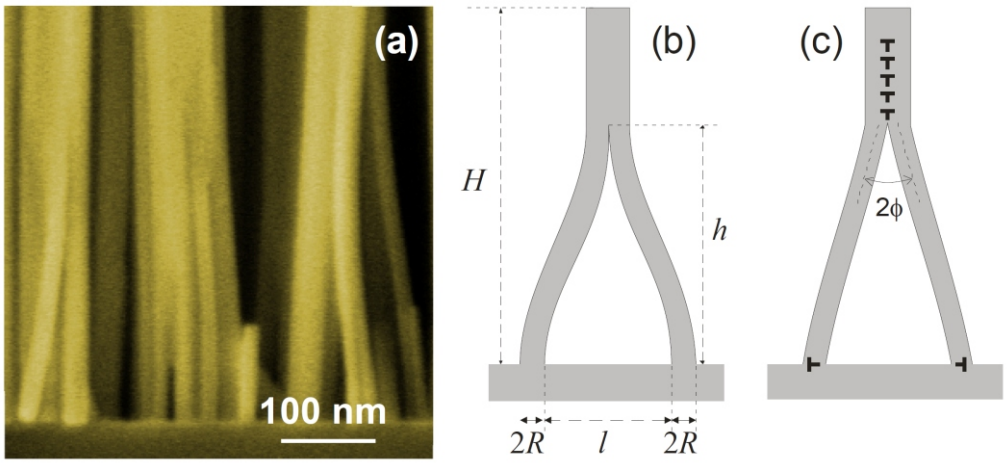

Figure 1. (a) Bottom part of coalesced nanowires, (b) coalescence by bending, (c) coalescence with creation of dislocations at the joints.

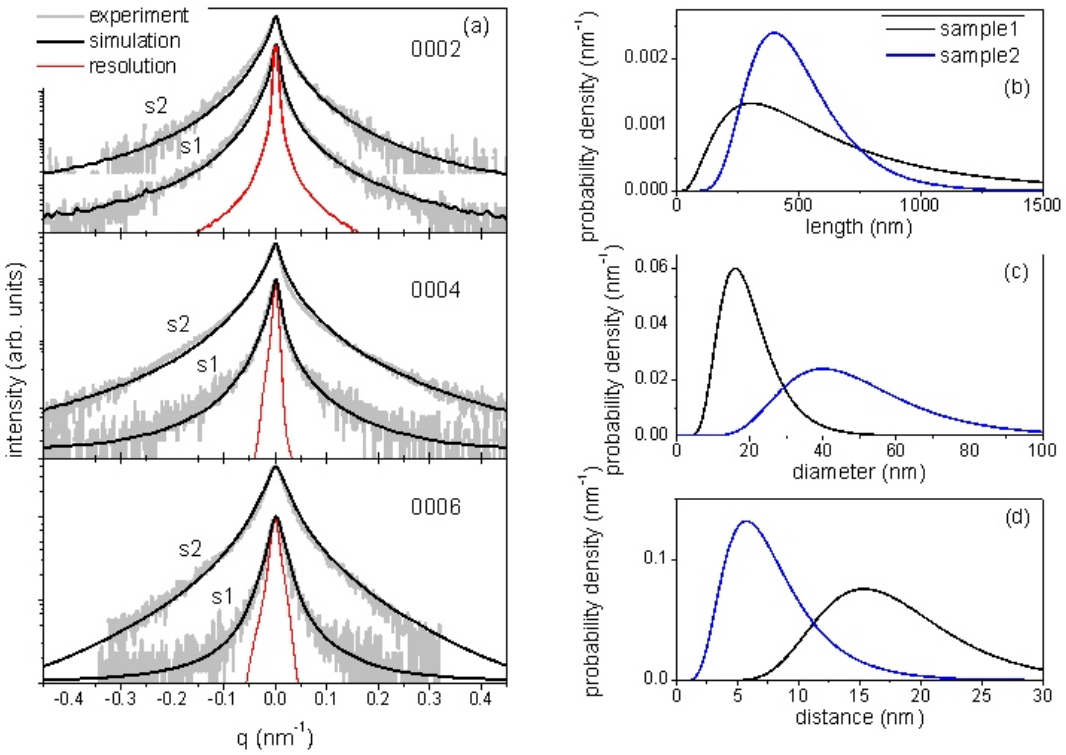

Figure 2. Measured and calculated X-ray diffraction profiles in successive reflection orders (a) and probability density distributions of the lengths of the bundled segments (b), nanowire diameters (c), and distances at the base of bundled segments (d) used in the Monte Carlo calculations.

2. V. M. Kaganer, B. Jenichen, O. Brandt, S. Fernández-Garrido, P. Dogan, L. Geelhaar, H. Riechert, *Phys. Rev. B* **86**, (2012), 115325.

C4

SCATTERING FROM FERROELECTRIC DOMAINS IN STRAINED (K, Na)NbO_3 EPITAXIAL FILMS ON (110) $TbScO_3$ SUBSTRATE

M. Schmidbauer[1], D. Braun[1], A. Kwasniewski[1], M. Hanke[2], L. von Helden[1], J. Schwarzkopf[1]

[1]Leibniz-Institute for Crystal Growth, Max-Born-Str. 2, D-12489 Berlin, Germany
[2]Paul-Drude-Institut für Festkörperelektronik, Hausvogteiplatz 5-7, D-10117 Berlin, Germany
martin.schmidbauer@ikz-berlin.de

Oxides with perovskite-like structure represent a fascinating class of advanced materials which have been extensively studied in the past decades since they exhibit a variety of functionalities, e.g., ferromagnetism, ferroelectricity or ferroelasticity. In ferroelectric materials phase symmetry and structural distortions are strongly coupled to piezoelectric properties. Periodic domain structures are of particular interest from both fundamental and technological point of view. Such periodic polarization modulations on a nanometre scale can be engineered by the use of substrates with suitable (anisotropic) misfit strains. However, understanding and controlling of ferroelectric phases and dimensions of the domain pattern is still hallenging.

We focus on $K_{0.75}Na_{0.25}NbO_3$ thin films grown on (110) $TbScO_3$ orthorhombic substrates using metal-organic chemical vapour deposition. A highly regular one dimensional ferroelectric domains pattern is formed which extends over several micrometres with a lateral periodicity of 50 nm (Fig.1a). The monoclinic symmetry of the domains is controlled by the anisotropic epitaxial lattice strain, which is highly compressive in one in-plane direction and weakly tensile in the corresponding orthogonal direction. Using piezoresponse force microscopy (PFM) and X-ray diffraction (Fig.1c,d) the monoclinic M_A phase is identified, which is associated with both a strong vertical and lateral electrical polarization component. The lateral

component of the polarization vector is collinear with the ± $[-110]_{pc}$ shear direction of the pseudocubic (pc) unit cell of the film and periodically changes by 180° in adjacent domains.

A structural variant of a 90° rotated M_A domain pattern, where the monoclinic distortion of the pseudocubic unit cells occurs along ± $[110]_{pc}$ is also observed (Fig.1b). However, this variant appears with significantly lower probability in agreement with energy considerations based on linear elasticity theory and cannot be independently resolved in a conventional X-ray diffraction experiment as shown in Fig.1c. Nevertheless, a 100 nm-focus experiment recently carried out at ID01 beamline (ESRF) could be used to individually investigate the two domain variants. Distinct differences between the 0° variant and the 90° variant were observed and will be discussed.

1. J. Schwarzkopf, D. Braun, M. Hanke, A. Kwasniewski, J. Sellmann, M. Schmidbauer, *J. Appl. Cryst.* **49**, (2016), 375.

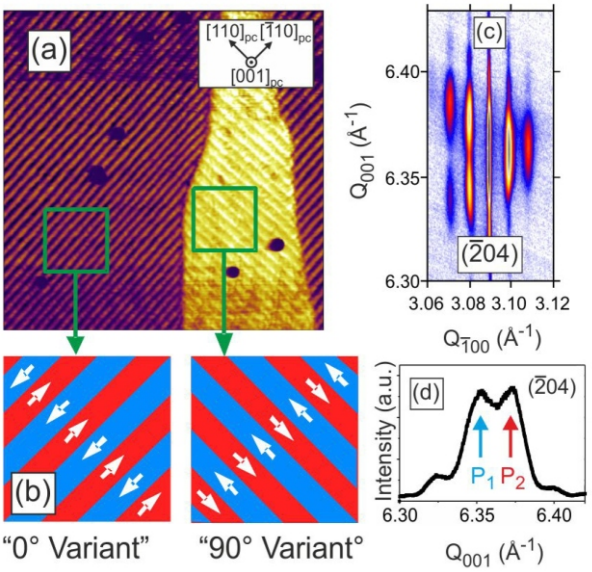

Figure 1. (a) Lateral PFM image (2 m x 2 m) of a 30 nm $K_{0.75}Na_{0.25}NbO_3$ film grown on (110) $TbScO_3$, (b) models of 0° and 90° variants (white arrows indicate the in-plane component of the polarization vector), (c) out-of-plane x-ray diffraction and, (d) section along the CTR at Q_{-100} = 3.09 $Å^{-1}$ (adapted from [1]).

Session II

Monday, September 4 - afternoon

I2

X-RAY PHASE-CONTRAST IN VIVO TOMOGRAPHY

Julian Moosmann

Helmholtz-Zentrum Geesthacht, Institute of Materials Research Metallic Biomaterials, Max-Planck-Str. 1, Geesthacht, 21502 Germany

Four-dimensional imaging techniques are essential tools in biology to understand the behaviour of cells during embryonic development. Here, we apply X-ray phase-contrast microtomography to capture the early development of the African clawed frog (Xenopus laevis), an important vertebrate model organism, over the course of time and in 3D. Early developmental stages of the Xenopus frog are optically opaque and lack conventional X-ray absorption contrast. For hard X-rays such embryos essentially are pure-phase objects. The probing wave front is thus characterised by a 2D phase map representing the projection of the object along the X-ray beam. Employing quasi-monochromatic and spatially coherent X-rays, we thus use propagation-based phase-contrast.

In Fresnel theory, the formation of 2D intensity contrast upon free-space propagation from a given phase map is studied and how linear approximations to the inverse problem of phase retrieval from a single-distance intensity measurement break down for large propagation distances and strong phase variations. Important properties of linear contrast transfer, which are conserved for a wide range of phase variations and propagation distances, are exploited in order to devise a phase-retrieval method which exhibits a high spatial resolution and contrast at low photon statistics.

Constraints imposed by in vivo imaging are discussed and results from experiments on living Xenopus embryos are presented.

component of the polarization vector is collinear with the ± $[-110]_{pc}$ shear direction of the pseudocubic (pc) unit cell of the film and periodically changes by 180° in adjacent domains.

A structural variant of a 90° rotated M_A domain pattern, where the monoclinic distortion of the pseudocubic unit cells occurs along ± $[110]_{pc}$ is also observed (Fig.1b). However, this variant appears with significantly lower probability in agreement with energy considerations based on linear elasticity theory and cannot be independently resolved in a conventional X-ray diffraction experiment as shown in Fig.1c. Nevertheless, a 100 nm-focus experiment recently carried out at ID01 beamline (ESRF) could be used to individually investigate the two domain variants. Distinct differences between the 0° variant and the 90° variant were observed and will be discussed.

1. J. Schwarzkopf, D. Braun, M. Hanke, A. Kwasniewski, J. Sellmann, M. Schmidbauer, *J. Appl. Cryst.* **49**, (2016), 375.

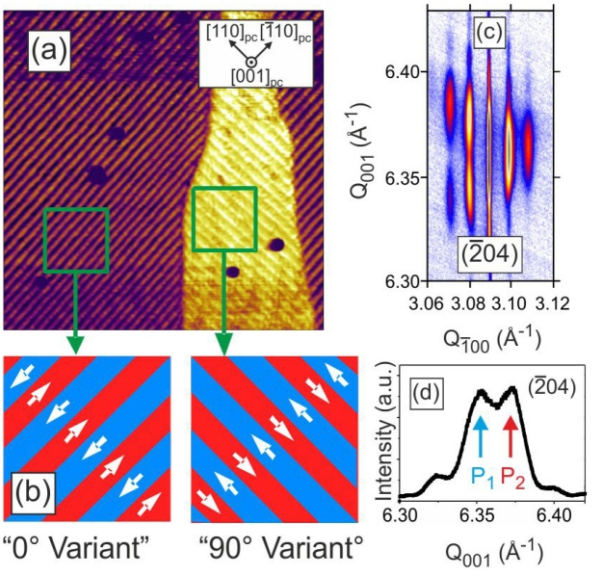

Figure 1. (a) Lateral PFM image (2 m x 2 m) of a 30 nm $K_{0.75}Na_{0.25}NbO_3$ film grown on (110) $TbScO_3$, (b) models of 0° and 90° variants (white arrows indicate the in-plane component of the polarization vector), (c) out-of-plane x-ray diffraction and, (d) section along the CTR at Q_{-100} = 3.09 $Å^{-1}$ (adapted from [1]).

Session II

Monday, September 4 - afternoon

I2

X-RAY PHASE-CONTRAST IN VIVO TOMOGRAPHY

Julian Moosmann

Helmholtz-Zentrum Geesthacht, Institute of Materials Research Metallic Biomaterials, Max-Planck-Str. 1, Geesthacht, 21502 Germany

Four-dimensional imaging techniques are essential tools in biology to understand the behaviour of cells during embryonic development. Here, we apply X-ray phase-contrast microtomography to capture the early development of the African clawed frog (Xenopus laevis), an important vertebrate model organism, over the course of time and in 3D. Early developmental stages of the Xenopus frog are optically opaque and lack conventional X-ray absorption contrast. For hard X-rays such embryos essentially are pure-phase objects. The probing wave front is thus characterised by a 2D phase map representing the projection of the object along the X-ray beam. Employing quasi-monochromatic and spatially coherent X-rays, we thus use propagation-based phase-contrast.

In Fresnel theory, the formation of 2D intensity contrast upon free-space propagation from a given phase map is studied and how linear approximations to the inverse problem of phase retrieval from a single-distance intensity measurement break down for large propagation distances and strong phase variations. Important properties of linear contrast transfer, which are conserved for a wide range of phase variations and propagation distances, are exploited in order to devise a phase-retrieval method which exhibits a high spatial resolution and contrast at low photon statistics.

Constraints imposed by in vivo imaging are discussed and results from experiments on living Xenopus embryos are presented.

C5

STATUS AND PERSPECTIVES OF SYNCHROTRON-BASED COHERENT X-RAY DIFFRACTION IMAGING

Y. Chushkin[1], F. Zontone[1], T. Beuvier[2], A. Gibaud[2], T. Latychevskaia[3], B. Maillot[6], P. Pernot[1], E.T.B. Skjønsfjell[4], D.W. Breiby[4], K. Giewekemeyer[5]

[1]ESRF, the European Synchrotron, CS40220 38043 Grenoble Cedex 9, France
[2]LUMAN, IMMM, UMR 6283 CNRS, Université du Maine, Faculté des Sciences, Le Mans Cedex 09, France
[3]Department of Physics, University of Zurich, Winterthurerstrasse 190, CH-8057 Zurich, Switzerland
[4]Norwegian University of Science and Technology, Høgskoleringen 5, 7491 Trondheim, Norway
[5] European XFEL GmbH, Albert-Einstein-Ring 19, 22761 Hamburg, Germany
[6] IGBMC, UDS, CNRS, INSERM, 1 rue Laurent Fries, 67404 Illkirch, France
chushkin@esrf.fr

After the first demonstration experiment [1], Coherent X-ray Diffraction Imaging (CXDI) attracted a lot of interest because of its promise of imaging isolated microscopic objects at high resolution which is beyond the values achieved with standard lens-based microscopy techniques. In spite of the huge potential [2-4] technical challenges have delayed the exploitation of the method for a regular application in science. Only recently CXDI turned out to be a reliable technique for high resolution 3D imaging [5].

In this work we report and discuss the opportunities and challenges of CXDI by showing examples of reconstructions of *Deinococcus radiodurans* bacteria in 2D Fig. 1(a), of a vaterite core-shell particle Fig. 1(b), a polymer microsphere coated with metallic multi-layers Fig. 1(c) and a gold test sample Fig. 1(d) in 3D. The high quality of the reconstructed images proves the power of CXDI: high sensitivity, full 3D capability, imaging the internal structure and high resolution. The improvement in the biological sample preparation and the development of large 2D (pixel) detectors remain the key elements for achieving the full potential of the technique.

1. J. Miao, P. Charalambous, J. Kirz, D. Sayre, *Nature*, **400**, (1999), 342.
2. H.N. Chapman, and K.A. Nugent, *Nature Photonics*, **4**, (2010), 833.
3. J. Miao, T. Ishikawa, B. Johnson, E.H. Anderson, B. Lai, K.O. Hodgson, *Phys. Rev. Letters*, **89**, (2002), 088303.
4. H.M. Chapman *et al, J. Opt. Soc. Am. A*, **23**, (2006), 1179.
5. Y. Chushkin *et al*, *J. Synchrotron Rad.,* **21**, (2014), 594.

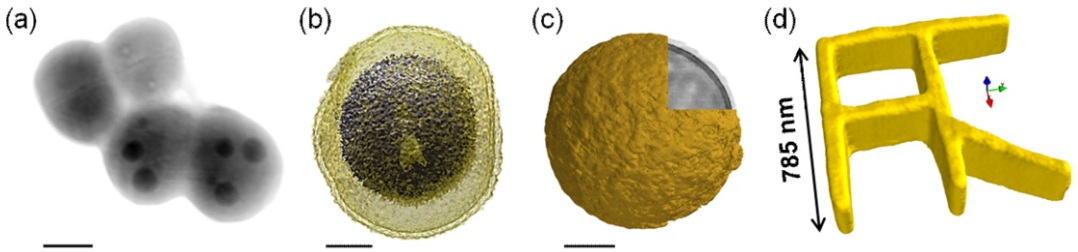

Figure 1. Reconstructed images: (a) *Deinococcus radiodurans* bacteria; (b) Vaterite core-shell particle (semitransparent iso-surface rendering); (c) Polymer microsphere with 3 coating layers (shown in a cut); (d) Tiny gold test sample. The scale bars are 1 m.

C6

STRUCTURAL INVESTIGATIONS OF SINGLE HETEROSTRUCTURE NANOWIRES

A. Davtyan[1], R. B. Lewis[1], H. Küpers[2], L. Geelhaar[2], D. Kriegner[3], S.M.M. Kashani[1], A. Al-Hassan[1], A. Seel[1], O. Loffeld[1], U. Pietsch[1]

[1]Faculty of Science and Engineering, University of Siegen, 57068 Siegen, Germany
[2]Paul-Drude-Institut für Festkörperelektronik, Hausvogteiplatz 5–7, D-10117 Berlin, Germany
[3]Department of Condensed Matter Physics, Charles University in Prague, Ke Karlovu 5, 121 16 Prague 2, Czech Republic
davtyan@physik.uni-siegen.de

GaAs/InGaAs/GaAs heterostructure nanowires (NWs) with 140nm GaAs core-10nm $In_{0.15}Ga_{0.85}As$ quantum well-30nm GaAs outer shell have been studied using Coherent X-ray diffraction imaging (CXDI) technique at ID1 beamline at ESRF. CXDI probes the structure of the wire by mapping the reciprocal space for example around the symmetric GaAs (333) (see Fig. 1 a,b) and asymmetric GaAs (331) (not shown here). In the direction of perpendicular to the NW growth axis the CDXI pattern shows a complex diffraction pattern as a result of the core-shell structure (Fig. 1a). Along the truncation rod the CXDI pattern shows displaced peaks indicating that coherently illuminated segment of the NW is composed from wurzite and zinc-blende segments (Fig. 1b). The electron density distribution in real space can be inverted from the diffraction patterns by means of dual space phase retrieval iterative algorithms. We demonstrate the feasibility of phase retrieval algorithms in case of symmetric and asymmetric reflections in 2D. Inverting the 2D diffraction pattern shown in Fig. 1a leads to the phase pattern (see Fig. 1c,d) where the phase anomalies are appearing at the corners of the hexagonal shaped nanowire indicating higher strain accumulation at the corners and strain relaxation towards the side facets of the NW. Fig.1d shows sensitivity of the phase to the presence of the InGaAs shell with phase shifts at the position of the embedded quantum well. Interpretation of these results by means of Finite Element Method simulations as well as 3D phase retrieval analysis are currently on the way in order to investigate the impact of strain caused by InGaAs inner shell and retrieve the 3D nanowire structure.

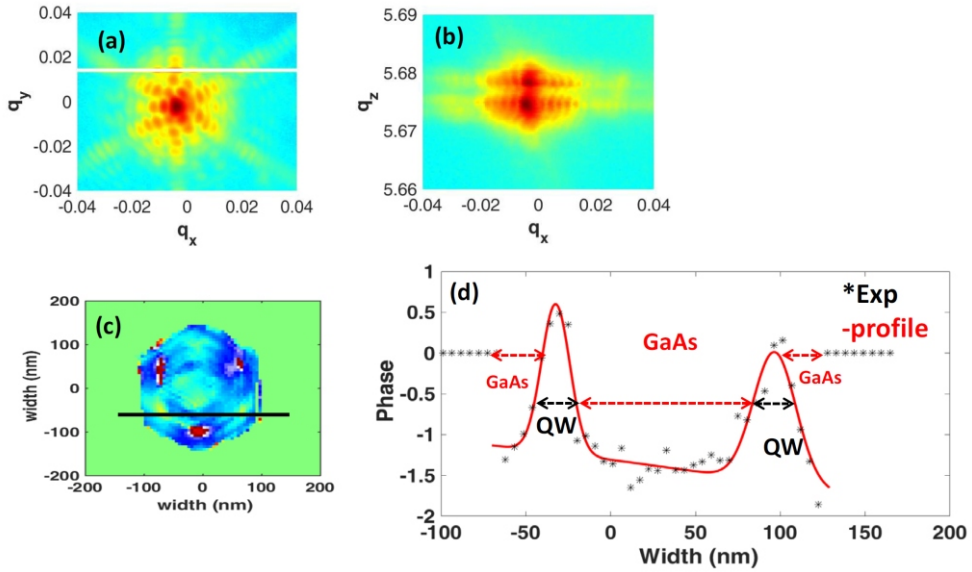

Figure 1. (a,b) Projections of the experimentally recorded 3D CXDI pattern from single NW around the GaAs (333) reflection.(c) Retrieved phase pattern of the nanowire. (d) Line cut from the phase shown in (c) black line.

Session III

Tuesday, September 6 - morning

I3

WHOLE POWDER PATTERN MODELLING OF NANOCRYSTALLINE AND PLASTICALLY DEFORMED MATERIALS "HANAVALT AWARD LECTURE"

Paolo Scardi

Department of Civil, Environmental & Mechanical Engineering, University of Trento, Via Mesiano 77, 38123 Trento, Italy
Paolo.Scardi@unitn.it

Whole Powder Pattern Modelling (WPPM) has been extensively used for nearly two decades in the characterization of nanocrystalline and plastically deformed materials, to gather information on crystalline domain shape and size distribution, and on the nature and amount of lattice defects, with special interest to those generating inhomogeneous strain fields [1,2]. In time the WPPM approach has been completed by a variety of microstructural models, with due consideration of diffuse scattering from static and dynamic disorder (Temperature Diffuse Scattering, TDS). The present talk reviews basic theory and applications, introducing the latest WPPM algorithm, adopted by the x-Dream software. Substantial improvements include structural models, as in Rietveld refinement, which add to the microstructural ones; detailed information on results and progress of the WPPM procedure are made visible directly in the user interface.

Among the latest results which will be presented, the growing integration between atomistic modelling, mostly based on Molecular Dynamics simulations, and WPPM. This combination is especially useful to understand how lattice defects – most remarkably, line defects and grain boundaries – contribute to the inhomogeneous strain and consequent line profile effects [2,3]. More results are presented on powders made of free-standing nanocrystals, as commonly produced and used in modern nanotechnology, e.g., for catalysis and biomedical applications.

1. P. Scardi, in *Powder Diffraction: Theory and Practice* (The Royal Chemistry Society, Cambridge, 2008), edited by R.E. Dinnebier & S.J.L. Billinge. Chap. 13, pp. 376–413. ISBN-13: 978-0854042319.
2. P. Scardi, A. Leonardi, L. Gelisio, M. R. Suchomel, B. T. Sneed, M. K. Sheehan & C.-K. Tsung, "Anisotropic atom displacement in Pd nanocubes resolved by molecular dynamics simulations supported by x-ray diffraction imaging", *Phys. Rev.* B 91 (2015) 155414. doi: 10.1103/PhysRevB.91.155414.
3. L. Rebuffi, A. Troian, R. Ciancio, E. Carlino, A. Amimi, A. Leonardi & P. Scardi, "On the reliability of powder diffraction Line Profile Analysis of plastically deformed nanocrystalline systems", *Scientific Reports* 6 (2016) 20712. doi: 10.1038/srep20712.

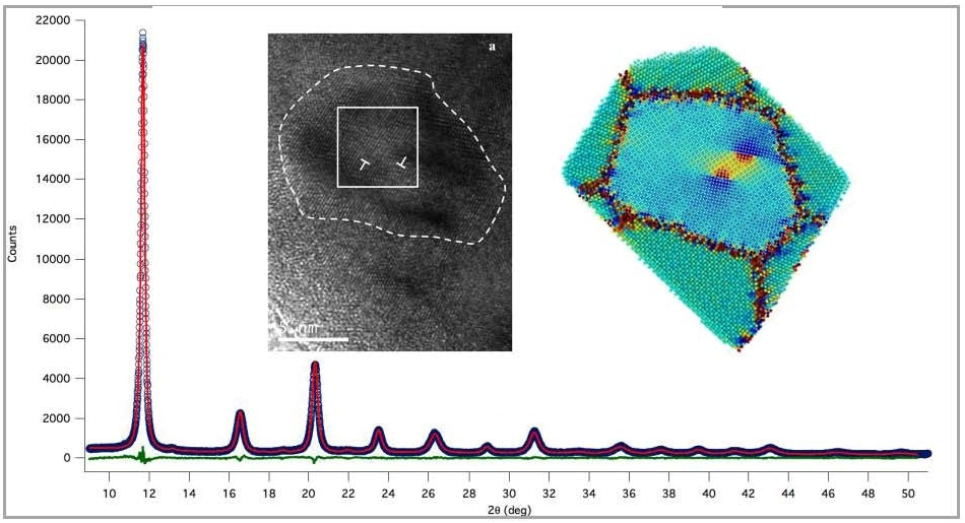

C7

TOWARDS REAL TIME X-RAY IMAGING OF CRACKS AND FRACTURE IN SILICON

A. N. Danilewsky[1], A. Rack[2] and M. Scheel[3]

[1]Kristallographie, Albert-Ludwigs-Universität, 79104 Freiburg i. Br., Germany
[2]European Synchrotron Radiation Facility, Grenoble, France
[3]Synchrotron Soleil, Gif sur Yvette, France
a.danilewsky@krist.uni-freiburg.de

Frank-Read sources in Si as well as thermal slip move in a ductile regime of the crystals at a speed in the order of magnitude of 10^{-5} – 10^{-6} m/s. In X-ray diffraction imaging, effects with a speed up to about 10^{-3} m/s are easily accessible [1]. In the brittle regime, the same driving forces may result in fracture of a crystal with a crack tip speed up to 3600 m/s where the experimental observation in real time becomes a challenge. In this paper we will be demonstrate, how the time structure of a brilliant synchrotron light source like ESRF, Grenoble, France can be used to follow ultra high speed events towards a time scale of less than microseconds [2]. In the so called four-bunch mode, only four highly populated electron bunches are used in the storage ring, separated from each other by a temporal delay of around 700 ns. The highest crack tip speed of 70 m/s is recently measured with a high-speed CMOS-based camera system providing frame rates of about 355.000 frames/sec. Based on a frame-transfer CMOS concept, such detector can operate at frame rates of up to 10 000 000 images per second: with a pixel size of about 40 µm it would allow one to follow cracks in real time up to a speed of 2000 m/s.

The experiments presented in this paper are performed on (001) oriented Si slices with artificial starting defects, done with an indentation method. At about 1100 °C, the slices are quenched by a water jet to produce enough thermal stress for crack formation and propagation. With 2 fast camera systems and acquisition rates of about 35 500 images per second the direct and diffracted image of a crack can be followed in parallel. Fig. 1 shows the starting indent in frame 210 and the appearance of the first crack c1 between frame 308 - 311, covering 84 µs. Information about the geometry and speed of a crack can be taken from the direct image from phase contrast, whereas the related local strain variation becomes visible in the 220 reflection. In this way and within about 42 ms a complex crack pattern of five cracks c1 - c5 originates from the indent, as shown in Fig. 2, frame 1495. Until frame 3000 the cracks elongate with varying strain fields and various crack tip velocities. Careful analysis indicates, that the deflection of the crack face into various high indexed, (hkl) planes is correlated with the short arrests of some microseconds of the crack tip. Obviously the local pile up of energy during the arrest allows to open the higher energy (hkl) faces. An irregular fracture results instead of a mirror like cleavage along the preferred low energy {111} or {110} planes as expected in the diamond structure.

Slow motion movies show this irregular crack propagation directly in phase contrast and in diffraction the related changes in the strain field.

1. A. N. Danilewsky, J. Wittge, A. Hess, A. Croell, A. Rack, T. dos Santos Rolo, D. Allen, P. McNally, P. Vagovic, Z. Li, T. Baumbach, E. Gorostegui-Colinas, J. Garagorri, M. R. Elizalde, D. Jaques, M. Fossati, D. K. Bowen and B. Tanner, Phys. Stat. Sol. (a) 208(11) (2011), 2499-2504.
2. A. Rack, M. Scheel and A. N. Danilewsky, IUCrJ 3(2) (2016), 108-114, DOI: http://dx.doi.org/10.1107/S205225251502271X..

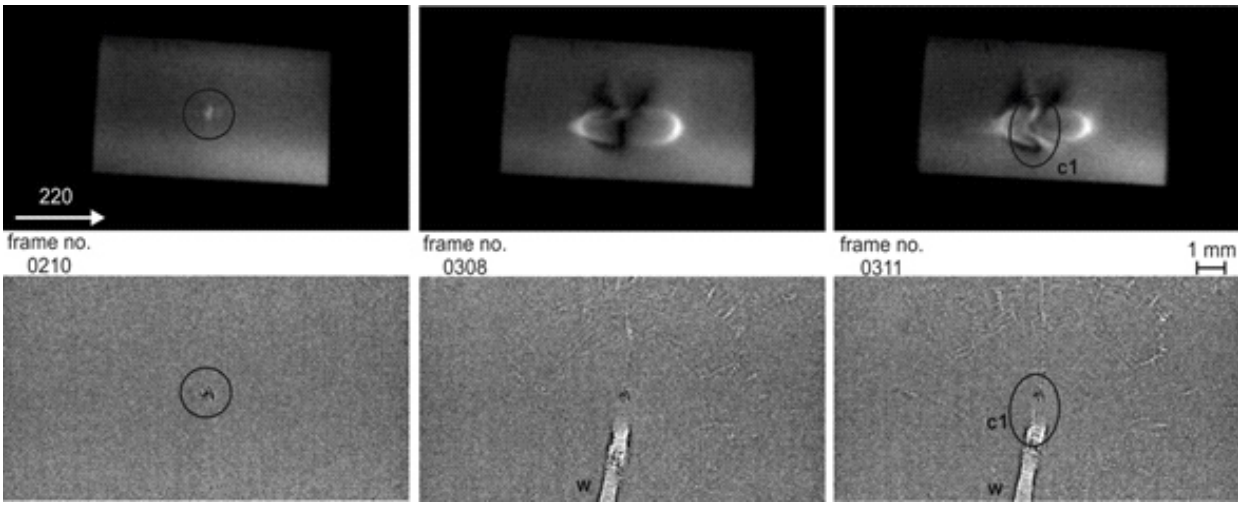

Figure 1. Beginning of high speed X-ray imaging of Si (100) wafer at about 1000 °C: (a) 220 Reflection (b) Radiography (phase contrast), both 1.28 s integration time and 28 s frame distance: Frame 210: indent marked by circle, Frame 308: locally quenching with a water jet (w) produces a strain field, Frame 311: 84 µs later the first crack c1 modifies the strain field (marked by ellipse).

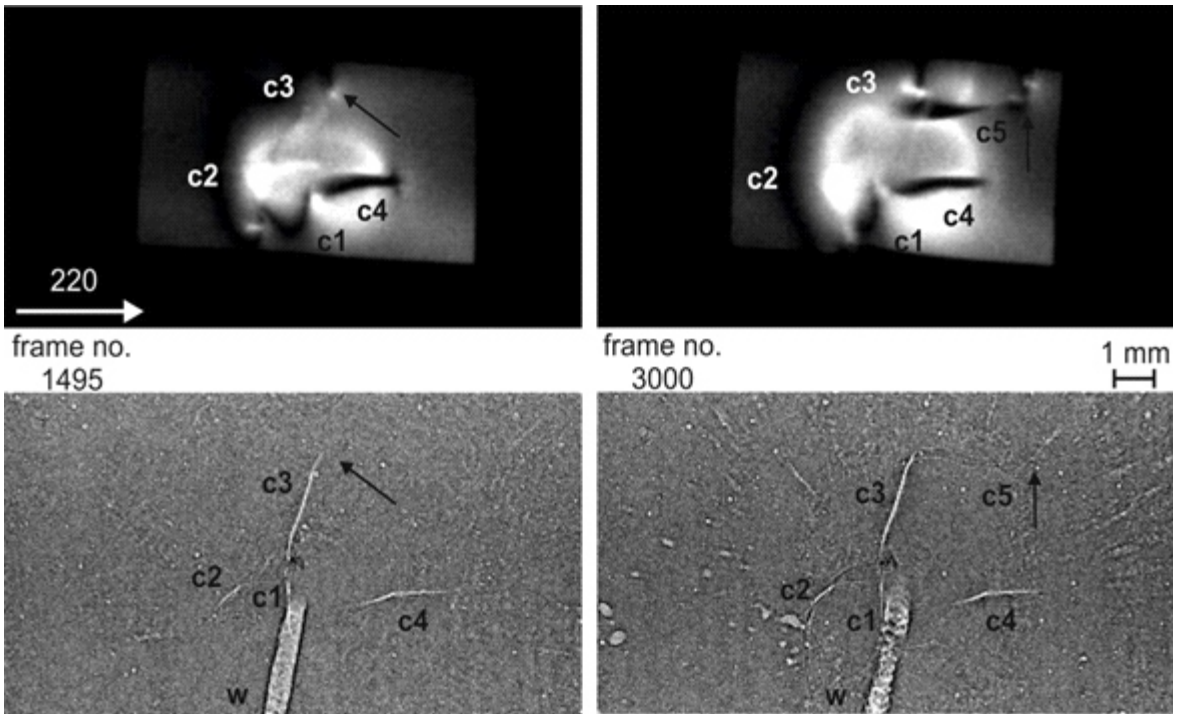

Figure 2. Continued high speed X-ray imaging of Si (100) wafer at about 1000 °C from Fig. 1 (a) 220 reflection (b) Radiography (direct image, phase contrast): Frame 1495 after 42 ms: cracks c2, c3, c4 and surrounding strain, arrow indicates tip of crack c3, Frame 3000 after about 0.1 s: last crack c5, tip marked by arrow.

The authors wish to acknowledge Prof. B. Tanner, Dept. of Physics, Durham, UK and Prof. P. McNally School of Electronic Engineering, Dublin City University, Dublin, Ireland for helpful discussions.

C8

NON-DESTRUCTIVE X-RAY DIFFRACTION MEASUREMENT OF WARPAGE IN SILICON DIE EMBEDDED IN INTEGRATED CIRCUIT PACKAGES

B. K. Tanner[1], A. N. Danilewsky[2], A. Bose[3], R. K. Vijayaraghavan[3], A. Cowley[3,4], V. Cherman[5] and P. J. McNally[3]

[1]Dept. of Physics, Durham University, South Road, Durham DH1 3LE, U.K
[2]Kristallographie, Albert-Ludwigs-Universität, Freiburg, German
[3]School of Electronic Engineering, Dublin City University, Dublin 9, Ireland
[4]Currently at European Astronaut Centre, European Space Agency, Köln, Germany
[5]IMEC, Kapeldreef 75, B-3001 Louvain, Belgium.
b.k.tanner@dur.ac.uk

Future integrated chip manufacturing must encompass complex chip systems capable of diverse functionality and application, so-called “More than Moore” manufacturing. Such systems include Micro-Electromechanical Systems, System in Package, System on Chip and 3-D Integrated Circuits, referred to collectively as “advanced packages”. This technology requires processing of thin semiconductor die (25-100µm thickness) and many packages include multiply-stacked silicon die. A recent review [1] revealed that none of today‘s commercially available metrology tools is capable of measuring, *in situ* and non-destructively across an entire die, the nature and scale of wafer/die strain or bow/warpage. Many techniques are destructive and those that are non-destructive tend to measure the package bow which, crucially, is not the same as wafer/die bow.

We have demonstrated that X-Ray Diffraction Imaging (XRDI) using B-Spline fitting techniques (B-XRDI) is capable of non-destructive, *in situ* mapping and analysis of major die warpage features in fully encapsulated advanced packages [2-3]. We describe how B-XRDI allows the user to reconstruct, from the image distortion of a series of section x-ray topographic images, a full profile of the warpage of the silicon die inside such a chip package. There is no requirement for pre-treatment or pre-processing of the chip package. We have used the technique to demonstrate the impact of elevated temperature on a commercially sourced micro quad flat nonlead (uQFN) chip package and have shown that the strain becomes locked in at a temperature between 94°C and 120°C [4]. Using synchrotron radiation at the Diamond Light Source, warpage maps for the entire 2.2 mm × 2.4 mm × 150 m Si die were acquired in 50 s and

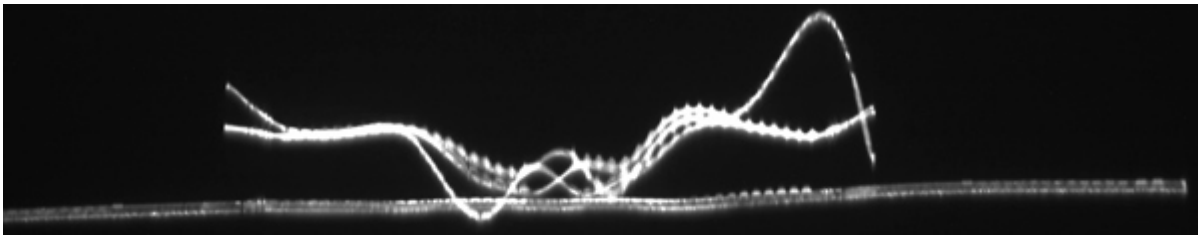

Figure 1. White beam section topographs of a package containing 4 stacked Si die. The 3 top dies are 5 mm 5 mm 50 m thick, while the bottom die is 8 mm 8 mm 200 m thick.

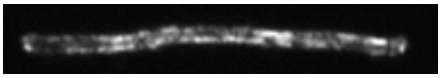

Figure 2. Image from a distorted (001) oriented uQFN die taken in transmission with a wide area monochromatic beam.

individual line scans in 500 ms. Warpage in multiple die packages (Fig1) has been measured.

We present examples of warpage measurement in several commercial chip packages and by measuring the image displacement as a function of detector distance and at several wavelengths, tilt and strain have been determined independently. The data have been shown to be in good agreement with warpage in test structures determined from mechanical profilometry.

Using a monochromatic beam, the warpage data can also be collected by recording transmission X-ray topographs at different angular positions across the rocking curve. Due to the wafer deformation, a narrow stripe of intensity only is imaged for any one angle (Fig 2). Addition of sequential stepped images creates the "zebra pattern" of Renninger [5] and this directly represents contours of effective misorientation. In this mode, strain sensitivity is limited by the X-ray optics. We have shown that statistically good data can be taken in transmission on single chip packages at 24.25keV (Fig 3), close to the wavelength of the AgK line. The total data collection time for the 20 images in Fig 3 was 75 seconds at B16 of the Diamond Light Source. By comparing 220 and reflections, we show that the deformation is almost symmetrical on 90 rotation about the [001] surface normal. Reversal of the entrance and exit surface results in similar patterns but with displacement of successive images in opposite directions. Contour analysis between these settings provides a means of separating tilts and dilations.

We compare the two approaches to warpage measurement in packaged die and examine the possibilities and challenges of converting the techniques into an in-fab tool.

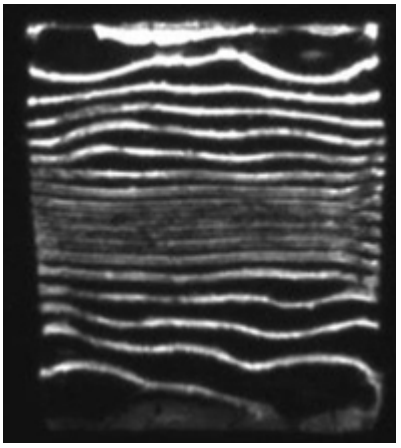

Figure 3. Summed monochromatic topographs taken at equal steps across the rocking curve for a packaged uQFN die. Adhesive is applied at the four corners of this die prior to encapsulation. 220 reflection.

1. M.R. Marks, Z. Hassan, K.Y. Cheong, *IEEE Trans. Comp. Manuf. Technol*., **4**, (2014) 2042.
2. C.S. Wong, N.S. Bennett, D. Manessis, A. Danilewsky, P.J. McNally, *Microelectronic Engineering* **117** (2014) 48.
3. A. Cowley, A. Ivankovic, C.S. Wong, N.S. Bennett, A.N. Danilewsky, M. Gonzalez, V. Cherman, B. Vandevelde, I. De Wolf, P.J. McNally, *Microelectronics Reliability*, 59, (2016), 108.
4. A. Bose, R.K. Vijayaraghavan, A. Cowley, V. Cherman, O. Varela Pedreira, B.K. Tanner, A.N. Danilewsky, I. De Wolf, P. J. McNally, *IEEE Trans. Comp. Packag. Manuf. Technol.,* **6** (2016) 653.
5. M. Renninger Phys Lett **1** (1962) 106.

C9

DETERMINABILITY OF DISLOCATION PATHS BY 3D DIFFRACTION LAMINOGRAPHIC IMAGING: THEORETICAL CONSIDERATIONS LEADING TO A NEW EXTINCTION RULE

D. Hänschke[1,2], T. Baumbach[1,2]

[1]*Karlsruhe Institute of Technology (KIT), Institute for Photon Science and Synchrotron Radiation (IPS/ANKA), 76344 Eggenstein-Leopoldshafen, Germany*
[2]*Karlsruhe Institute of Technology (KIT), Laboratory for Applications of Synchrotron Radiation (LAS), 76128 Karlsruhe, Germany*
daniel.haenschke@kit.edu

Recently, X-ray diffraction laminography (XDL) has been developed and successfully applied to the 3D imaging of dislocation networks inside large monocrystals like e.g. industrial silicon wafers [1]. Similar to X-ray topo-tomography [2] and related electron tomographic approaches [3], XDL is based on the acquisition of topographic (i.e. Bragg diffraction contrast) projection images of the investigated crystal volume during its rotation about a selected reciprocal lattice vector. The average distribution of the local reflectivity (for suitable contrast conditions increased close by crystal defects like dislocations) can then be estimated by means of 3D laminographic reconstruction with suitable algorithms. In many cases, this enables the determination of the spatial dislocation arrangement with few micrometres precision.

It turns out, however, that few dislocation segments with certain configurations of local line direction $\boldsymbol{l}$, Burgers vector $\boldsymbol{b}$, diffracting reciprocal lattice vector $\boldsymbol{h}_{hkl}$, and direction $\boldsymbol{k}_h$ of the diffracted beam, cannot be localized inside the reconstruction volume in this way. In the simplest case, this is due to the well-known extinction rule for vanishing or reduced topographic contrast of dislocations (basically $\boldsymbol{b}.\boldsymbol{h}_{hkl} = 0$), i.e. the defects are already not sufficiently visible in the entire projection data in the first place. But, more intriguingly, in some cases only the paths of particular dislocation segments cannot be determined, despite these being clearly visible in most projections. Up to now, this effect has not been understood.

We will report on our recent investigation of the X-ray diffraction contrast of dislocations during XDL measurements, using linear elasticity theory [4]. We will show that for projection acquisition with both full excitation (e.g. by white beam) and so-called weak-beam conditions [5] analytic expressions can be derived for the size of the excited crystal volume V per dislocation line length, in dependence of the projection angle , see Fig. 1 and Fig. 2. Based on this, we will formulate a new extinction rule, which correctly predicts the inaccessibility of a certain class of dislocation segments. For the future this will allow a more careful interpretation of dislocation arrangements determined by any projection based 3D diffraction imaging.

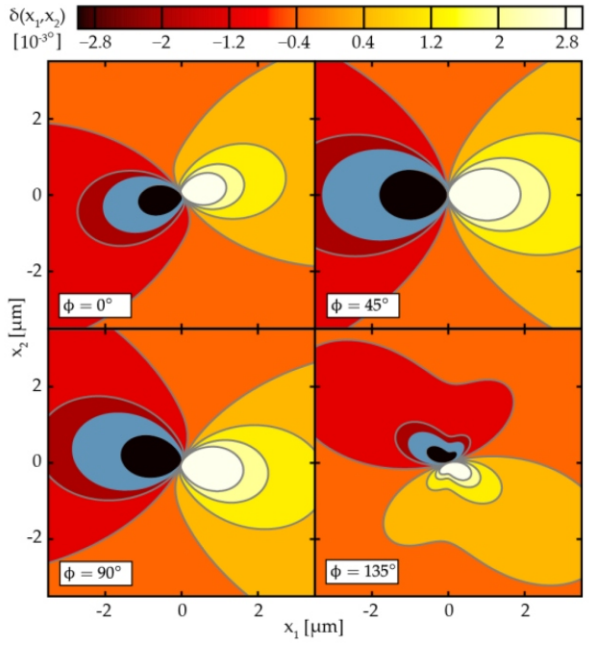

Figure 1. Numerical simulation of the effective misorientation (x_1,x_2) of the diffracting lattice planes close by a dislocation in silicon, for different view angles during rotation about the reciprocal lattice vector $\boldsymbol{h}_{-2-20}$. Line direction is $\boldsymbol{l} = \boldsymbol{e}_3 = [_{01-1}]$, the Burgers vector is $\boldsymbol{b} = a/2[101]$ and $E = 40$ keV. The corresponding excited crystal regions V for a fixed interval are indicated as blue areas.

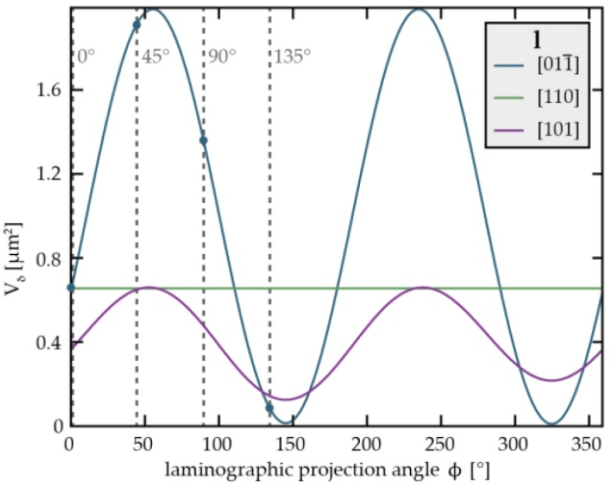

Figure 2. Fully analytic calculation of the excited crystal volume per line length V (fixed , the same as for Fig. 1), in dependence of the rotation angle . Three line directions $\boldsymbol{l}$ are compared (blue corresponding to Fig. 1), revealing significant differences. From the underlying analytic expressions an extinction rule can be derived, predicting the failure of dislocation path determination by 3D reconstruction from projections.

1. D. Hänschke, L. Helfen, V. Altapova, A. Danilewsky, T. Baumbach, *Appl. Phys. Lett.,* **101**, (2012), 244103.
2. W. Ludwig, P. Cloetens, J. Härtwig, J. Baruchel, B. Hamelin, P. Bastie, *J. Appl. Crystallogr.,* **34**, (2001), 602-607.
3. J. S. Barnard, J. Sharp, J. R. Tong, P. A. Midgley, *Science,* **313**, (2006), 319.
4. J. P. Hirth, J. Lothe, *Theory of dislocations*. New York: MacGraw-Hill. 1968.
5. A. Authier, *Dynamical theory of X-ray diffraction*. Oxford: Oxford University Press. 2002.

The presented work is partially funded by the EU-FP7 project No. 216382 SIDAM and by the German Federal Ministry of Education and Research by the grant 05K14VKA STROBOS-CODE. We thank for the support and valuable contributions by all members of these collaborations as well as by the staff of IPS, LAS, and IBPT/ANKA.

C10

COMBINING QUALITATIVE AND QUANTITATIVE DIFFRACTION TOPOGRAPHY AT THE ESRF TO CHARACTERISE PV SILICON AND DIAMOND CRYSTALS

T. N. Tran Thi[1], V. A. Oliveira[2], D. Camel[2], S. Connell[3], D. Caliste[4], D. Eon[5], J. Härtwig[1], T. Lafford[6], J. Baruchel[1]

[1]European Synchrotron Radiation Facility (ESRF), BP 220, 38043 Grenoble, France
[2]INES, CEA, Le Bourget du Lac, F-73000, France
[3]University of Johannesburg, Auckland Park, South Africa
[4]L Sim, MEM, UMR-E CEA/UGA, INAC, Grenoble F-38054, France
[5]Institut Néel, CNRS, Grenoble, France
[6]IBEX Innovations Ltd., NETPark, Sedgefield, TS21 3FH, UK

The need for high quality diamonds, for electronics, detectors and X-ray optics purposes, and for "inexpensive, reduced-defects" silicon for photovoltaic (PV) purposes, has strongly promoted the use of X-ray Bragg diffraction imaging ("X-ray topography") techniques to study their defects. This led us to develop, at the ESRF, enhanced capabilities in the portfolio of Bragg imaging techniques we now propose. This includes some automation, and a new diffractometer on the BM05 beamline. Within this portfolio, projection and section white beam topography and monochromatic Rocking Curve Imaging (RCI) [1] are mostly used to qualitatively and quantitatively characterise the crystalline quality, in deposited layers, deep bulk structures and the interface between them, with an angular precision in the µrad range and a spatial resolution in the µm range.

Diamond exhibits many attractive properties for electronic and detector applications (wide band gap, high mobility of charge carriers, high electric field breakdown strength and thermal conductivity). In addition, diamond, because of its thermal and X-ray transparency properties, is a material of choice for diffractive and refractive X-ray optics [2]. High voltage diodes and FET switches are based on Boron- and phosphorus-doped diamond, these devices being expected to efficiently commute high power at high frequency. But their performances are a function of the crystalline quality, and the material available from commercial suppliers covers a wide variety of qualities and prices. Figure 1 shows examples of topographic images made at BM05: the high quality type-IIa diamonds (Fig. 1 iii and vi) display areas of the (001) growth sector that are

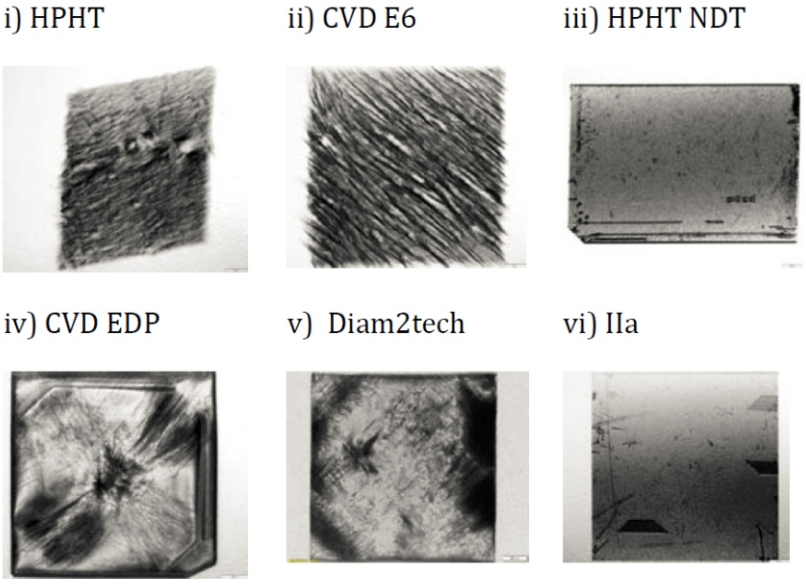

Figure 1: White beam topographs of different single diamond plates characterized at BM05

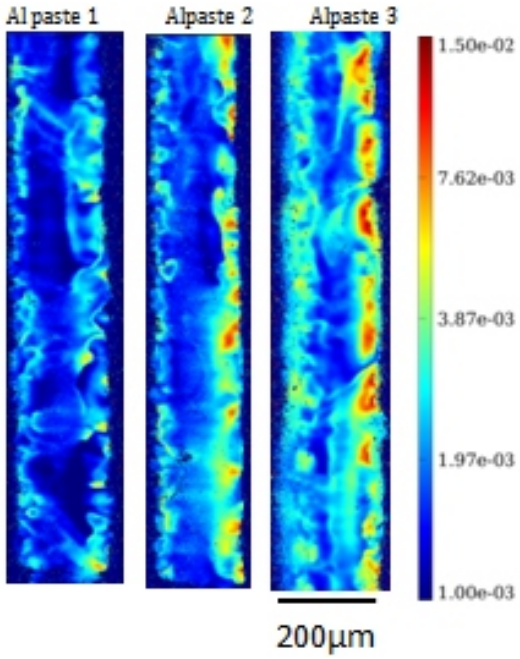

Figure 2. 220 section FWHM maps (in degrees) of mono-like Si, with Al back-planes made from three different Al pastes. The face with the Al back plane is on the right of the image. The Al back plane produces an increased distortion of the Si 220 planes, higher than the one associated with the mono-like Si defects formed during the growth (visible within the bulk of the sample). The different Al pastes produce different effects: the Si 220 FWHM values vary significantly when going from the Al paste 1 ("good" photovoltaic efficiency, less distortion of the Si wafer, FWHM values ~ $2x10^{-3}$ degrees) to, Al paste 3 ("less good", FWHM misorientations of the Si wafer up to $8x10^{-3}$ degree).

almost dislocation-free, with only a few stacking-faults visible. The dislocation densities of 'low grade' commercial diamonds (images i, ii, iv and v) are in the 10^3-10^4cm^{-2} range. The crystalline quality of a boron-doped layer grown onto a diamond plate was quantified via section RCI measurements (FWHM maps). It shows that the distortion of the boron-doped layer (FWHM > 3.5 10^{-3} degrees) is much higher than that of the substrate bulk (FWHM ~2.4 10^{-3}degrees). But attention should also be paid to the defects that exist in the diamond substrate itself (dislocations, stacking faults, growth sectors, and (sub-) surface damage from polishing processes), these defects being often detrimental for the final electronic performance.

Silicon is today the most widely-used material for PV applications. Both the quality of PV-Si substrates and the preparation of the device, strongly influence the PV efficiency and price of the solar-cell. We have therefore studied both the growth of "mono-like" Si (less expensive than Cz Si, but sufficient quality for PV applications) and aspects of the cell processing (Al back electrical contacts).

The "mono-like" Si is grown by directional solidification, on a series of seeds located at the bottom of the crucible. Dislocation sources, leading to a dislocation multiplication very detrimental for the PV efficiency, occur during growth, both at the level of the junction of the seeds [3] or higher in the ingot through the piling up of dislocations belonging to several gliding systems [4]. These two mechanisms have been widely studied through white beam and RCI measurements.

The distortion and strain of the Si in contact with the Al back layer have been characterised by coupling RCI section topography with X-ray nano-diffraction measurements (at ID01). The results show a correlation between the lattice distortion of the Si in contact with the eutectic and Al layers, and the PV efficiency. This distortion, and the PV performances, vary as a function of the Al paste used. The higher PV efficiency ("good" paste) appears to be associated with a higher homogeneity of the eutectic layer and, consequently, a lower distortion of the Si back surface region (Fig.2). The difference between the various commercial pastes rests on the amount of Al, Al grain size, and their precise composition. We determined some of the characteristics of a "good Al paste", a crucial ingredient for producing efficient solar cells.

1. R.T. Kluender, A. Philip, J. Meyssonier, J. Baruchel, *Phys. Status Solidi* **208**, 2505 (2011).
2. P. Van Vaerenbergh, C. Detlefs, J. Härtwig, et al., *AIP Conf. Proc.* 1234, 229 (2010).
3. M. Tsoutsouva, V.A. Oliveira, D. Camel, T.N. Tran Thi, et al., *J. Cryst Growth* **401**, 397 (2014).
4. V. Amaral de Oliveira, PhD Thesis, Université Grenoble Alpes (2016).
5. T. N. Tran Thi, S. Dubois, J. Baruchel et al. *Solar Energy Materials and Solar Cells* **135**, 17 (2015).

Session IV

Tuesday, September 6 - morning

I4

MINERALIZED TISSUE FORMATION DESCRIBED BY SYNCHROTRON-BASED X-RAY ANALYSIS AND IMAGING TECHNIQUES

I. Zlotnikov

Department of Biomaterials, Max Planck Institute of Colloids and Interfaces, Potsdam, Germany
igor.zlotnikov@mpikg.mpg.de

Living organisms form complex mineralized composite materials that perform a variety of essential functions, ranging from structural support and mechanical strength, to optical, magnetic or sensing capabilities. This remarkable diversity in functionality is accomplished from a relatively narrow range of constituent inorganic materials via hierarchical mineral-organic functional architectures. Therefore, these structures routinely serve as a source of inspiration for scientists and engineers. The control over biomineral shape, at all hierarchical levels, is a key aspect of structure-to-function relationship in biological materials. Although many studies have emphasized the critical role of biological regulation during biomineral formation, the physical constraints governing the growth process of naturally occurring architectures and determining the form of biomineral building blocks are not understood.

In this talk, I will address the fundamental question of how nature takes advantage of thermodynamic principles to generate complex morphologies. I will highlight two structures where, using synchrotron based X-ray analysis and imaging techniques, it was shown that the microstructure formation process during biomineralization is analytically defined and can be quantitatively described both in time and in space. The structures are the prismatic layer in the shell of a bivalve mollusc *Pinna nobilis* [1] and the anchor spicule of a glass sponge *Monorhaphis chuni* [2, 3].

1. B. Bayerlein, P. Zaslansky, Y. Dauphin. A. Rack, P. Fratzl, I. Zlotnikov, Nat. Mater., 13(12), (2014), 1102.
2. I. Zlotnikov, P. Werner, H. Blumtritt, A. Graff, Y. Dauphin, E. Zolotoyabko, P. Fratzl, Adv. Mater., 26(1), (2014), 1682.
3. I. Zlotnikov, P. Werner, P. Fratzl, E. Zolotoyabko, Small, 11(42), (2015), 5636.

C11

DARK-FIELD HARD X-RAY MICROSCOPY IMAGING FOR THE STUDY OF BIOMINERALS

P. K. Cook[1], A. C. Jakobsen[2], H. Simons[2], H. F. Poulsen[2], C. Detlefs[1]

[1]ESRF-The European Synchrotron, CS40220, 38043 Grenoble Cedex 9, France
[2]Department of Physics, Technical University of Denmark, Fysikvej, building 311, 2800 Kgs. Lyngby, Denmark
philip.cook@esrf.fr

A full-field Hard X-ray Microscope (HXRM) has been constructed at ESRF ID06 for the study of polycrystalline materials. Used in dark-field mode, the Bragg diffracted beam produced by a given grain is selected and magnified using a stack of Be compound refractive lenses. The resulting image, a real space projection of the grain, is captured by an imaging detector. Coupled to a high-precision goniometer, this permits characterisation of orientation and mosaicity with a real space resolution of 100 nm and angular resolution of 10 mrad. Strain within a grain can be measured with a resolution of 10^{-5}. A single projection can be recorded in one second, and mosaicity maps can be recorded in a few hours, providing the possibility for studies of dynamics. The microscope has so far been used for characterisation of metal and ferroelectric samples, and work is underway to expand the technique to new areas.

One such example is the study of biominerals, biological hierarchical materials combining an organic template with a mineral structural component. Biominerals exhibit a wide variety of functions, with forms which are controlled by the animal's physiology. Their microstructure is often tailored to provide particular material properties, making them interesting as natural models for the inspiration of new engineered materials.

We will show results from our initial examinations of pearl, bivalve shell, and fish otoliths, highlighting some of the challenges in their analysis and the potential of dark-field HXRM to reveal structures on scales from

micrometric to nanometric in these and other complex polycrystalline materials.

1. H. Simons, A. King, W. Ludwig, C. Detlefs, W. Pantleon, S. Schmidt, F. Stöhr, I. Snigireva, A. Snigirev, H. F. Poulsen, *Nat. Comm.*, **6**, (2015), 6098.

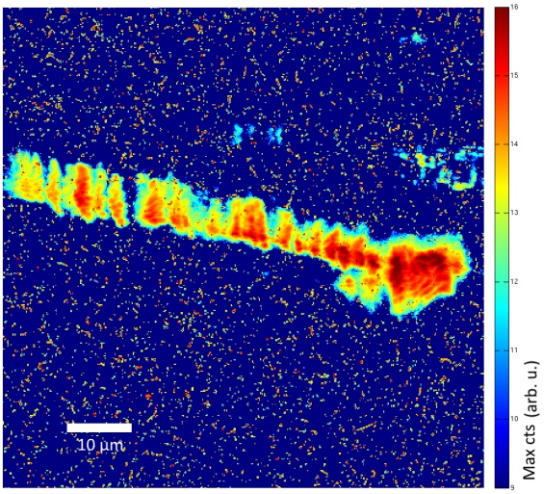

Figure 1. A dark-field image of an aragonite fibre from a fish otolith shows its growth from left to right in sequential layers, each composed of multiple crystalline units.

C12

COMBINED USE OF X-RAY FLUORESCENCE MICROSCOPY, PHASE CONTRAST IMAGING AND NANOTOMOGRAPHY FOR HIGH RESOLUTION QUANTITATIVE Fe MAPPING IN INFLAMED CELLS

Chiara Gramaccioni[1,5], Alessandra Procopio[2], Alessandra Frioni[3], Emil Malucelli[2], Stefano Iotti[2], Andrea Notargiacomo[4], Michela Fratini[5,6], Yang Yang[7], Peter Cloetens[7], Inna Bukreeva[5], Sylvain Bohic[7], Piera Valenti[3], Luigi Rosa[3], Lorenzo Massimi[5], Francesca Berlutti[7] and Stefano Lagomarsino[5].

[1]Dept. of Physics, Univ. of Cosenza, Arcavata di Rende, (Cosenza), Italy
[2]Dept. of Pharmacy and biotechnology, Univ. Bologna, Bologna, Italy
[3]Dept. of Public Health and Infectious Diseases, Univ. Sapienza, Roma, Italy
[4]Institute for Photonics and Nanotechnologies - CNR, Roma Italy
[5]CNR-Nanotec, c/o Dept. of Physics Univ. Sapienza, Roma, Italy
[6]Fondazione Santa Lucia, Roma, Italy
[7]ESRF, Grenoble, France
chiara.gramaccioni@gmail.com

Iron is a primary component of fundamental processes which can become toxic when present in excess. In human fluids, free iron is maintained at 10-18M concentration thanks to several proteins as lactoferrin (Lf) in secretions and transferrin in blood. The altered iron balance favors bacterial infection and the related inflammatory response as occurs in cystic fibrosis [1, 2]. Therefore, it is of great importance to provide quantitative mapping of iron concentration at high spatial resolution. Here we studied human phagocytic cells unstimulated or stimulated with bacterial lipopolysaccharide (LPS) or/and Lf to map the intracellular density and iron concentration. For this aim, X-ray fluorescence microscopy (XRFM), atomic force microscopy (AFM) and phase contrast imaging were combined, as previously demonstrated [3, 4]. To determine the concentration map, we normalized the fluorescence intensity with the volume of the illuminated region Fig.1. The volume of freeze-dried cells has been obtained by AFM with lateral resolution of 100 nm. The XRFM and phase contrast measurements have been carried out at the beamline ID16A-NI at ESRF, with spatial resolution of 100 nm and 50 nm, respectively. Moreover, we determined the weight fraction distribution map, normalizing the fluorescence intensity with the projected density obtained by phase contrast imaging Fig.2 [5]. Indeed, we obtained the density distribution Fig.3 by normalizing phase reconstruction maps with AFM data. Similar evaluations were carried out for Lf- and LPS plus Lf-treated cells. We also carried out nanotomography measurements, to obtain the three-dimensional density distribution Fig.4. Information about the electron density combined with the average density of the sample allows to calculate its thickness, value which can be compared with alternative techniques AFM. The nanotomography is of paramount importance to reach the volumetric information in frozen-hydrated cells because AFM cannot be used since frozen hydrated cells are stored in liquid nitrogen.

1. R. Paesano et al. Pathogens and Global Health 2012, 106, 200.

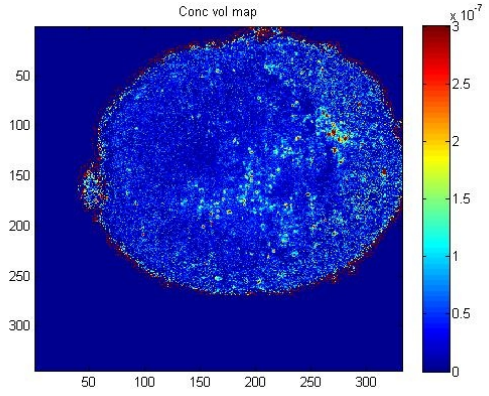

Figure 1. Iron concentration map of cell treated with LPS.

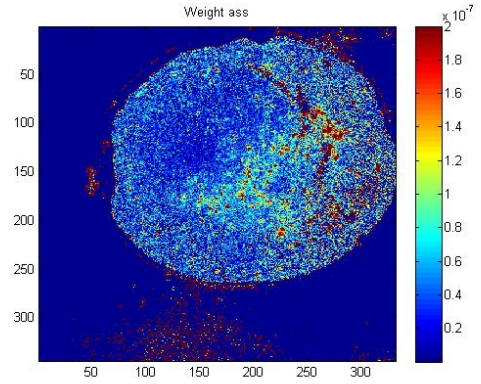

Figure 2. Iron Weight fraction distribution map of cell treated with LPS.

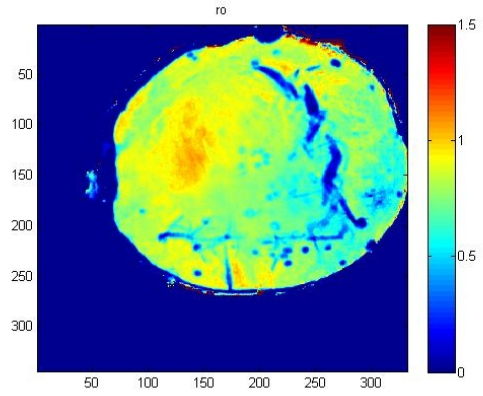

Figure 3. Density distribution map of cell treated with LPS**.**

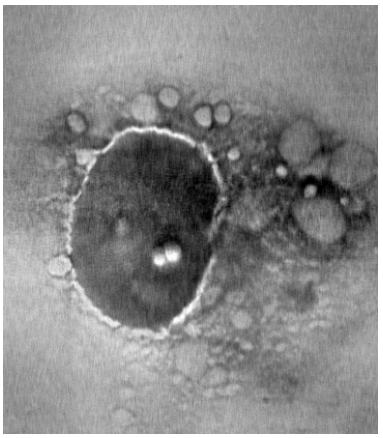

Figure 4. Electron density map of cell treated with LPS + Lf**.**

2. P. Valenti et al., Lactoferrin and cystic fibrosis airway infection. In: Diet and Exercise in Cystic Fibrosis. 2015, 30, 259.

3. S. Lagomarsino et al., *Spectrochim. Acta B* 2011 66, pp767-866 .

4. E. Malucelli et al., *Anal. Chem.*, 2014, 86 , pp 5108–5115.

5. E. Kosior et al., *J. Struct. Biol.* 2012 177(2):239-47.

The research was granted by Sapienza University of Rome to PV and FB and by Cystic Fibrosis Foundation (Italy) (FFC#16/2014 and FFC#12/2015) to FB.

C13

TOWARDS DOSE EFFICIENT IN-VIVO X-RAY MICROSCOPY OF BIOLOGICAL SYSTEMS USING BRAGG MAGNIFIER MICROSCOPE

S. Hrivňak[1], L. Mikeš[4], M. Franko[1], J.Uličný[1], L. Švéda[5], A.Cecilia[6], E. Hamann[6], E. N. Gimenez[7], Z. Zápražný[8], D. Korytár[8], U. Wagner[7], and T. Baumbach[6], P. Vagovič[2,3]

[1]Department of Biophysics, Faculty of Science, P. J. Šafárik University, Jesenná 5, 04154 Košice, Slovakia
[2]Center for Free-Electron Laser Science, DESY, Notkestrasse 85, 22607 Hamburg, Germany
[3]European XFEL, Albert Einstein Ring 19, 22761 Hamburg, Germany
[4]Department of Computer Science, Faculty of Science, P. J. Šafárik University, Jesenná 5, 04154 Košice Slovakia
[5]FNSPE CTU, B□ehová 7, 115 19 Prague 1, Czech Republic
[6]ANKA Light Source, Karlsruhe Institute of Technology, Hermann-von-Helmholtz-Platz 1 D-76344 Eggenstein-Leopoldshafen, Germany
[7]Diamond Light Source, Harwell Science and Innovation Campus, Fermi Ave, Didcot OX11 0QX, UK
[8]Institute for Electrical Engineering, Slovak Academy of Sciences, Dúbravská cesta 9, 841 04 Bratislava, Slovakia
stanislav.hrivnak@student.upjs.sk

In this work we present the actual status of the development of Bragg Magnifier Microscope based on in-line Germanium crystals [1, 2] with the focus on the improved phase retrieval algorithm. This imaging system is using asymmetric Bragg reflections to geometrically magnify X-ray beam up to 250 times and the beam is directly detected by single photon counting detector. We performed successful testing of this imaging system at Diamond Light Source I13 and B16 and at Spring 8 radiation facilities and applied it for full field, single distance, holographic imaging of biological samples. The improved phase retrieval algorithm [3] takes advantage from the combination of the modified shrink-wrap algorithm for phase objects, robust unwrapping algorithm as well as other reasonable constraints applied to the wavefield at the object and the detector plane. The spatial resolution, achieved after successful phase retrieval of recorded holograms (Fig. 1), was ~300 nm and the acquisition time for one frame at ID13 was 0.3s, which can be still minimized to millisecond region. In diffraction limited sources the throughput of the device will be maximized due to matching divergences, which will bring additional exposure time decrease. According to achieved state of the development: high resolution, short acquisition time, single distance phase retrieval, we propose this system for in-vivo 2D/3D quantitative imaging of biological samples such as cells or small animals. In this work we will summarize recent state of the development, introduce single distance phase retrieval method and demonstrate it on successful 3D reconstruction of biological organism (Tardigrade).

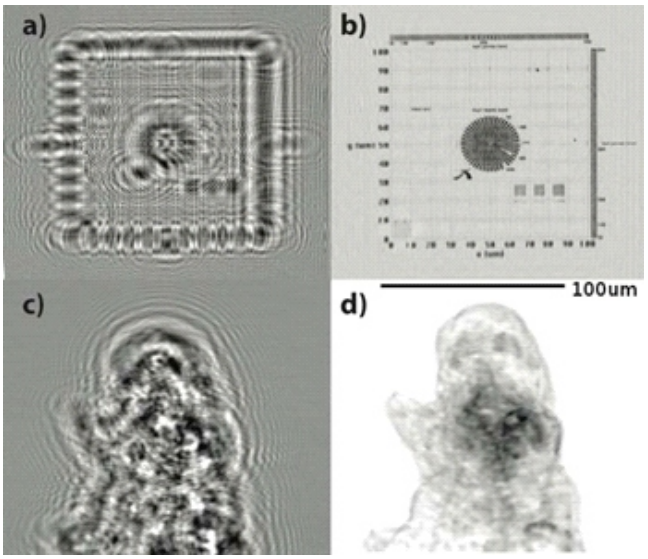

Figure 1. Measured holograms of X-radia X-50-30-20 test pattern a) and Tardigrade (water bear) c) and the corresponding retrieved phase maps b), d) recovered by single distance phase retrieval algorithm [3]. Spatial resolution achieved was about 300 nm.

1. P. Vagovič, D. Korytár, A. Cecilia, E. Hamann, L. Švéda, D. Pelliccia, J. Härtwig, Z. Zápražný, P. Oberta, I. Dolbnya, K. Shawney, U. Fleschig, M. Fiederle, T. Baumbach, *J. Synchrotron Radiat.*, **20**, (2013), 153–159.
2. P. Vagovič, L. Švéda, A. Cecilia, E. Hamann, D. Pelliccia, E. N. Gimenez, D. Korytár, K. M. Pavlov, Z. Zápražný, M. Zuber, T. Koenig, M. Olbinado, W. Yashiro, A. Momose, M. Fiederle, T. Baumbach, *Opt. Express* **22**, (2014), 21508–21520.
3. S. Hrivňak et. al., in preparation.

This work was supported by projects KVARK ITMS-26110230084 and VVGS-PF-2015-470.

Session V

Tuesday, September 6 - afternoon

I5

OPERANDO HIGH ENERGY SURFACE SENSITIVE X-RAY DIFFRACTION

Andreas Stierle

DESY NanoLab and University of Hamburg, Physics Department, Germany
Andreas.Stierle@desy.de

The atomic structure determination of surfaces and nano-objects under operando conditions is an important step towards tailoring their properties for applications in the field of heterogeneous catalysis or corrosion science. Recently significant progress towards faster surface sensitive x-ray characterization has been made by the use of higher energy x-rays in the 70 keV - 90 keV range [1,2].

I will discuss in my presentation the principles of surface sensitive high energy x-ray diffraction and I will elucidate in several examples why it is beneficial for operando studies: during ambient pressure CO oxidation over a Pd(100) single crystal the full 3D surface structure of the catalytically active phase could be determined in data recording times below 10 minutes [2,4]. The shape dependent sintering of Pt-Rh nanoparticles during CO oxidation can be monitored by instantaneous reciprocal space mapping [1]. A combinatorial sample design in combination with grazing incidence high energy x-ray diffraction allowed to identify a composition dependent oxidation mechanism for Pd-Rh nanoparticles on $MgAl_2O_4(100)$. With the advent of diffraction limited synchrotron light sources in the near future, improved nanofocussing of high energy x-ray beams will enable single nano object studies under operational conditions.

1. U. Hejral, P. Müller, O. Balmes, D. Pontoni, A. Stierle, *Nature Communications* **7**, 10964 (2016).
2. J. Gustafson, M. Shipilin, C. Zhang, A. Stierle, U. Hejral, U. Ruett, O. Gutowski, P.-A. Carlsson, M. Skoglundh, E. Lundgren, *Science* **343** (6172) 758-61 (2014).
3. P. Müller, U. Hejral, U. Rütt and A. Stierle, *Phys. Chem. Chem. Phys.* **16**, 13866 (2014).
4. M. Shipilin, U. Hejral, E. Lundgren, L.R. Merte, C. Zhang, A. Stierle, U. Rütt, O. Gutowski, M. Skoglundh, P.-A. Carlsson, J. Gustafson, *Surf.Sci.* **630**, 229 (2014).

C14

IN OPERANDO X-RAY CHARACTERIZATION OF NANOWIRE DEVICES

J. Wallentin[1,2]*, M. Osterhoff[1], and T. Salditt[1]

[1]Institute for X-Ray Physics, University of Göttingen, GERMANY
[2]Synchrotron Radiation Research, Lund University, SWEDEN
jesper.wallentin@sljus.lu.se

To characterize strain in nanodevices it is important to measure complete devices, since the strain is affected by deposited metal and oxide films. In addition to these static effects, semiconductor devices in operation are exposed to high electric fields and temperatures. We demonstrate how in operando hard X-ray diffraction using a nanofocused beam can quantitatively measure both strain and bending in a nanowire device under electric bias, and how nanowires can be used as X-ray detectors.

Nanowire transistors were mounted in a special sample holder which allows simultaneous X-ray and electrical measurements, and characterized with nanofocused X-rays at the ESRF and PETRA-III synchrotrons. Scanning X-ray Bragg diffraction was performed with 100 nm real-space resolution along the nanowire axis, also behind the metal contacts. The 3D shape of the nanowire was reconstructed from the XRD data.

In the as-processed device, the strain was small but the nanowire was bent in an arch between the contacts. The device was then exposed to increasing bias voltages until breakdown, while simultaneously measuring the electrical current and performing scanning X-ray Bragg diffraction at each bias. We observed small and non-reversible bending at 2V bias. At higher bias voltages the arch gradually disappeared while the lattice constant changed in the contact regions. The structural changes were correlated with a reduction in electrical conductance [1].

Measurements with another nanowire device show that carriers generated by X-ray absorption increased the electrical conductance by five orders of magnitude. By 2D scanning the device, and measuring the current at constant electrical bias for each point, we created an image of the X-ray nanofocus with submicron resolution [2].

1. J. Wallentin, M. Osterhoff, and T. Salditt, “In operando X-ray diffraction reveals electrically induced strain and

bending in single nanowire device" *Adv. Mater.* **28** (9), 1788 (2016) http://dx.doi.org/10.1002/adma.201504188

2. J. Wallentin, M. Osterhoff, R. N. Wilke, K.-M. Persson, L.-E. Wernersson, M. Sprung, and T. Salditt, "Hard X-ray detection using a single 100 nm-diameter nanowire" *Nano Lett.* **14** (12), 7071 (2014) http://dx.doi.org/10.1021/nl5040545.

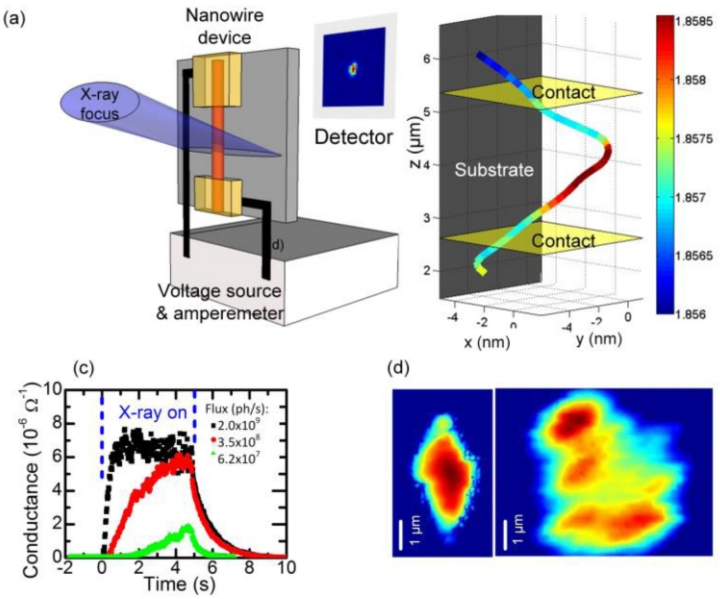

Figure 1. (a) Experimental setup, (b) 3D model of nanowire in the device [1], (c) Conductance of a nanowire device as function of time, for three different X-ray fluxes [2], (d) Imaging of a focused X-ray beam using the nanowire device, at (left) and 24 mm (right) after the nanofocus.

C15

GROWING SELF-CATALYSED GaAs NANOWIRES PROBED BY TIME-RESOLVED IN-SITU HIGH-RESOLUTION X-RAY DIFFRACTION

Philipp Schroth[1,2,3], Julian Jakob[2,3], Martin Köhl[3], Ludwig Feigl[3], Seyed Mohammad Mostafavi Kashani[1], Jonas Vogel[1], Arman Davtyan[1], Jörg Strempfer[4], Tilo Baumbach[2,3] and Ullrich Pietsch[1]

[1]*Universität Siegen, Siegen, Germany*
[2]*Laboratory for Application of Synchrotron Radiation (LAS), Faculty of Physics, Karlsruhe Institute of Technology*
[3]*Institute for Photon Science and Synchrotron Radiation (IPS), Karlsruhe Institute of Technology (KIT), Karlsruhe, Germany*
[4]*Deutsches Elektronen Synchrotron (DESY), Hamburg, Germany*

Time-resolved X-ray measurements can provide valuable insight in the dynamics of the growth of semiconductor nanostructures as e.g. GaAs nanowires, in particular in the evolution of their crystallographic properties and their shape. Here, we report on the growth of self-catalysed GaAs nanowires onto Silicon (111) substrates using the portable molecular beam epitaxy setup of LAS/IPS [1] at KIT. These nanowires are grown by the vapor-liquid-solid mode using a liquid Ga-droplet as catalyst. We probe the crystallographic properties and the shape of the growing nanowires *in-situ* by means of time-resolved high-resolution X-ray diffraction.

The X-ray experiments have been performed at the P09 beamline of PETRA III at DESY, where the (311) and (220) zinc-blende and (10.3) wurtzite Bragg reflections have been monitored during growth.

We gain insight in the evolution of polytypism in self-catalyzed GaAs nanowires during growth. Further, we obtain information on radial growth processes of wurtzite and zinc-blende segments in the growing GaAs nanowires. In particular, we separate radial facet growth processes from tapering caused by an inflation of the liquid Ga droplet and compare the findings with ex-situ SEM and theoretical growth models.

We are grateful for Thomas Keller and Andreas Stierle at the Nanolab@DESY, David Reuther at P09, Hans Gräfe, Bärbel Krause and Annette Weißhardt at the UHV-laboratory@ANKA, KIT. The project was supported by German BMBF (05ES7CK and 05K13PS3).

1. T. Slobodskyy, et al., *Rev. Sci. Instrum.* **83**, 105112 (2012).

C16

SYNCHROTRON X-RAY BRAGG DIFFRACTION IMAGING TECHNIQUES TO CHARACTERISE ICE DISTORTION UNDER LOADING

A. Philip[1], R. T. Kluender[2], L. Capolo[1]*, J. Meyssonnier[1], J. Baruchel[2]

[1]LGGE, UGA-CNRS, Grenoble, France; [2]ESRF, Grenoble, France
** now at Grenoble Université Presses*

The way ice distorts under an external force is an important topic for both mechanics (because ice is an example of very anisotropic solids [1]), and environmental science. Indeed strain and orientation heterogeneities occur in each of the crystallites of polycrystalline ice when submitted to applied stresses. These intra-granular inhomogeneities, as well as the interactions of dislocations with grain boundaries [2], play an important role in processes like yielding, creep, recrystallisation or fracture. We investigated, at the ESRF beamline BM05, a high crystalline quality tricrystal of ice (initial dislocation density less than 100 cm/cm^3), which constitutes the simplest model for a polycrystal. This tricrystal was submitted, within a specially designed cold cell, to several steps of compression.

A first, qualitative, approach, was carried out by using white beam diffraction topography, which allows following the movement and multiplication of the dislocations at the inception of the deformation. Their velocity was found to be in the 0.5 - 1 ms^{-1} range at -10 °C under a compression stress of 0.3 MPa, in agreement with the order of magnitude of the mobility of dislocations in ice found in the literature [3]. The dislocation density increases during loading, and stress concentrations occur at the level of grainb boundaries: they appear as areas of increased diffracted intensity ('black', with the usual convention) on the

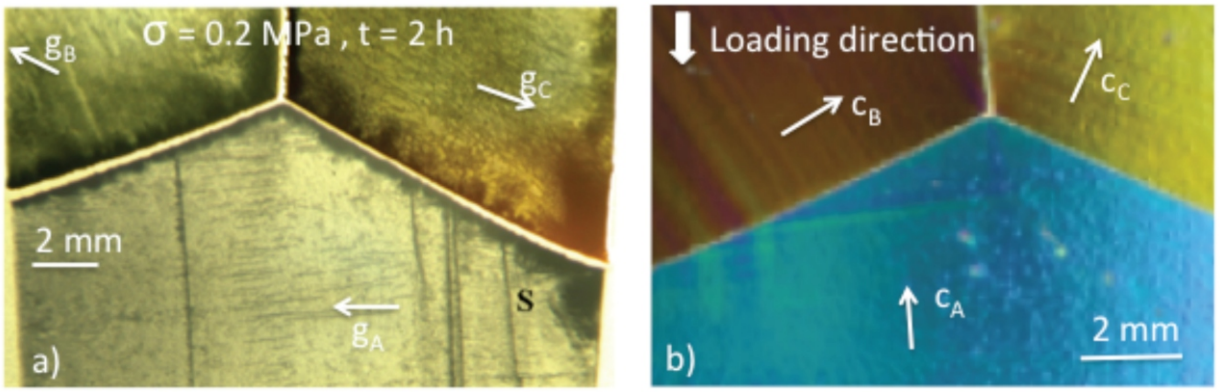

Figure 1. a) Bragg diffraction composite image (the reflection used is different for the different grains, but the images are simultaneous) of the deformation of an ice tri-crystal under a compression of 0.2 MPa. b) Photo taken with polarised light. The projection of the c-axis of each grain on the plane is indicated by the arrows. The c-axes are perpendicular to the basal slip lines.

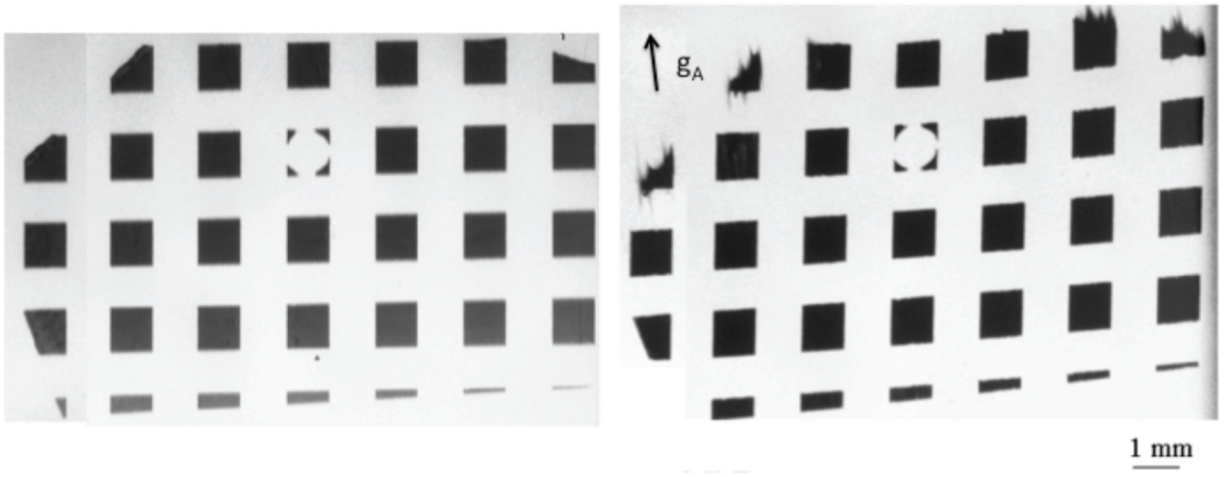

Figure 2. Example of the measurement of the curvature field map (which is directly related to the geometrically necessary dislocation density map) through the use of "reticulography": a tungsten grid located in front of the crystal lead to a number of spatially independent Bragg spots (in this case corresponding to the (1-100) reflecting planes), allowing measuring the variation of position/orientation of the areas imaged on these spots in the deformed state with respect to the position in the initial (non-deformed) one.

composite topograph shown on Fig. 1a. At the beginning of loading, the black regions appear to be related to the internal elastic strain since they disappear when the external load is removed. However, after the specimen has been loaded for some time then unloaded, the topographs still exhibit black areas at the grain boundaries, suggesting that this distortion is related to the dislocations piling up at the level of the grains, as already observed in the Fe-Si bicrystal case [4]. The orientation of the grains (fig1b) determines their degree of strain compatibility: if the two grains have a-axes in the same direction, they behave as "strain-compatible", because the Burgers vectors of the basal dislocations in both grains are parallel to each other. We observe distortions associated with the energy stored by the dislocation piling up, which are stronger for grains where the dislocation Burgers vectors are not compatible than for those where they are.

More quantitative results were obtained by using 3D-RCI [5], which combines rocking curve imaging with section and pinhole topography, in order to measure lattice distortions in all three spatial dimensions. This 3D-RCI method allowed quantifying the lattice orientations with a spatial voxel of about 50 × 50 × 50 m^3, and an angular resolution is in the few radians range. 3D-RCI is a sophisticated and powerful technique, but, as it rests on the assumption that an elementary volume in the crystal always diffract on a given pixel of the detector (size p), it can only be applied when the local mosaic spread of this elementary volume is such that < p / (2D sin), where D is the sample-to-detector distance. This leads, with our usual experimental conditions, to a limit 1 mrad) which remains low with respect to the distortions that are important to investigate.

Another technique, "reticulography" [6], allows characterising distortions induced under higher or longer compressions. It implies locating an absorbing grid in front of the sample, to split the beam into a series of sub-beams. Each diffraction spot is thus split into sub-regions. By pointing the grid nodes on the topographic image obtained by using various reflecting lattice planes (at least two), it is possible to obtain the components of the diffraction vectors, and consequently the crystallographic orientation at each node. An example of application of reticulography is presented on Figure 2.

These two techniques (3D-RCI for the lower statesof distortion, and reticulography) were used to measure the crystalline orientation in a whole grain volume. From these experimental results we have calculated the gradient of lattice rotation, and estimated the curvature tensor field in the grain. This later tensor allows reaching the density of "geometrically necessary dislocations"[7], which is directly related to the viscoplastic deformation of the crystalline material. To our knowledge no experimental results as these ones have been published up to now. These results are very promising, but have to be improved both for RCI (where an enhanced stability is required) and reticulography (where the grid size must be reduced), if we wish acquiring measurements of the strong strain gradients that occur in ice, which are actually useful for the mechanical simulations that are developing nowadays.

1. V. F. Petrenko, R. W. Whitworth, "Physics of Ice', Oxford University Press, 1999.
2. D.A. Smith, http://dx.doi.org/10.1051/jphyscol:1982621.
3. Y. Okada, T. Hondoh, S. Mae, *Phil. Mag. A,* **79**, (1996), 2853.
4. M. Polcarová, J. Gemperlová, A. Jacques, J. Brádler, A. George*, J. Phys. D: Appl. Phys.* **39**, (2006), 4440.
5. R.T. Kluender, A. Philip, J. Meyssonier, J. Baruchel, *Phys. Status Solidi* **208**, (2011), 2505.
6. A.R. Lang, A.P.W. Makepiece, *J. Synchrotron Rad*. **3**, (1996), 313.
7. M. F. Ashby, *Phil. Mag.* **13**, (1970), 399.

C17

HIGH-ENERGY LOW-DOSE MAMMOGRAPHY USING EDGE ILLUMINATION X-RAY PHASE-CONTRAST IMAGING

P. C. Diemoz[1], A. Bravin[2], A. Sztrókay-Gaul[3], M. Ruat[2], S. Grandl[3], D. Mayr[4], A. Mittone[2,5], M. F. Reiser[3], P. Coan[3,5], A. Olivo[1]

[1]Department of Medical Physics and Biomedical Engineering, UCL, London WC1E 6BT, UK
[2]European Synchrotron Radiation Facility, 38043 Grenoble, France
[3]Institute for Clinical Radiology, Ludwig-Maximilians University, 81377 Munich, Germany
[4]Institute for Pathology, Ludwig-Maximilians University, 80337 Munich, Germany
[5]Department of Physics, Ludwig-Maximilians University, 85748 Garching, Germany
p.diemoz@ucl.ac.uk

Edge illumination (EI) is an X-ray phase-contrast imaging (XPCI) technique that has been under intensive development at University College London (UK) in recent years. Besides being applicable at synchrotron radiation facilities [1], EI was also demonstrated to be compatible with table-top setups based on non-microfocal X-ray tubes [2]. In fact, EI is insensitive to both beam polychromaticity and relatively large source sizes (up to at least 100 μm). This directly follows from the incoherent nature of the method, which in fact can be described accurately through simple geometrical optics.

The goal of this study was to demonstrate that EI, when used at X-ray energies much larger than those employed in clinical practice, enables the achievement of very low

doses in mammography. Since the first days of XPCI, mammography has been considered as one of the most important candidates for a clinical application [3]. In fact, the imaging of breast can greatly benefit from soft tissue contrast improvements and/or from radiation dose reductions provided by XPCI.

In order to achieve this aim, a proof-of-principle experiment was performed at the European Synchrotron Radiation Facility (ESRF, France), on excised human breast specimens. A photon-counting detector achieving almost 100% efficiency at high X-ray energies was used in order to minimize the image noise. Moreover, a new retrieval algorithm capable of extracting the phase shift from a single EI image was exploited to process the acquired images [4]. This method presents the twofold advantage of being stable with respect to noise (thus allowing further dose reductions) [5] and of needing only one input image, thus significantly simplifying and speeding up the acquisition. Importantly, although this proof-of-principle study was carried out with synchrotron radiation, the method has potential for an application in table-top setups, which represents an essential requirement for any future clinical implementation.

In this talk, we will first introduce the EI technique and its main features. We will then present the recently developed single-image retrieval algorithm and the pilot experiment carried out at the ESRF, and suggest ways to exploit these results for potential future clinical applications.

1. A. Olivo, et al., *Med. Phys.*, **28**, (2001), 1610.
2. A Olivo, R. D. Speller, *Appl. Phys. Lett.*, **91**, (2007), 074106.
3. V. N. Ingal, E. A. Beliaevskaya, A. P. Brianskaya, R. D. Merkurieva, *Phys. Med. Biol.*, **43**, (1998), 2555.
4. P. C. Diemoz, F. A. Vittoria, C. K. Hagen, M. Endrizzi, P. Coan, E. Brun, U. H. Wagner, C. Rau, I. K. Robinson, A. Bravin, A. Olivo, *J. Synchrotron Radiat.*, **22**, (2015), 1072.
5. P. C. Diemoz, F. A. Vittoria, C. K. Hagen, M. Endrizzi, P. Coan, A. Bravin, U. H. Wagner, C. Rau, I. K. Robinson, A. Olivo, *submitted*.

Session VI

Tuesday, September 6 - afternoon

I6

SYNCHROTRON-BASED X-RAY STRUCTURAL ANALYSIS OF FUNCTIONAL MATERIALS TOWARDS CATALYTIC STRUCTURE-ACTIVITY RELATIONSHIPS

J. P. Hofmann

Laboratory of Inorganic Materials Chemistry, Department of Chemical Engineering and Chemistry, Eindhoven University of Technology, P.O. Box 513, 5600MB Eindhoven, The Netherlands
j.p.hofmann@tue.nl

Heterogeneous catalysis plays a significant role in chemical industry. To arrive at a knowledge-based catalyst design, fundamental insight into relations between structure and catalytic properties, such as activity, selectivity and stability, is needed. During this lecture, examples from recent work at ESRF beamlines ID01 and ID03 will be discussed. Three showcase applications from the field of heterogeneous model catalysis will be highlighted.

1) Zeolites are commonly used as solid acid catalysts in many large scale industrial processes, such as the Methanol-to-Hydrocarbons process. Zeolite H-ZSM-5 is a well-known candidate and has been studied extensively because of its intriguing 3D intergrowth structure. We have applied micro-focused X-ray diffraction imaging at higher order Bragg reflections to unravel the intergrowth pattern of individual large H-ZSM-5 crystals [1]. Additionally, information about aluminium zoning, which sensitively impacts on catalytic properties, could be obtained based on subtle changes of the lattice constants. Recently, we extended the μXRD approach by coupling optical detection of X-ray excited optical fluorescence (XEOF) of labelled H-ZSM-5 crystals [2]. Recording XEOF of styrene oligomers as a Brřnsted acid site specific label together with μXRD response led to the simultaneous characterization of local crystallinity and the presence and nature of catalytically active sites.

2) *Operando* surface X-ray scattering experiments under electrochemical conditions have been carried out to arrive at catalytic structure-activity relationships for single crystal (here Pt(111)) model electrodes [3]. In this experiment, SXRD, XRR and GISAXS have been applied together with On-Line-Electrochemical Mass Spectrometry (OLEMS) to study the influence of surface structural changes on activity of the model electrode in hydrogen and oxygen evolution reactions. OLEMS adds chemical specificity to electrochemically measured currents and plays to its strength when reactions with a selectivity dimension are studied.

3) Most recently, nanocrystal model catalysts have been introduced for *in-situ* studies of individual nanoparticle catalysis. Real space structure and strain distribution is studied by Coherent X-ray Diffraction Imaging (CXDI). *In-situ* cells for both heterogeneous gas phase catalysis and electrocatalysis have been constructed and successfully applied; showcases from both field will be highlighted.

doses in mammography. Since the first days of XPCI, mammography has been considered as one of the most important candidates for a clinical application [3]. In fact, the imaging of breast can greatly benefit from soft tissue contrast improvements and/or from radiation dose reductions provided by XPCI.

In order to achieve this aim, a proof-of-principle experiment was performed at the European Synchrotron Radiation Facility (ESRF, France), on excised human breast specimens. A photon-counting detector achieving almost 100% efficiency at high X-ray energies was used in order to minimize the image noise. Moreover, a new retrieval algorithm capable of extracting the phase shift from a single EI image was exploited to process the acquired images [4]. This method presents the twofold advantage of being stable with respect to noise (thus allowing further dose reductions) [5] and of needing only one input image, thus significantly simplifying and speeding up the acquisition. Importantly, although this proof-of-principle study was carried out with synchrotron radiation, the method has potential for an application in table-top setups, which represents an essential requirement for any future clinical implementation.

In this talk, we will first introduce the EI technique and its main features. We will then present the recently developed single-image retrieval algorithm and the pilot experiment carried out at the ESRF, and suggest ways to exploit these results for potential future clinical applications.

1. A. Olivo, et al., *Med. Phys.*, **28**, (2001), 1610.
2. A Olivo, R. D. Speller, *Appl. Phys. Lett.*, **91**, (2007), 074106.
3. V. N. Ingal, E. A. Beliaevskaya, A. P. Brianskaya, R. D. Merkurieva, *Phys. Med. Biol.*, **43**, (1998), 2555.
4. P. C. Diemoz, F. A. Vittoria, C. K. Hagen, M. Endrizzi, P. Coan, E. Brun, U. H. Wagner, C. Rau, I. K. Robinson, A. Bravin, A. Olivo, *J. Synchrotron Radiat.*, **22**, (2015), 1072.
5. P. C. Diemoz, F. A. Vittoria, C. K. Hagen, M. Endrizzi, P. Coan, A. Bravin, U. H. Wagner, C. Rau, I. K. Robinson, A. Olivo, *submitted*.

Session VI

Tuesday, September 6 - afternoon

I6

SYNCHROTRON-BASED X-RAY STRUCTURAL ANALYSIS OF FUNCTIONAL MATERIALS TOWARDS CATALYTIC STRUCTURE-ACTIVITY RELATIONSHIPS

J. P. Hofmann

Laboratory of Inorganic Materials Chemistry, Department of Chemical Engineering and Chemistry, Eindhoven University of Technology, P.O. Box 513, 5600MB Eindhoven, The Netherlands
j.p.hofmann@tue.nl

Heterogeneous catalysis plays a significant role in chemical industry. To arrive at a knowledge-based catalyst design, fundamental insight into relations between structure and catalytic properties, such as activity, selectivity and stability, is needed. During this lecture, examples from recent work at ESRF beamlines ID01 and ID03 will be discussed. Three showcase applications from the field of heterogeneous model catalysis will be highlighted.

1) Zeolites are commonly used as solid acid catalysts in many large scale industrial processes, such as the Methanol-to-Hydrocarbons process. Zeolite H-ZSM-5 is a well-known candidate and has been studied extensively because of its intriguing 3D intergrowth structure. We have applied micro-focused X-ray diffraction imaging at higher order Bragg reflections to unravel the intergrowth pattern of individual large H-ZSM-5 crystals [1]. Additionally, information about aluminium zoning, which sensitively impacts on catalytic properties, could be obtained based on subtle changes of the lattice constants. Recently, we extended the μXRD approach by coupling optical detection of X-ray excited optical fluorescence (XEOF) of labelled H-ZSM-5 crystals [2]. Recording XEOF of styrene oligomers as a Brřnsted acid site specific label together with μXRD response led to the simultaneous characterization of local crystallinity and the presence and nature of catalytically active sites.

2) *Operando* surface X-ray scattering experiments under electrochemical conditions have been carried out to arrive at catalytic structure-activity relationships for single crystal (here Pt(111)) model electrodes [3]. In this experiment, SXRD, XRR and GISAXS have been applied together with On-Line-Electrochemical Mass Spectrometry (OLEMS) to study the influence of surface structural changes on activity of the model electrode in hydrogen and oxygen evolution reactions. OLEMS adds chemical specificity to electrochemically measured currents and plays to its strength when reactions with a selectivity dimension are studied.

3) Most recently, nanocrystal model catalysts have been introduced for *in-situ* studies of individual nanoparticle catalysis. Real space structure and strain distribution is studied by Coherent X-ray Diffraction Imaging (CXDI). *In-situ* cells for both heterogeneous gas phase catalysis and electrocatalysis have been constructed and successfully applied; showcases from both field will be highlighted.

1. Z. Ristanovic, J. P. Hofmann, U. Deka, T. U. Schülli, M. Rohnke, A. M. Beale, B. M. Weckhuysen, *Angew. Chem. Int. Ed.* **52**, (2013), 13382.

2. Z. Ristanovic, J. P. Hofmann, M.-I. Richard, T. Jiang, G. A. Chahine, T. U. Schülli, F. Meirer, B. M. Weckhuysen, *Angew. Chem. Int. Ed.*, (2016) in press.

3. A. Goryachev, A. H. Wonders, F. Carlŕ, J. Drnec, R. Felici, P. P. T. Krause, E. J. M. Hensen, J. P. Hofmann, ChemistrySelect, (2016), in press, DOI: 10.1002/slct.201600355.

C18

TRANSMISSION SURFACE DIFFRACTION: A NEW TOOL FOR IN-SITU AND OPERANDO SURFACE SCIENCE

F. Reikowski[1], T. Wiegmann[1], J. Stettner[2], J. Drnec[2], V. Honkimäki[2], F. Maroun[3], O. M. Magnussen[1]

[1]*Institute of Experimental and Applied Physics, Kiel University, Kiel 24098, Germany*
[2]*Experimental division, ESRF, 71 Avenue des Martyrs, 38000 Grenoble, France*
[3]*Physique de la Matière Condensée, Ecole Polytechnique, CNRS, 91128 Palaiseau, France*
drnec@esrf.fr

A new surface diffraction method for in situ studies of buried interfaces which employs synchrotron X-ray radiation of high photon energy is presented. In contrast to the standard geometry with grazing incidence angles [1], in this technique a transmission geometry where the X-ray beam passes through the sample is used (Fig. 1). Transmission surface diffraction (TSD) is a powerful and user-friendly method that enables fast simultaneous imaging of the full in-plane structure of solid surfaces. Furthermore, it allows surface X-ray diffraction studies with micrometer spatial resolution, opening up the way to map the atomic interface structure of spatially inhomogeneous systems or to study the surface properties of small samples. The feasibility of this approach is demonstrated by TSD measurements of Co and Bi electrodeposition on Au(111) electrodes [2], performed at beamline ID 31 of the ESRF. The formation of the crystal truncation rods (CTRs), changes in the Au CTRs due to epitaxial strain, and the disappearance of the rods corresponding to the (22 x 3) phase of the Au surface reconstruction can be directly observed without lengthy searches in reciprocal space. In addition, in situ microscale mapping of the deposit and substrate properties and studies during Co dissolution are discussed.

1. J. Gustafson, M. Shipilin, C. Zhang, A. Stierle, U. Hejral, U. Ruett, O. Gutowski, P.-A. Carlsson, M. Skoglundh, E. Lundgren, Science 343, 758 (2014).

2. F. Reikowski, F. Maroun, N. Di, P. Allongue, M. Ruge, J. Stettner, O. M. Magnussen, Electrochimica Acta 197, 273 (2016).

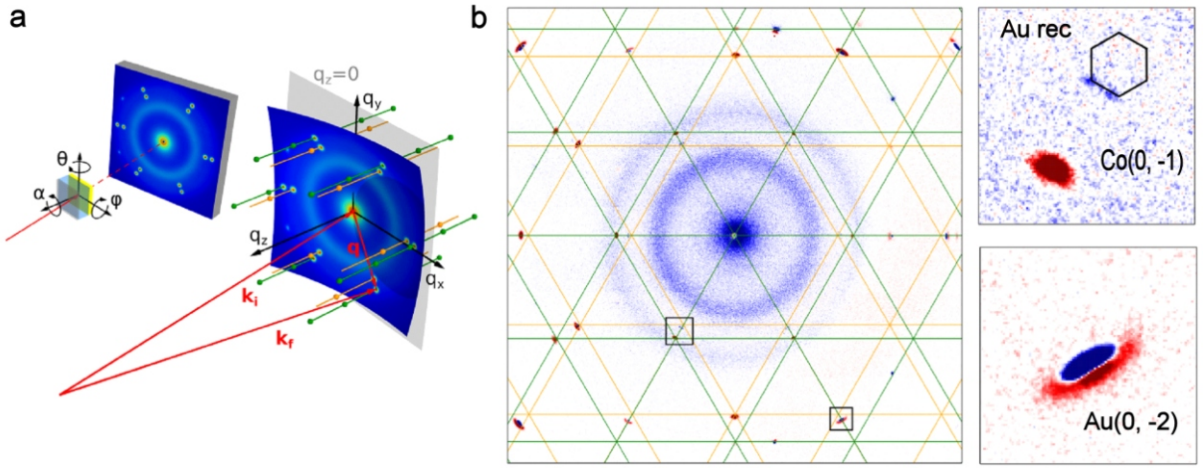

Figure 1. (a) Real space and reciprocal space geometry of TSD. (b) In situ TSD of Au(111) in 0.1 M $NaClO_4$ + 1.3 mM HCl + 1mM $CoCl_2$, recorded at 40 keV. Shown is the intensity difference between detector images of the Au sample at -0.2 $V_{Ag/AgCl}$ and after electrodeposition of a 20 ML thick epitaxial Co(001) film at -1.05 $V_{Ag/AgCl}$.

C19

INTERMIXING IN SINGLE Ge-Si CORE-SHELL NANOWIRES: A COHERENT X-RAY IMAGING STUDY

S. Fernández[1,2], M.-I. Richard[1,2], S. Labat[2] , P. Gentile[3], T. Schülli[2], O. Thomas[1]

[1]Aix-Marseille Université, CNRS, IM2NP UMR 7334, Campus de St-Jérôme, 13397 Marseille, France
[2]ESRF, The European Synchrotron, 71 Avenue des Martyrs, 38043 Grenoble Cedex, France
[3]CEA Grenoble/ INAC/PHELIQS, 17 Avenue des Martyrs, 38054, Grenoble

Characterising the structural properties (strain gradients, chemical composition, crystal orientation and defects) inside nanostructures is a grand challenge in materials science. In this context, the temperature evolution of the interface structure in a core-shell nanostructure is especially interesting to study. It raises fundamental questions about intermixing at the nanoscale where a strong interplay between strain and interfacial energies is expected to play an important role. Coherent diffraction imaging (CDI) in Bragg condition is a promising and attractive method to map the shape, the concentration and deformation fields simultaneously inside *single* nanostructures. It also permits *in situ* experiments owing to its non-destructive nature.

We demonstrate the capabilities of the CDI technique in Bragg condition on single Ge-Si core-shell nanowires (NWs) with a typical diameter of 300 nm and a length of 10 micrometers. NWs are grown by Vapor-Liquid-Solid (VLS) phase epitaxy and then isolated using a SEM/FIB instrument.

High resolution X-ray diffraction experiments have been performed at the ID01 beamline of ESRF (France). A Fresnel Zone Plate focused the beam on a 150 (V) × 400 (H) nm^2 spot. X-ray reciprocal space maps around four different Bragg reflections were recorded, evidencing a Ge core completely relaxed (*i.e.*, at its bulk lattice parameter). Also a lattice tilt in the growth direction of the NW was observed during the measurements. Then, an *in-situ* study as function of temperature was performed on the isolated wire, yielding changes in the recorded diffraction patterns. Phase retrieval analysis and reconstruction of the studied NW are in progress.

Session VII

Wednesday, September 7 - morning

I7

FOLLOWING MACROSCOPIC, MESOSCOPIC AND ATOMIC MOTIONS IN MULTI-DOMAIN CRYSTALS UNDER ALTERNATING ELECTRIC FIELD

S. Gorfman[1], H. Choe[1], N. Zhang[2], M. Ziolkowski[1], U. Pietsch[1]

[1] *Department of Physics, University of Siegen, Siegen, Germany*
[2] *Electronic Materials Research Laboratory, Xi'An Jiaotong University, Xi'An, China*
gorfman@physik.uni-siegen.de

Physical property is a response of a material to an external perturbation, as e.g. converse piezoelectricity accounts for mechanical deformation in response to an electric field. Being observable and applicable in devices on a macroscopic level, physical properties are underpinned by some deeper structural or / and microstructural motions. Importantly, many functional properties (e.g. giant piezoelectricity, super-elasticity and shape-memory effect) are attributed to the mesoscopic length scale, where external electric field or stress move domain walls and change the volume ratios between domains. Mesoscopic length scale and multi-domain structure plays pivotal role in ferroic (e.g. ferroelastic and ferroelectric) crystals, where domains naturally appear after a phase transition from higher- and lower-symmetry phases. Surprisingly, the tremendous potential of mesoscopically dominated properties in devices remains unexplored as long as simultaneous probing of macroscopic, mesoscopic and atomic dynamics in multi-domain crystals remains to be a serious challenge.

In this talk we explore the capabilities of the state-of-the-art high-resolution X-ray diffraction for combined in-situ probes of multi-domain processes in ferroics under alternating and quasi-static electric fields. We will focus on the recent insights to the functional ferroelectric and ferroelastic materials and show how high-resolution reciprocal space scans / 2D maps / 3D volumes can be measured simultaneously with e.g. macroscopic *P-E* hysteresis loops. We will discuss the separation of intrinsic response (displacement of atoms in a unit cell [1], changes of lattice parameters [2]) and extrinsic responses (field-induced domain-wall motion, volumetric exchange between domains) as well as their possible interconnection.

We will demonstrate and discuss *in-situ* X-ray diffraction data (the example is in the Figure 1) from uniaxial $Sr_{0.5}Ba_{0.5}Nb_2O_6$ ferroelectric, where only 180° (inversion) domains are present [2] and from the perovskite-based $PbZr_{1-x}Ti_xO_3$ and $Na_{0.5}Bi_{0.5}TiO_3$, where tetragonal, rhombohedral and monoclinic strain domains are present.

1. S. Gorfman, H. Simons, T. Iamsasri, S. Prasertpalichart, D.P. Cann, H. Choe, U. Pietsch, Y. Watier, J.L. Jones. *Scientific Reports* **6**, 20829, (2016).
2. S. Gorfman, H. Choe, V.V. Shvartsman, M. Ziolkowski, M. Knapp, M. Vogt, J. Strempfer, T. Łukasiewicz, U. Pietsch, *J. Dec. Physical Review Letters* **114**, 097601, (2015).

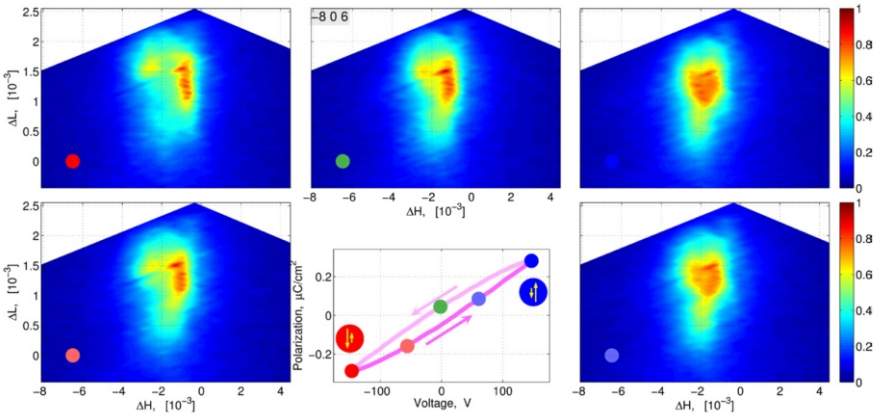

Figure 1. Reciprocal space maps around -8 0 6 Bragg reflections of uniaxial $Sr_{0.5}Ba_{0.5}Nb_2O_6$ ferroelectric, stroboscopically collected under alternating external electric field (P08 beamline at PETRA III). X-ray diffraction was measured simultaneously with the polarization-electric field hysteresis loop (bottom middle). The maps are composed of two Bragg peak components which are displaced against one another due to the opposite (positive / negative) piezoelectric responses in 180° / inversion ferroelectric domains.

C20

TWIN DOMAIN MAPPING IN TOPOLOGICAL INSULATOR Bi_2X_3 (X = Se,Te) BY SCANNING XRD AND ELECTRON BACKSCATTERING DIFFRACTIONG

D. Kriegner[1], P. Harcuba[1], A. Lesnik[2], G. Springholz[3], G. Bauer[3], V. Holy[1]

[1]Faculty of Mathematics and Physics, Charles University in Prague, Praha, Czech Republic
[2]Otto-von-Guericke Universität Magdeburg, FNW/IEP/AHE, Magdeburg, Germany
[3]Institute of Semiconductor and Solid State Physics, Johannes Kepler University Linz, Linz, Austria
dominik.kriegner@gmail.com

3D topological insulators are a new kind of matter with inverted bulk band gap and Dirac cone-like surface states [1]. Bi_2X_3 with X = Se and Te are prime members of this material class and were shown to exhibit the predicted topological properties [2]. For electrical devices made from these materials large area high quality thin films are required which, however, commonly show the formation of twin defects as can be seen in Fig.1a. Horizontal (c-plane) twin defects were shown to influence the electronic properties [3] whereas little is known about vertical twin defects. We have investigated the horizontal and vertical twin defect formation in molecular beam epitaxy grown Bi2Se3 and Bi_2Te_3 thin films by scanning X-ray diffraction (SXRD) [4] and electron backscatter diffraction (EBSD). With EBSD we directly obtain the crystal orientation in the vicinity of the surface as shown in Fig. 1b. Scanning X-ray diffraction probes the bulk of the thin films and thus complements the surface sensitive electron imaging techniques. For SXRD a focused X-ray beam (~150nm diameter) is used and with the samples mounted on piezo-scanners the XRD intensity is mapped in real space. Performing measurements at the asymmetric (10-1.20) Bragg peak the XRD intensity (Fig. 1c) therefore reveals that defects separating the two twin domains are not strictly vertical but that one twin domain might also overgrow another second one. Based on these results we are able to present a strategy to reduce the surface density of such defects which has important implications for the study of topological surface states.

1. H. Zhang, C.-X. Liu, X.-L. Qi, X. Dai, Z. Fang and S.-C. Zhang, Nature Physics 5, 438 - 442 (2009).
2. Y. L. Chen, J. G. Analytis, J.-H. Chu, Z. K. Liu, S.-K. Mo, X. L. Qi, H. J. Zhang, D. H. Lu, X. Dai, Z. Fang, S. C. Zhang, I. R. Fisher, Z. Hussain and Z.-X. Shen, Science 325, 178-181 (2009).
3. H. Aramberri, J. I. Cerdá, and M. C. Muńoz, Nano Lett., 15 3840–3844 (2015).
4. J. Stangl, C. Mocuta, A. Diaz, T. H. Metzger, and G. Bauer, ChemPhysChem 10, 2923-2930 (2009).

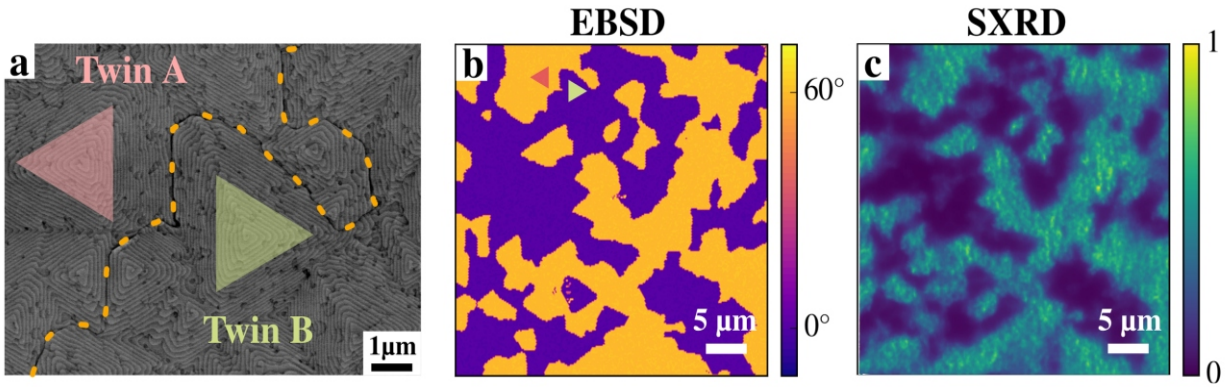

Figure 1. Twin formation in Bi_2Te_3 thin films. a) Scanning electron micrograph of a twin boundary (dashed line) separating two crystallographically twinned areas. b) Electron backscatter diffraction (EBSD) inplane orientation map showing the twin domains in a larger area. c) bulk sensitive scanning XRD measurement of the very same area shown in b), however, with bulk sensitivity.

C21

IN SITU NANO-MECHANICAL TESTS IN THE LIGHT OF SYNCHROTRON X-RAY DIFFRACTION

T. W. Cornelius[1], Z. Ren[1], C. Leclere[1], M. Dupraz[2], G. Beutier[2], M. Verdier[2], O. Robach[3], J.-S. Micha[3], E. Rabkin[4], G. Richter[5], O. Thomas[1]

[1]*Aix-Marseille Université, CNRS, IM2NP UMR 7334, 13397 Marseille Cedex 20, France*
[2]*Grenoble Institute of Technology & CNRS, BP 75, 38402 Saint-Martin d'Hčres Cedex, France*
[3]*CRG-IF BM32 Beamline at the European Synchrotron (ESRF), CS40220, 38043 Grenoble Cedex 9, France*
[4]*Technion -Israel Institute of Technology Department of Materials Engineering, 32000 Haifa, Israel*
[5]*MPI for Intelligent Systems, Heisenbergstrasse 3, 70569 Stuttgart, Germany*
thomas.cornelius@im2np.fr

In the recent past, low-dimensional materials attracted enormous attention due to the extraordinary properties compared to their bulk counterparts. For instance, micro-and nano-mechanical tests revealed an increasing yield strength with decreasing structure size reaching the ultimate limit of the material for nanowires [1, 2]. To shed additional light on the mechanical behavior of low-dimensional materials, *in situ* experimental setups are being designed for monitoring the evolution of the structures during the mechanical deformation. So far, in situ mechanical tests coupled with X-ray diffraction techniques concentrated on micrometric samples [3, 4]. For in situ nano-mechanical tests, a scanning force microscope was developed which can be installed at different 3rd generation synchrotron beamlines [5, 6, 7]. Here, we will present the coupling of this new tool with Bragg coherent X-ray diffraction imaging (BCDI) and µLaue diffraction for *in situ* nano-indentation on Au nanocrystals and *in situ* three-points bending tests on self-suspended Au nanowires, respectively [7, 8]. These *in situ* experiments enabled us for the first time to image by BCDI a prismatic loop in a Au crystal which had been induced by nano-indentation. A scanning electron micrograph and the reconstructed electron density of the indented Au nanocrystal are presented in Fig. 1(a). Moreover, the in situ coupling with µLaue diffraction allowed for measuring the complete profile of a mechanically loaded nanowire giving access to the elastic as well as the plastic deformation of the nanostructure. Figure 1(b) displays integrated diffraction patterns of the Au 222 Laue spot recorded along the nanowire at different deformation stages employing a newly developed KB scanning method [8]. From these integrated diffraction patterns, the bending angle and the complete nanowire profile also shown in this figure were determined.

This work was funded by the French National Research Agency through project ANR-11-BS10-01401 MecaniX.

1. B. Wu et al., Nature Materials 4 (2005) 525.
2. G. Richter et al., Nano Lett. 9 (2009) 3048.
3. C. Kirchlechner et al., Acta Materialia 60 (2012) 1252.
4. R. Maaß et al., Mater. Sci. Eng. A 524 (2009) 40.
5. Z. Ren et al., J. Synchrotron Radiat. 21 (2014) 1128.
6. C. Leclere et al., J. Appl. Cryst. 48, 291 (2015).
7. M. Dupraz, PhD thesis, Université Grenoble Alpes, Grenoble, France (2015)
8. C. Leclere et al., to be submitted.

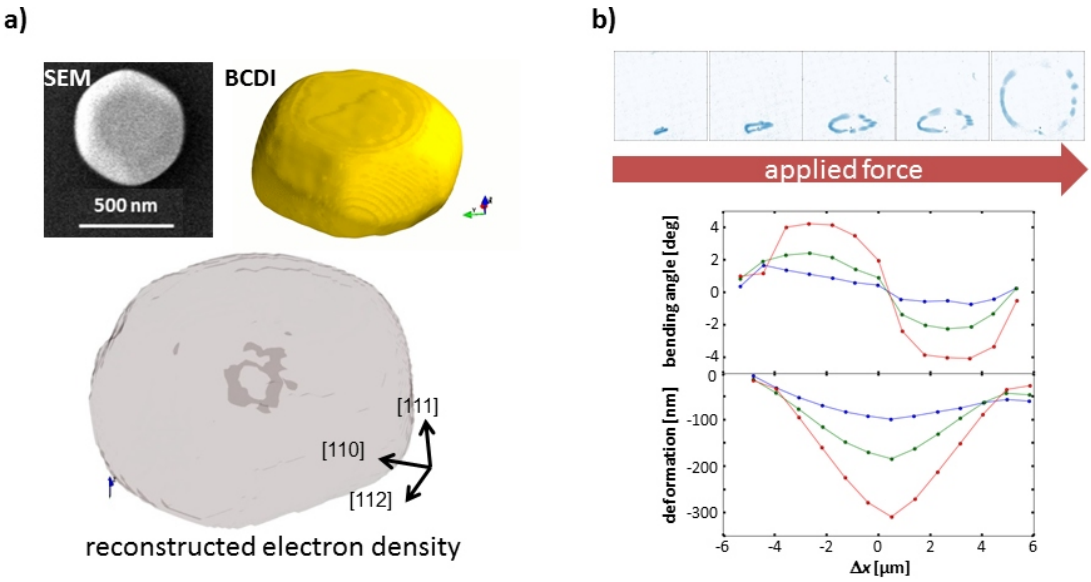

Figure 1. a) SEM image, reconstructed shape and electron density of an indented Au nanocrystal. b) Integrated diffraction patterns of the Au 222 Laue spot recorded along the deformed nanowire, bending angle and nanowire profile inferred from the diffraction patterns.

C22

OBSERVATION OF SAGITTAL X-RAY DIFFRACTION OF SURFACE ACOUSTIC WAVES IN BRAGG GEOMETRY

S. Vadilonga[1,2], I. Zizak[1], A. Erko[1,2], D. V. Roshchupkin[3]

[1]Helmholtz-Zentrum Berlin, Albert Einstein str. 15, 12489 Berlin, Germany
[2]Freie Universität Berlin, Arnimallee 14, 14195 Berlin, Germany
[3]Institute of Microelectronics Technology and High Purity Materials, Russian Academy of Sciences, 6 Academic Ossipyan str., Chernogolovka, Moscow region 142432, Russia
simone.vadilonga@helmholts-berlin.de

X-ray diffraction on surface acoustic waves (SAW) was previously demonstrated in meridional diffraction geometry in several works [1, 2]. SAW travel on the crystal surface, temporarily creating grating-like structures with amplitude up to one nanometer and near-sinusoidal deformation profile. Using this effect *Tucoulou et al.* demonstrated the feasibility of a high frequency chopper for synchrotron radiation at ESRF [2]. But due to the fact that the velocities of the SAW are typically on the order of 3000 m/s, the time resolution of the device was limited by the value of ~1 μs due to the large travel distance of the SAW pulse through the footprint of the X-ray beam at a small grazing incidence angle. In this work we observed an X-ray beam splitting by SAW in sagittal diffraction geometry. A similar experiment was already done by *Roshchupkin et al.* [3]. The (200) Bragg reflection on a langasite ($La_3Ga_5SiO_{14}$) single crystal was used. SAW with frequencies up to 500 MHz were excited in piezoelectric materials using interdigital transducers deposited on the crystal surface. The experiment was performed in sagittal diffraction geometry (Fig. 1 b) by electronic pulsing of the SAW emission and synchronization with the arrival of the synchrotron x-ray pulses. The achieved time resolution was in the order of 50 ns, and it was smeared by the time that the SAW need to cross the beam footprint. In Fig. 2 it is shown the Bragg reflection without and with SAW. Once the SAW are excited the 0-th order is suppressed and only the m=+/-1 satellites are visible. The observed effect can be used for fast modulation of X-ray beams with the time resolution better of 50 ns, which is faster than most mechanical choppers. The results of the measurement were compared with theoretical calculations using GSolver, a rigorous diffraction grating analysis program.

1. D.V. Roshchupkin et al., *Applied Physics A*, **114** (2014).
2. R. Tucoulou et al., *Nuclear Instruments and Methods in Physics Research B,* **132**, 207-213 (1997) .
3. D.V. Roshchupkin et al., *Journal of Applied Physics*, **110** (2011).

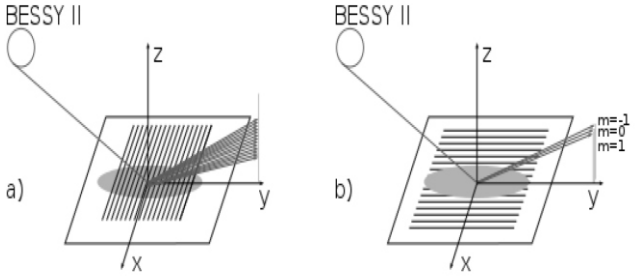

Figure 1. SAW experiment in meridional a) and sagittal b) geometry.

Figure 2. Bragg peak recorded with a CCD b) geometry camera.When SAW are switched on the 0-th order is suppressed and the satellite peaks appear

C23

SUSTAINED kHZ FRAME RATES FOR ULTRAFAST TOMOGRAPHY - INTRODUCING GigaFRoST

C. M. Schlepütz[1], R. Mokso[2], G. Theidel[3], H. Billich[4], E. Schmid[3], T. Celcer[5], G. Mikuljan[1], F. Marone[1], N. Schlumpf[3], M. Stampanoni[1,6]

[1]Swiss Light Source, Paul Scherrer Institut, 5232 Villigen PSI, Switzerland
[2]Max IV Laboratory, Lund University, SE-22100 Lund, Sweden
[3]Electronics and Measuring Systems, Paul Scherrer Institut, 5232 Villigen PSI, Switzerland
[4]Information Technology Division, Paul Scherrer Institut, 5232 Villigen PSI, Switzerland
[5]Controls Section, GFA Division, Paul Scherrer Institut, 5232 Villigen PSI, Switzerland
[6]Institute for Biomedical Engineering, University and ETH Zurich, 8092 Zurich, Switzerland
christian.schlepuetz@psi.ch

Developing the means to observe a sample's full volumetric structural evolution during dynamic processes with high temporal and spatial resolution has been a key project of the tomographic microscopy beamline TOMCAT [1] at the Swiss Light Source. We have achieved the acquisition of tomographical scans with 3 microns voxel size at 20 Hz [2], and were able to push the time-resolution into the kHz regime for quasi-periodic motions [3].

A major technical innovation enhances the capabilities of our high-speed camera system. Commercially available CMOS detectors able to collect images at multi-kHz rates are designed for burst operation. Images are first buffered in on-board memory, and the subsequent readout process to external storage is slow, thus precluding a sustained data acquisition. The available amount of internal memory limits the total number of frames that can be recorded, and is in many cases much too small to capture the entire duration of dynamic processes at a sufficient temporal resolution and field of view. To overcome this limitation, we have developed the "Gigabit Fast Read-out System for Tomography", coined *GigaFRoST*. The data collected by a pco.Dimax fast imaging sensor are read out by custom-designed readout electronics and directly streamed to the processing servers via eight parallel 10 Gbit fiber-optic links, reaching a transfer rate of 7.7 GB/s, which is sufficient to handle the maximum data rate produced by the chip. On the server side, independent processes can access the data simultaneously to produce real-time previews and write data to permanent disk storage. In parallel, we plan to perform on-the-fly data reconstruction and analysis to select only the useful data for storage or to provide on-line feedback to the experiment. GigaFRoST also offers very flexible trigger schemes, providing an adaptable and versatile interface for complex *in situ, in operando,* and *in vivo* experiments.

We will present an overview of the system architecture and its implementation at TOMCAT, as well as examples of experiments that will greatly profit from the GigaFRoST capabilities, ranging from the observation of crack propagation in metals [2], and self-healing in ceramics [4], to *in vivo* measurements of lung tissue during breathing in mice [5] and the musculoskeletal motion of a fly thorax in flight [3]. The sustained high-speed acquisition has already enabled the detailed observation of sintering dynamics in volcanic materials in real-time for up to 30 minutes.

1. M. Stampanoni, A. Groso, A. Isenegger, G. Mikuljan, Q. Chen, A. Bertrand, S. Henein, R. Betemps, U. Frommherz, P. Böhler, D. Meister, M. Lange, and R. Abela, *Proc. of SPIE* **6318** (2006) , 63180M.
2. E. Maire, C. Le Bourlot, J. Adrien, A. Mortensen, and R. Mokso, *Int J Fract* **1** (2016).
3. R. Mokso, D. A. Schwyn, S. M. Walker, M. Doube, M. Wicklein, T. Müller, M. Stampanoni, G. K. Taylor, and H. G. Krapp, *Scientific Reports* **5** (2015) , 8727.
4. W. G. Sloof, R. Pei, S. A. McDonald, J. L. Fife, L. Shen, L. Boatemaa, A.-S. Farle, K. Yan, X. Zhang, S. van der Zwaag, P. D. Lee, and P. J. Withers, *Scientific Reports* **6** (2016) , 23040.
5. G. Lovric, PhD Thesis, ETH Zürich (2015).

Session VIII

Wednesday, September 7 - morning

I8

BIOMINERALS IN THE LIGHT OF BRAGG COHERENT X-RAY DIFFRACTION IMAGING

V. Chamard

Aix-Marseille Université, CNRS, Centrale Marseille, Institut Fresnel, Marseille, France
virginie.chamard@fresnel.fr

Biomineralization integrates complex physico-chemical processes leading to an extraordinary diversity of calcareous biomineral crystalline architectures, in intriguing contrast with the consistent presence of a submicrometric granular structure [1]. Understanding how the mineral granules organize is a key element to gain knowledge on the biomineralization processes. While evidences for the existence of a mesoscale crystalline organization, spanning over a few granules, have been reported, a 3D image of the spatial organization of the crystalline domains is still lacking.

In this context, we have proposed to apply 3D X-ray Bragg ptychography microscopy [2], a recently demonstrated coherent diffraction imaging approach, based on the inversion of a set of intensity-only data [3]. Ptychography exploits the partially redundant information obtained by scanning a finite beam spot size transversally to the sample, while measuring the corresponding 3D far-field coherent diffraction pattern. Thereby, 3D imaging of extended crystalline samples becomes possible [4, 5].

In this presentation, we first briefly review the evolution of the Bragg ptychography approach, before detailing the results obtained in the framework of biomineralization. Specifically, we show the 3D images of the prismatic part of a *Pinctada margaritifera* shell, revealing this way the spatial arrangement of the crystalline structure with a nanometric resolution. We evidence a crystalline coherence extending over a few granules and further prove the existence of larger iso-oriented crystalline domains, slightly misoriented with respect to each other around a single rotation axis [6]. These original results bring new structural information, which will be discussed in the framework of recently proposed biomineralization growth schemes.

1. Y. Dauphin, *Mineralogical Magazine* **72**, (2008), 243.
2. P. Godard, G. Carbone, M. Allain, F. Mastropietro, G. Chen, L. Capello, A. Diaz, T. H. Metzger, J. Stangl and V. Chamard, *Nature Communications,* **2**, (2011), 568.
3. P. Godard, M. Allain, V. Chamard, and J. Rodenburg, *Optics Express*, **20**, (2012), 25914.
4. V. Chamard, M. Allain, P. Godard, A. Talneau, G. Patriarche and M. Burghammer, *Scientific Reports*, **5**, (2015), 9827.
5. I. Pateras, M. Allain, P. Godard, L. Largeau, G. Patriarche, A. Talneau, K. Pantzas, M. Burghammer, A. A. Minkevich and V. Chamard, *Physical Review B*, **92**, (2015), 205305.
6. F. Mastropietro, P. Godard, M. Burghammer, C. Chevallard, J. Daillant, J. Duboisset, M. Allain, P. Guenoun, J. Nouet, V. Chamard, *submitted*.

The co-authors of reference [6] are warmly acknowledged for their participation to this work. This research program was funded by the French ANR under project number ANR-11-BS20-0005.

C24

NEW LABORATORY IMPLEMENTATIONS OF EDGE ILLUMINATION X-RAY PHASE CONTRAST IMAGING

G. K. Kallon,[1*] P. C. Diemoz,[1] M. Endrizzi,[1] F. A. Vittoria,[1] M. Wesolowski,[2] T. P. Millard,[1] D. Basta,[1] and A. Olivo,[1]

[1]Department of Medical Physics and Biomedical Engineering, Malet Place, London WC1E 6BT
[2]Department of Medical Imaging, University of Saskatchewan, Saskatoon, SK, Canada, S7N 0W8
[*]gibril.kallon.10@ucl.ac.uk

Edge illumination X-ray phase contrast imaging (EI XPCI) is a technique that enables quantitative retrieval of the absorption, differential phase and ultra-small angle X-ray scattering properties of an object using commercially available, polychromatic sources in a laboratory environment [1,2]. Two periodic masks, consisting of long, vertical slits are normally used. The first (sample) mask is placed before the sample and reshapes the incoming beam, while the second is placed just before the detector pixels, partially intercepting the beamlets, thereby making the system sensitive to refraction caused by the sample. A single image taken at a given sample mask displacement contains a mixture of absorption, differential phase and scattering effects. To retrieve the two (phase & absorption) or three (phase, absorption & scattering) channels of information, two or three images need to be acquired at different sample mask displacements and then mathematically combined.

In this presentation, we report on a new laboratory implementation of EI based on the use of a single mask. Besides simplifying the set-up and relaxing the system alignment constraints, it also enables phase and absorption retrieval through the simultaneous acquisition of two images in a single shot. This is realised by removing the second mask and using the boundary between detector pixels as the edge sensing mechanism (Fig. 1(a)). Figure 1(b) shows the image captured by a single mask EI system for all the detector pixels, and how alternating sets of pixels are then used to obtain a pair of images with inverted refraction contrasts. The single mask EI set-up can also potentially reduce the dose delivered to the sample by the current, "standard" double mask set-up by up to a factor of two, as only a single exposure is needed.

We will additionally show how two-directional EI sensitivity can be achieved by replacing the vertical slits with L-shapes and acquiring images at six different sample mask displacements [3]. This yields the refraction and scattering channels in both directions. In general, 2D differential phase images have the advantage of enabling easy phase integration and removing the streak artefacts common to the 1D case [4].

Furthermore, these developments can be combined with new detector technology, e.g. PixiRad a photon counter with a sharp PSF [5], and high-quality masks to improve the aforementioned set-ups. This will lead to the realisation of new designs (single mask 2D EI, dual-energy EI etc.) which even better exploit the advantages provided by the EI technique.

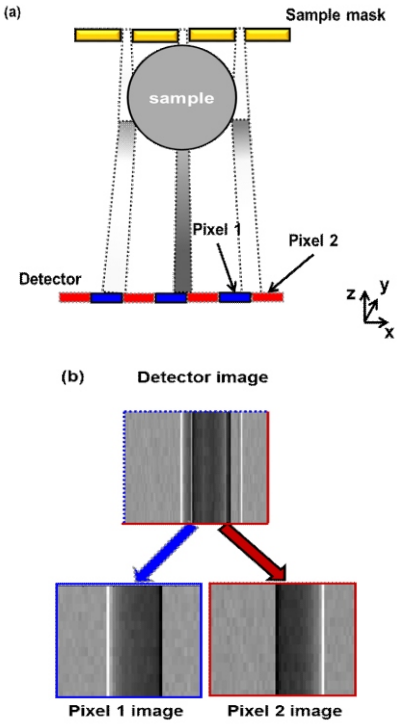

Figure 1. (a) Schematic for the single mask edge illumination set-up, (b) an unprocessed image using all detector pixels (top), and the images formed by the two sets of pixels (bottom).

1. A. Olivo & R. Speller, *Appl. Phys. Lett.*, **91**(7), (2007).
2. A. Olivo, K. Ignatyev, P.R.T. Munro, R. D. Speller, *Appl. Opt.*, **50, (**2011), pp. 1765-1769.
3. G. K. Kallon, M. Wesolowski, F. A. Vittoria, M. Endrizzi, D. Basta, T. P. Millard, P. C. Diemoz, A. Olivo, *Appl. Phys. Lett.*, **107**(20), (2015).
4. C Kottler, C David, F Pfeiffer, O Bunk, *Opt. Express*, **15**(3), (2007), pp. 1175-1181.
5. R. Bellazzini, G. Spandre, A. Brez, M. Minuti, M. Pinchera, P. Mozzo, *J. Instrum.*, **8**(02), (2013), C02028.

C25

SYRIS: A FLEXIBLE AND EFFICIENT FRAMEWORK FOR SIMULATING X-RAY IMAGING EXPERIMENTS

T. Faragó[1,2], P. Mikulík[3], A. Ershov[1,2], M. Vogelgesang[4], D. Hänschke[1,2], T. Baumbach[1,2]

[1]Institute for Photon Science and Synchrotron Radiation, Karlsruhe Institute of Technology, Herrmann-von-Helmholtz-Platz 1, 763444 Eggenstein-Leopoldshafen, Germany
[2]Laboratory for Applications of Synchrotron Radiation, Karlsruhe Institute of Technology, Herrmann-von-Helmholtz-Platz 1, 763444 Eggenstein-Leopoldshafen, Germany
[3]CEITEC – Central European Institute of Technology, Masaryk University, Kotlářská 2, 611 37 Brno, Czech Republic
[4]Institute for Data Processing and Electronics, Karlsruhe Institute of Technology, Herrmann-von-Helmholtz-Platz 1, 763444 Eggenstein-Leopoldshafen, Germany
tomas.farago@kit.edu

With *syris* we present a software tool to simulate the complete image formation process from an X-ray source through an arbitrary number of objects to a detector system. Our current implementation takes sample and beam motion, wavefield propagation, its detection process and coherence effects into account. This allows us to simulate a broad range of X-ray imaging experiments and their peculiarities like motion blur, beam drift and realistic noise.

Syris is organized as a framework and consists of basic abstract building blocks with a well-defined application programming interface (API) in Python. We provide implementations of all building blocks to conduct full virtual experiments. These implementations are optimized to achieve a reasonable compromise between efficiency and physical correctness. Moreover, they are written in OpenCL [1] and can thus be executed on numerous platforms, e.g. modern highly parallel GPUs which greatly speed up the computations. Users can provide their own implementations of this API which increases the framework's flexibility.

Combining flexibility with an efficient implementation makes *syris* a powerful tool to investigate novel imaging approaches [2, 3] and validate sophisticated data processing pipelines [4, 5]. Because the data processing parameters depend on experimental conditions, systematic studies of mutual dependencies will help to develop more robust algorithms optimized for particular scientific use cases.

To demonstrate the potential of the framework we first show the simulation of a high-speed radiography experiment conducted with different exposure times giving rise to varying noise levels. We then show the accuracy of a selected motion estimation algorithm as a function of the noise level. Afterwards we pick a noise level and optimize one of the algorithm's parameters to obtain the most accurate flow field. Finally, we employ *syris* to create a complex 3D resolution pattern and use it as a sample in a virtual tomographic experiment to investigate the impact of various imaging conditions on the precision of different reconstruction algorithms.

1. Stone, J. E., Gohara, D. & Shi, G. (2010). *Computing in science & engineering*, 12(1-3), 66–73.
2. Moosmann, J., Ershov, A., Altapova, V., Baumbach, T., Prasad, M. S., LaBonne, C., ... & Hofmann, R. (2013). *Nature*, 497(7449), 374-377.

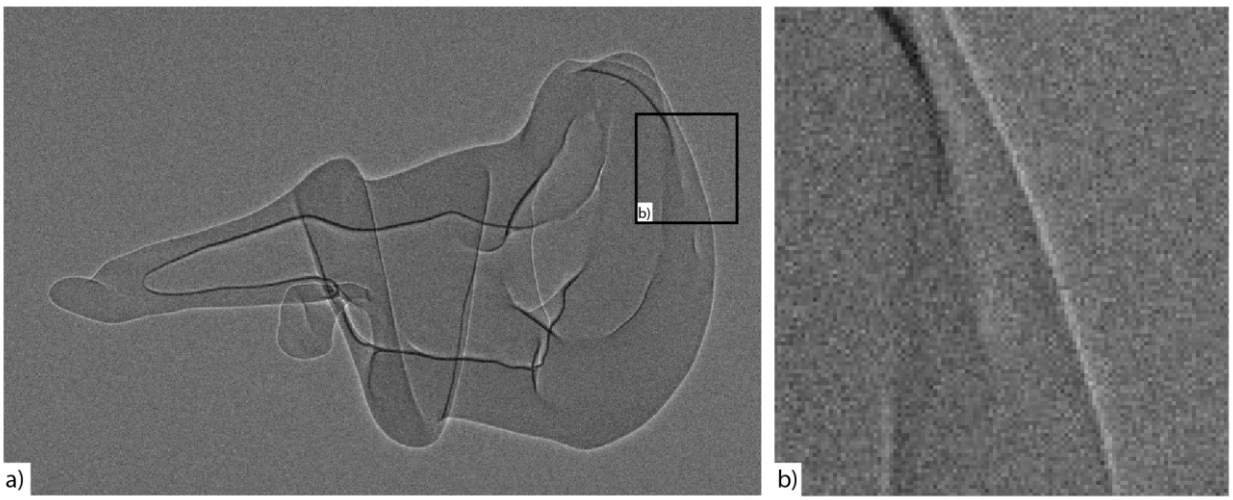

Figure 1. Simulation of a white beam X-ray radiograph of a biological screw joint found in Trigonopterus oblongus [6] based on data from a real CT measurement. The detailed crop in b) shows the appearance of realistic noise and the edge enhancement by free-space propagation visible as a white outlier on the sample boundary.

3. dos Santos Rolo, T., Ershov, A., van de Kamp, T. & Baumbach, T. (2014). *Proceedings of the National Academy of Sciences*, 111(11), 3921–3926.

4. Paganin, D., Mayo, S., Gureyev, T. E., Miller, P. R. & Wilkins, S. W. (2002). *Journal of microscopy*, 206(1), 33-40.

5. Van Nieuwenhove, V., De Beenhouwer, J., De Carlo, F., Mancini, L., Marone, F. & Sijbers, J. (2015). *Optics express*, 23(21), 27975– 27989.

6. van de Kamp, T., Vagovič, P., Baumbach, T. & Riedel, A. (2011). *Science*, 333(6038), 52-52.

C26

IN-SITU X-RAY TOMOGRAPHY STUDY OF CO_2 - INDUCED HEALING IN FRACTURED CEMENT

E. A. Chavez Panduro[1], M. Torsæter[2], K. Gawel[2], R. Bjørge[3], A. Gibaud[4], Y. Yang[5], Y. Zheng[6], H. O. Sørensen[5], D. W. Breiby[1]

[1]Norwegian University of Science and Technology, Høgskoleringen 5, 7491 Trondheim, Norway
[2]SINTEF Petroleum Research, Trondheim, Norway
[3]SINTEF Materials and Chemistry, Trondheim, Norway
[4]LUMAN, IMMM, UMR 6283 CNRS, Université du Maine, Le Mans Cedex 09, France
[5]University of Copenhagen, Department of Chemistry, Copenhagen, Denmark
[6]Technical University of Denmark, Department of Physics, Lyngby, Denmark
elvia.a.c.panduro@ntnu.no

The special report on Carbon Capture and Storage (CCS) published by the Intergovernmental Panel of Climate Change (IPCC) outlines that wells are among the most probable leakage paths from CO_2 storage reservoirs [1]. Whether they are in operation, or permanently plugged and abandoned, these wells are man-made structures of steel and cement that connect the storage reservoir with the atmosphere. If the steel or cement barriers break, leakage paths are likely to develop. To estimate potential leakage rates over time, and to optimize well remediation protocols, the compatibility of cement with CO_2 has been studied [2-5]. An important recent finding is that defects in cement (e.g. cracks) gradually heal when exposed to CO_2 [3-5]. The healing process, and its kinetics, has not yet been fully understood. In order to make use of this beneficial cement healing process in practice, a more detailed understanding is required of how and when it occurs. For that purpose we report in-situ µ-CT measurement in an environment of CO_2 saturated in brine to study both the carbonation and the healing processes on fractured cement.

Cement blocks with artificial channels were used to mimic fractures in cement. The sample was submerged in a saline solution (1%wt NaCl) inside the pressure cell and exposed to CO_2 for 20 hours at 50 bars and ambient temperature. Figure 1 shows that CO_2 exposure of cement induces $CaCO_3$ precipitation in all confined areas (e.g. in fractures, microcavities, non-connected pores and at cement/aluminum interfaces). The volume rate at which $CaCO_3$ precipitated was found to be 4.6×10^{-5} mm^3/min. High resolution µ-CT shows us a varying $CaCO_3$ content within carbonated front of cement block suggesting dissolution of $CaCO_3$ during CO_2 exposure.

1. IPCC Special report on CO_2 Capture and Storage. Eds: B. Metz et al. Cambridge UniversityPress, (2005) 244 pp.

2. B. G. Kutchko et al *Environmental Science & Technology* **42** (2008) 6237–6242.

3. H. E. Mason et al .*Environmental Science & Technology* **47** (2013) 1745-1752.

4. S.D.C. Walsh et al. *Int. J. Greenh. Gas Con.* **22** (2014) 176-188.

5. C. Kjøller et al. *Energy Procedia* **86** (2016) 342-351.

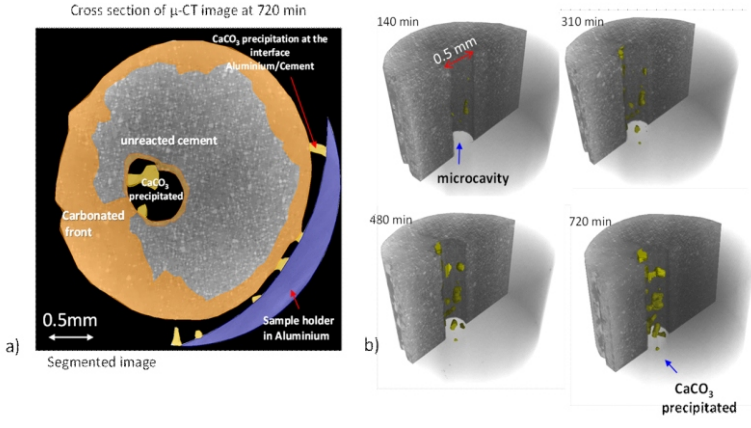

Figure 1. Results obtained from µ-CT. a) Cross section measured after 820 min, b) 3D representations of $CaCO_3$ precipitation in the microcavity as a function of time during the CO_2 exposure.

Session IX

Wednesday, September 7 - afternoon

I9

FROM GLOBAL AND LOCAL Ge INTEGRATION APPROACHES ON Si(001): NOVEL INSIGHTS BY ADVANCED SYNCHROTRON-BASED SCANNING XRD

M. H. Zoellner[1,*], G. Chahine[2], M.-I. Richard[2,3], P. Zaumseil[1], C. Reich[1], M. Häberlen[4], G. Capellini[1], F. Montalenti[5], A. Marzegalli[5], P. Storck[4], T. U. Schülli[2], and T. Schroeder[1,6]

[1]IHP, Im Technologiepark 25, 15236 Frankfurt (Oder), Germany
[2]European Synchrotron Radiation Facility, BP 220, 38043 Grenoble, France
[3]Aix-Marseille Université, CNRS, IM2NP UMR 7334, 13397 Marseille, France
[4]Siltronic AG, Hans-Seidel-Platz 4, 81737 München, Germany
[5]Dipartimento di Scienza dei Materiali, Universita B degli Studi di Milano-Bicocca, Italy
[6]Brandenburgische Technische Universität Cottbus, Konrad -Zuse-Strasse 1, 03046 Cottbus, Germany
**zoellner@ihp-microelectronics.com*

Global and local integration schemes of Germanium (Ge) based heteroepitaxial systems on a Silicon (Si) platform are of crucial importance for advanced complementary metal-oxide-semiconductor (CMOS) technology and electronic photonic integrated circuits (EPICs). To improve the performance of such heterostructures for Ge-based devices, fundamental insights into the local crystal structure are required. This information can be a valuable input to engineers for theoretical simulations to correlate the structural properties with materials electronic and photonic properties.

A recently developed synchrotron-based scanning X-ray diffraction microscopy technique, called quic*K-map*ping (K-map), from the beam line ID01 of the European Synchrotron radiation facility (ESRF) is ideally suited to non-destructively image with sub-micron resolution local tilt and lattice constant variations (a/a) with a sensitivity down to 10^{-3} degree and 10^{-5}, respectively. Local lattice orientations and constants are extracted by the X-ray Strain Orientation Calculation Software (XSOCS) [1]. In the presentation, K-map results from SiGe buffer layers and Ge micro-stripes are demonstrated as examples for global and local Ge heterostructures.

SiGe „virtual substrates“ are a promising approach for the very large scale integration (VLSI) of Ge as closed films on Si(001). Although, growth and relaxation processes of SiGe buffer layers on Si(001) are well investigated and major achievements were made, control over the structural homogeneity of SiGe buffers below micro-meter scale is still a challenge for global integration on 300 mm Si(001) wafers. The capability of the K-map technique to determine lattice parameters in a quantitative way demonstrates the achieved quality given by the influence of plastic relaxation to the tilt, strain and composition of Ge/SiGe/Si(001) systems.[2,3]

Ge micro-structures on Si(001) achieved by top-down or bottom-up approaches suffer as well from inhomogeneities due to growth and relaxation processes. Additionally, process steps as capping layers and local etching or doping may further influence the crystal structure. However, these approaches enable to engineer local structural properties as the strain distribution.[4]

1. G.A. Chahine, M.-I. Richard, R.A. Homs-Regojo, T.N. Tran-Caliste, D. Carbone, V.L.R. Jacques, R. Grifone, P. Boesecke, J. Katzer, I. Costina, H. Djazouli, T. Schroeder, and T.U. Schülli, *J. Appl. Cryst.*, **47**, 762 (2014).
2. M.H. Zoellner, M.-I. Richard, G.A. Chahine, P. Zaumseil, C. Reich, G. Capellini, F. Montalenti, A. Marzegalli, Y.-H. Xie, T.U. Schülli, M. Häberlen, P. Storck, and T. Schroeder, *ACS Appl. Mater. Interfaces. Instrum.*, **7**, 9031 (2015).
3. M.-I. Richard, M.H. Zoellner, G.A. Chahine, P. Zaumseil, G. Capellini, M. Häberlen, P. Storck, T.U. Schülli, and T. Schroeder, *ACS Appl. Mater. Interfaces*, **7**, 26696 (2015).
4. G.A. Chahine, M.H. Zoellner, M.-I. Richard, S. Guha, C. Reich, P. Zaumseil, G. Capellini, T. Schroeder, and T.U. Schülli, *Appl. Phys. Lett.*, **106**, 071902 (2015).

C27

TABLE-TOP SAXS/WAXS (SCANNING) MICROSCOPY PROBES HYDROXYAPATITE CONCENTRATION GRADIENTS IN ENGINEERED BIO-SCAFFOLDS

Davide Altamura[1], Stella G. Pastore[1], Maria G. Raucci[2], Dritan Siliqi[1], Rocco Lassandro[1], Fabio De Pascalis[3], Michele Nacucchi[3], Luigi Ambrosio[2,4] and Cinzia Giannini[1]

[1]Institute of Crystallography (IC), National Research Council, Bari 70125, Italy
[2]Institute of Polymers, Composites, and Biomaterials (IPCB), National Research Council, Naples, Italy
[3]Italian National Agency for New Technologies, Energy and Sustainable Economic Development (ENEA), Brindisi 72100, Italy
[4]Department of Chemical Sciences and Materials Technology (DSCTM), National Research Council, Rome 000133, Italy

A structural study of a scaffold made of bovine gelatin and hydroxyapatite (HA) is carried out, for bone tissue engineering purposes [1]. The great relevance of such a material relies on its potential application in the healing process of osteochondral defects, which are responsible for the damage of cartilage and adjacent subchondral bone, compromising the quality of life of millions of patients. Two techniques exploiting X-ray radiation, with table-top setups, are used: micro-CT and microdiffraction. The former allowes 3D imaging at the micrometer scale spatial resolution, the latter provides combined 2D structural/morphological information at the atomic and nano-scale, with a hundred microns spatial resolution. The combination of these two techniques allowed the study of the scaffold density gradient, related to the HA concentration gradient, engineered on purpose to mimic the natural bone structure model. Micro-CT defines the directionality of the gradient; WAXS probes the crystalline phases in the sample; SAXS microscopy selectively probes HA distribution through mapping of the SAXS intensity in specific q-ranges. Scanning SAXS micrographs and WAXS patterns were collected by using a high brilliance Rigaku Fr-E+ SuperBright microsource, coupled to a SMAX3000 three pinhole camera through a focusing multilayer optics (CMF 15-105) [2].

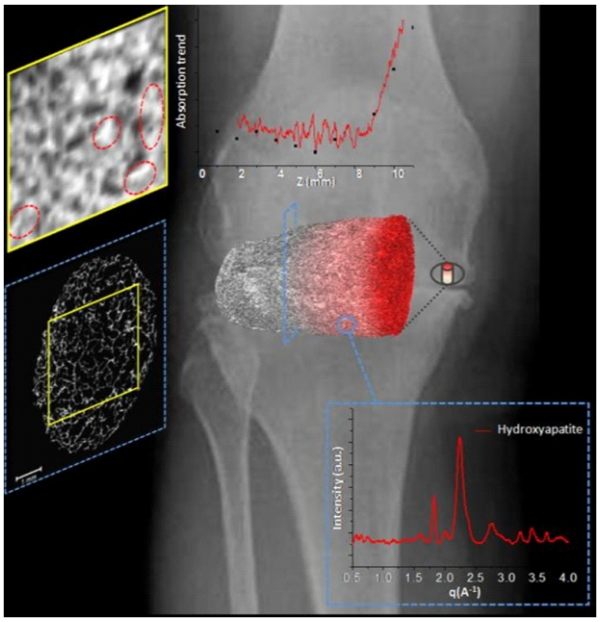

1. D. Altamura, S. G. Pastore, M. G. Raucci, D. Siliqi, F. De Pascalis, M. Nacucchi, L. Ambrosio, and C. Giannini.Scanning Small- and Wide-Angle X-ray Scattering Microscopy Selectively Probes HA Content in Gelatin/Hydroxyapatite Scaffolds for Osteochondral Defect Repair. ACS Appl. Mater. Interfaces (2016). 8, 8728-8736.
2. D. Altamura, R. Lassandro, F. A. Vittoria, L. De Caro, D. Siliqi, M. Ladisa & C. Giannini, X-ray MicroImaging Laboratory (XMI-LAB), J. Appl. Cryst. (2012). 45, 869-873.

C28

EXTENDED RANGE ULTRA SMALL-ANGLE X-RAY, SMALL-ANGLE, AND WIDE-ANGLE SCATTERING FOR ADVANCED ALLOY DEVELOPMENT

J. Ilavský[1], F. Zhang[2], L.E. Levine[2], A.J. Allen[2]

[1]Advanced Photon Source, Argonne National Laboratory, Argonne, IL, USA
[2]National Institute of Standard and Technology, Gaithersburg, MD, USA
ilavsky@aps.anl.gov

Development of new high-performance materials, e.g., new aluminum or steel alloys, is critical for advances in energy production and utilization (and many other areas). These materials often exhibit complex microstructures spanning multiple length scales that control their performance. In this context, it is important to simultaneously characterize, ideally *in situ* or *in operando*, various facets of the microstructure – for example precipitate shape and size, together with their phase and chemical composition. Over many years, the Advanced Photon Source (APS) with NIST has developed and optimized a combined Ultra-Small, Small, & Wide Angle X-ray Scattering

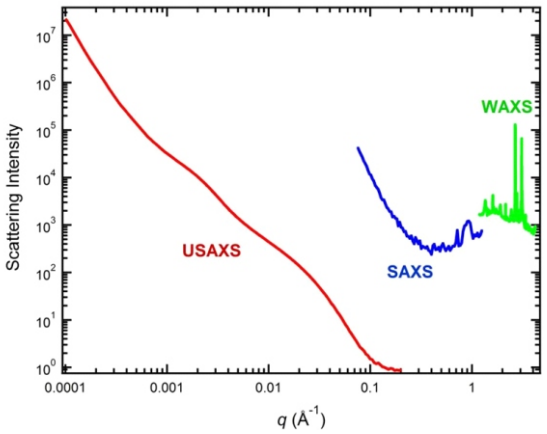

Figure 1 Example of combined USAXS, SAXS, and WAXS for AA202024 alloy.

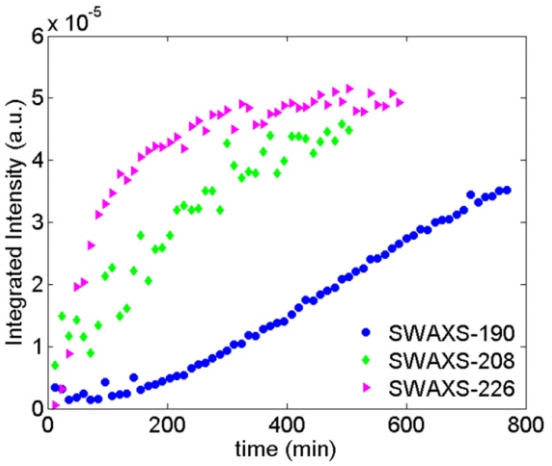

Figure 2. Evolution of the integrated 112 reflection of the S phase precipitate peak intensity at d = 2.570 Å (or q = 2.445 Å^{-1}) at 190 °C, 208 °C, and 226 °C,...

(USAXS/SAXS/WAXS) facility [1]. Data spanning over 5 decades in microstructural size can be collected sequentially in 4 to 6 minutes, from the same volume during one *in-situ* experiment. In the case presented, we have studied the Al-Cu-Mg alloys, e.g., AA2024, at different aging conditions.

The precipitate structure and precipitation kinetics in the Al-Cu-Mg alloy, AA2024, aged at 190 °C, 208 °C, and 226 °C have been studied using *ex situ* TEM and *in situ* combined USAXS/SAXS/WAXS at the APS across a length scale from sub-Angstrom to several micrometers, Fig.1. TEM provided information concerning the nature, morphology, and size of the precipitates, while USAXS/SAXS/WAXS provided qualitative and quantitative information concerning the time-dependent size and volume fraction evolution of the precipitates at different stages of the precipitation sequence.

Using a three-parameter scattering model constructed on the basis of the TEM results, we established the temperature-dependent kinetics for the cluster-dissolution and S-phase formation processes. These two processes, while occurring simultaneously, have different kinetic rates, with the cluster-dissolution rate approximately double the S-phase formation rate. We also identified a dissolution activation energy at (149.5 ± 14.6) kJ mol^{-1}, which translates to (1.55 ± 0.15) eV/atom, as well as an activation energy for the formation of S precipitates at (129.2 ± 5.4) kJ mol^{-1}, i.e. (1.33 ± 0.06) eV/atom. The SAXS/WAXS results show the absence of an intermediate GPB2/S" phase in the samples under the experimental ageing conditions. These results are further validated by precipitation simulations that are based on Langer-Schwartz theory and a Kampmann-Wagner numerical method. This study [2] clearly shows how the extended-range USAXS/SAXS/WAXS facility simplifies and speeds up new advanced materials characterization and development.

1. J. Ilavsky, P.R. Jemian, A.J. Allen, F. Zhang, L.E. Levine, G.G. Long, *Journal of Applied Crystallography*, 42, (2009), 469-479.

2. Zhang, F., L. E. Levine, A. J. Allen, C. E. Campbell, A. A. Creuziger, N. Kazantseva and J. Ilavsky, *Acta Materialia* **111**, (2016), 385-398.

This research used resources of the Advanced Photon Source, a U.S. Department of Energy (DOE) Office of Science User Facility operated for the DOE Office of Science by Argonne National Laboratory under Contract No. DE-AC02-06CH11357.

C29

NANODIFFRACTION OF HIGHLY MISMATCHED COMPOSITIONALLY GRADED SiGe/Si MICROCRYSTALS

M. Meduňa[1,2], F. Isa[3,4], A. Jung[3,4], A. Marzegalli[5], Y. Arroyo Rojas Dasilva[4], G. Isella[6], R. Erni[4], P. Niedermann[7], K. Zweiacker[8], A. Neels[8], A. Dommann[8], P. Gröning[5], and H. von Känel[3,4]

[1]Department of Condensed Matter Physics, Masaryk University, Kotlářská 2, Brno, CZ-61137, Czech Republic
[2]CEITEC, Masaryk University, Kamenice 5, Brno, CZ-60177, Czech Republic
[3]Laboratory for Solid State Physics, ETH Zürich, Otto-Stern-Weg 1, Zürich, CH-8093, Switzerland
[4]Electron Microscopy Center, Empa, Überlandstrasse 129, Dübendorf, CH-8600, Switzerland
[5]L-NESS and Department of Materials Science, Universita di Milano-Bicocca, Via Cozzi 55, Milano, I-20125, Italy
[6]L-NESS and Department of Physics, Politecnico di Milano, Via Anzani 42, Como, I-22100, Italy
[7]CSEM, Rue Jaquet-Droz 1, Neuchâtel, CH-2002, Switzerland
[8]Center for X-Ray Analytics, Empa, Überlandstrasse 129, Dübendorf, CH-8600, Switzerland
mjme@physics.muni.cz

The heteroepitaxial growth of materials with different lattice and thermal expansion coefficients, particularly in the form of various semiconductor layers on silicon, is one of the cornerstones of functional scaling for integrating high-speed electronic and optoelectronic devices. Unfortunately, the mismatched materials suffer from misfit (MDs) and threading (TDs) dislocations formed at the material interface and from wafer bowing. Both MDs and TDs negatively impact the electrical and optical properties of the potential device. Wafer bowing can lead even to cracking of whole chips.

Recently Falub et al. achieved a breakthrough in the attempt to eliminate threading dislocations from heteroepitaxial SiGe/Si layers. This was realized by using a novel kind of epitaxial growth in which densely packed 3D SiGe crystals are formed on patterned Si substrates instead of continuous films [1]. Thanks to a fully faceted morphology and limited lateral crystal size, all threading dislocations stemming from the heavily defected heterointerface are forced to leave the crystals through their sidewalls, leaving the upper crystal region defect-free [2].

Although this method is highly effective in eliminating threading dislocations, it does not prevent the formation of misfit dislocations at the SiGe/Si heterointerface, as presented in our previous experiments using scanning X-ray nanodiffraction [3]. However M. Salvalaglio et al. have recently proposed [4] an innovative approach to eliminate misfit dislocations in highly mismatched, compositionally graded SiGe/Si heterostructures. The misfit stress may be relaxed entirely elastically by choosing the appropriate crystal width and Ge grading rate. Such heterostructures have been recently realised [5] and form the basis for this paper.

In this work we present X-ray nanodiffraction experiments performed at the ID01 beamline of the ESRF in Grenoble on isolated 3D $Si_{1-x}Ge_x$ microcrystals (see Fig. 1), in which the Ge content x is linearly increased from 0 to

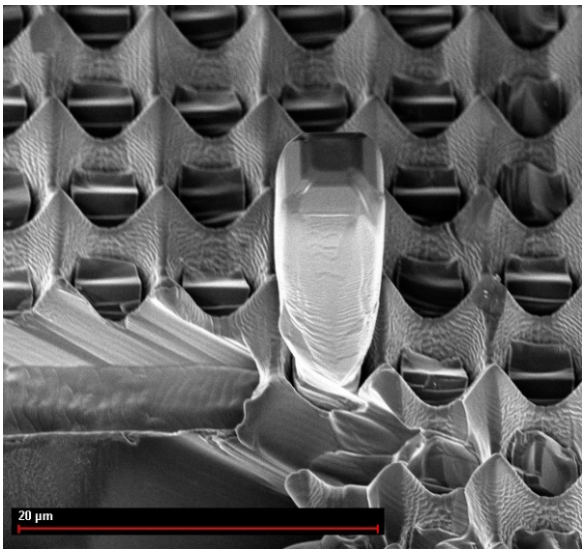

Figure 1. Perspective scanning electron microscope (SEM) image of an individual graded SiGe crystal probed by an X-ray nanobeam.

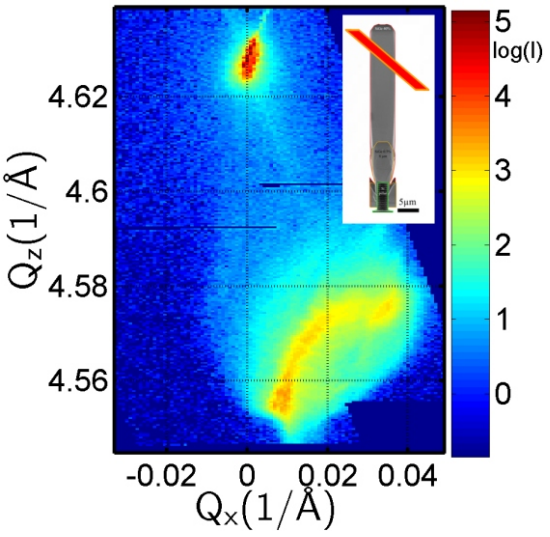

Figure 2. RSM around the (004) Bragg reflection of a SiGe crystal probed by a skewed nanobeam through the top part of the crystal.

40% at the rate of 1.5% μm^{-1}. Depending on the crystal width, the 3D SiGe crystals are expected to be completely free from misfit and threading dislocations. During the experiment we have performed series of scanning X-ray diffraction microscopy (SXDM) images for different incidence angles from which 3D reciprocal space maps (RSMs) have been built (see Fig. 2). RSMs around the (004) and (115) Bragg reflections have been collected on 2D meshes for microcrystals with different Ge grading rates and different widths, and on an unpatterned area. By combining series of RSMs we obtain an evolution of the crystal lattice tilt and strain depending on the Ge grading rate and crystal width at various positions inside the crystal. The X-ray data are compared with finite element calculations.

1. C. V. Falub, H. von Känel, F. Isa, R. Bergamaschini, A. Marzegalli, D. Chrastina, G. Isella, E. Müller, P. Niedermann, and L. Miglio, *Science*, **335**, (2012), 1330.
2. C.V. Falub, M. Meduňa, D. Chrastina, F. Isa, A. Marzegalli, T. Kreiliger, A. G. Taboada, G. Isella, L. Miglio, A. Dommann, and A. H. von Känel, *Sci. Rep.*, **3**, (2013). 2276.
3. M. Meduňa, C.V. Falub, F. Isa, A. Marzegalli, D. Chrastina, G. Isella, L. Miglio, A. Dommann, and H. von Känel, *J. Appl. Cryst*, **49**, (2016) in press, doi: 10.1107/S1600576716006397.
4. M. Salvalaglio and F. Montalenti, J. Appl. Phys., **116**, (2014), 104306.
5. F. Isa, M. Salvalaglio, Y.A.R. Dasilva, M. Meduňa, M. Barget, A. Jung, T. Kreiliger, G. Isella, R. Erni, F. Pezzoli, E. Bonera, P. Niedermann, P. Gröning, F. Montalenti, and H. von Känel, *Adv. Mater.* **28**, (2016), 884.

Supported by the Sinergia project NOVIPIX CRSII2_147639 of the Swiss National Science Foundation. One author wishes to acknowledge the projects INGO LG 13058, EE2.3.20.0027 and ED1.1.00/02.0068. This research has been also financially supported by the MEYS of the Czech Republic under the project CEITEC 2020 (LQ1601).We acknowledge the staff of the ID01 beamline at the ESRF, Grenoble; FIRST Center for Micro- and Nanoscience of ETH Zurich; and helpful discussions with B. Batlogg.

C30

TITLE X-RAY DIFFRACTION STUDY OF THE (MAGNETO-)STRUCTURAL TRANSITION IN FeRh THIN LAYERS

L. Horák

Faculty of Mathematics and Physics, Charles University in Prague, Ke Karlovu 5, 121 16 Praha 2
horak@karlov.mff.cuni.cz

The $Fe_{50}Rh_{50}$ material exhibits a reversible magneto-structural transition between a room-temperature antiferromagnetic (AFM) and a high-temperature ferromagnetic (FM) phase approximately at 350 K [1]. After the transition to the FM state, the lattice is discretely expanded and this transition shows the temperature/field hysteresis in the lattice parameter and in the magnetic net moment [2]. Most probably, the initial growth of the ferromagnetic phase is stimulated by the defects located at the surface and/or the interface with the substrate [2]. Further, in the thin FeRh layers, the presence of the stable residual FM volume located at the layer/substrate or layer/capping interfaceis is being observed [3].

Using High-Resolution X-ray diffractometry (HR-XRD), we have measured several samples of FeRh thin layers with various thicknesses benefiting from the different lattice parameter of the AFM and the FM phase. We performed the temperature dependent measurements (during the heating and the cooling) of the distribution of diffracted intensity in the reciprocal space. For the simulation we assumed the mosaic-like model of FM and AFM domains that allowed to interpret the experimental data. From the fitting we determined the vertical and lateral size of domains together the relative volume of both phases.

We confirmed the presence of the FM volume at the room tempereature. However, in contrary to the common interpretation based on thin FM interlayer, the diffraction

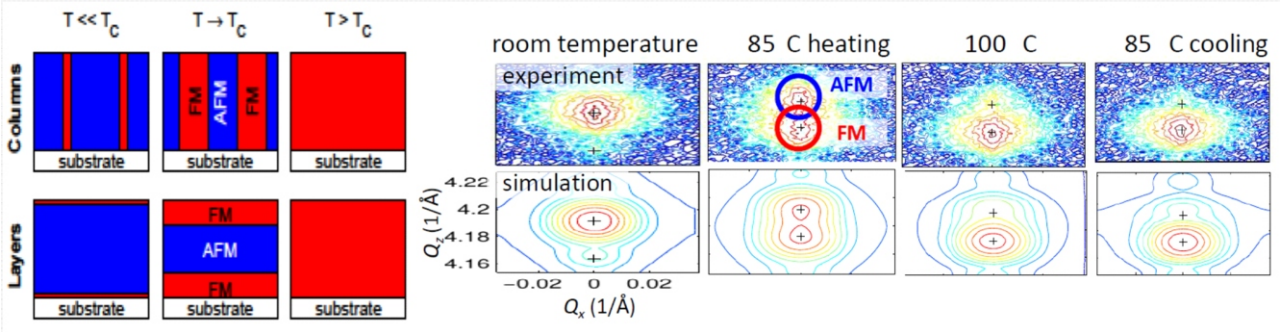

Figure 1. The sketch of two competitive model of FM/AFM domains arrangement (left panel). The comparison of the measured and simulated reciprocal space maps at various temperatures (right panel).

data indicated that both the FM and the AFM domains have constant vertical size being equal to the layer thickness obtained from the X-ray reflectivity. At room temperature, the FM volume (although very small) is spread from the very bottom to the top of the thin layer, probably in the form of thin columns laterally distributed in the layer. Just these columns could be the seeds for the emerging FM phase during the heating.

1. Zakharov, A. (1964). *Soviet Physics JETP*, 46(6), 2003–2010.
2. Lu, W., Huang, P., Chen, Z., He, C., Wang, Y., & Yan, B. (2012). *Journal of Physics D: Applied Physics*, **45**, 435001.
3. Baldasseroni, C., Pálsson, G. K., Bordel, C., Valencia, S., Unal, a. a., Kronast, F., ... Hellman, F. (2014). *Journal of Applied Physics*, **115**, 043919

We acknowledge the financial support by the Czech Science Foundation (proj. num. 14-37427G).

Session X

Wednesday, September 7 - afternoon

I10

HIGH RESOLUTION X-RAY SPECTROSCOPY OF ELECTRONIC AND ATOMIC STRUCTURE OF TIO2 NANOSTRUCTURES AND CHARGE TRANSFER PROCESSES

Federico Boscherini[1]*, Lucia Amidani[2], Luca Pasquini[1], Giacomo Rossi[1], Marco Malvestuto[3] and Alberto Naldoni[4]

[1]Department of Physics and Astronomy, University of Bologna, Italy
[2]ESRF, The European Synchrotron, Grenoble, France
[3]Elettra, Sincrotrone Trieste, Trieste, Italy
[4]CNR-ISTM, Milano, Italy
federico.boscherini@unibo.it

Refined X-ray spectroscopy can play a key role in understanding the fundamental mechanisms responsible for the physical and chemical properties of advanced functional materials and devices. In this contribution, we will focus on TiO_2 – based nanostructures, which are actively studied for many applications, including photocatalysis. Despite many potential advantages, one limitation of TiO_2 is the wide band gap, which limits solar light absorption. By using high resolution X-ray absorption spectroscopy (XAS) and resonant inelastic X-ray scattering (RIXS) we have recently studied the atomic and electronic structure of two materials systems designed to overcome this limitation: nanostructures formed by close assembly of Au and TiO_2 nanoparticles [1] and V-doped TiO_2 [2].

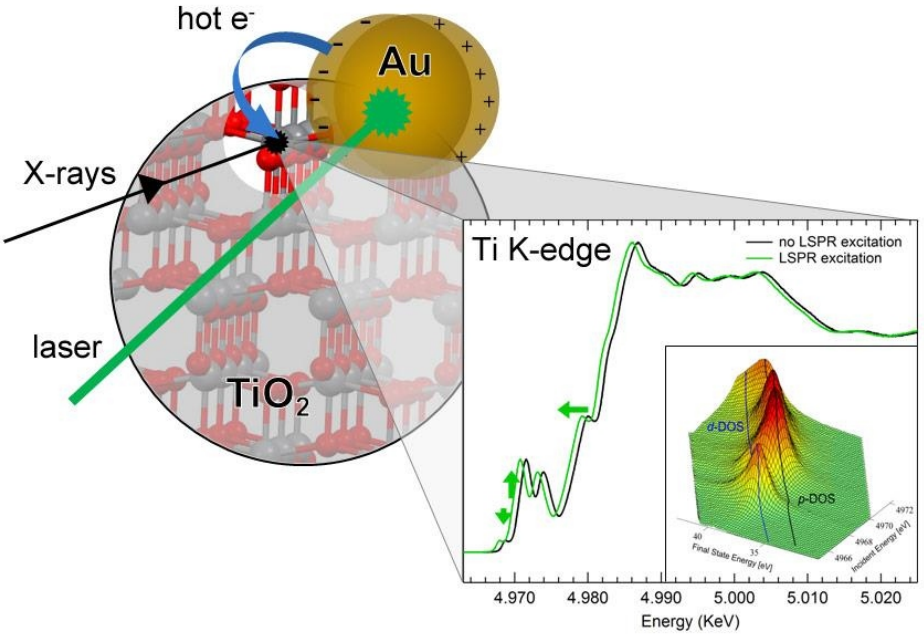

Figure 1: Graphical description of the experiment on Au:TiO_2 and of hot electron charge transfer. The inset reports the effect of laser illumination on high resolution XAS spectra and a typical RIXS plane.

data indicated that both the FM and the AFM domains have constant vertical size being equal to the layer thickness obtained from the X-ray reflectivity. At room temperature, the FM volume (although very small) is spread from the very bottom to the top of the thin layer, probably in the form of thin columns laterally distributed in the layer. Just these columns could be the seeds for the emerging FM phase during the heating.

1. Zakharov, A. (1964). *Soviet Physics JETP*, 46(6), 2003–2010.
2. Lu, W., Huang, P., Chen, Z., He, C., Wang, Y., & Yan, B. (2012). *Journal of Physics D: Applied Physics*, **45**, 435001.
3. Baldasseroni, C., Pálsson, G. K., Bordel, C., Valencia, S., Unal, a. a., Kronast, F., ... Hellman, F. (2014). *Journal of Applied Physics*, **115**, 043919

We acknowledge the financial support by the Czech Science Foundation (proj. num. 14-37427G).

Session X

Wednesday, September 7 - afternoon

I10

HIGH RESOLUTION X-RAY SPECTROSCOPY OF ELECTRONIC AND ATOMIC STRUCTURE OF TIO2 NANOSTRUCTURES AND CHARGE TRANSFER PROCESSES

Federico Boscherini[1]*, Lucia Amidani[2], Luca Pasquini[1], Giacomo Rossi[1], Marco Malvestuto[3] and Alberto Naldoni[4]

[1]Department of Physics and Astronomy, University of Bologna, Italy
[2]ESRF, The European Synchrotron, Grenoble, France
[3]Elettra, Sincrotrone Trieste, Trieste, Italy
[4]CNR-ISTM, Milano, Italy
federico.boscherini@unibo.it

Refined X-ray spectroscopy can play a key role in understanding the fundamental mechanisms responsible for the physical and chemical properties of advanced functional materials and devices. In this contribution, we will focus on TiO_2 – based nanostructures, which are actively studied for many applications, including photocatalysis. Despite many potential advantages, one limitation of TiO_2 is the wide band gap, which limits solar light absorption. By using high resolution X-ray absorption spectroscopy (XAS) and resonant inelastic X-ray scattering (RIXS) we have recently studied the atomic and electronic structure of two materials systems designed to overcome this limitation: nanostructures formed by close assembly of Au and TiO_2 nanoparticles [1] and V-doped TiO_2 [2].

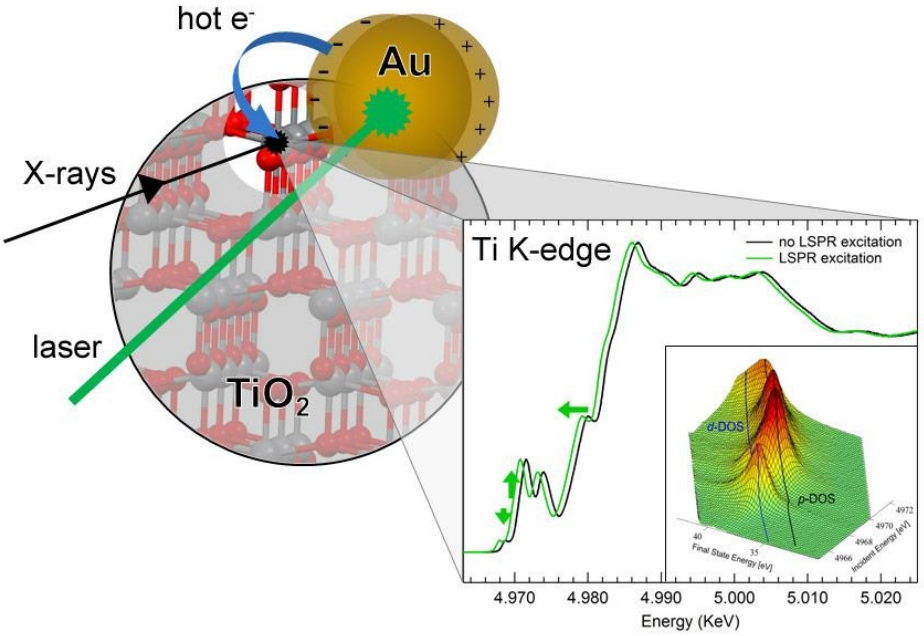

Figure 1: Graphical description of the experiment on Au:TiO_2 and of hot electron charge transfer. The inset reports the effect of laser illumination on high resolution XAS spectra and a typical RIXS plane.

Exploiting plasmonic Au nanoparticles to sensitize TiO_2 to visible light is a widely employed route to produce efficient photocatalysts. However, a description of the atomic and electronic structure of the semiconductor sites in which charges are injected is still not available. Such a description is of great importance in understanding the underlying physical mechanisms and to improve the design of catalysts with enhanced photoactivity. We investigated changes in the local electronic structure of Ti in pure and N-doped nanostructured TiO_2 loaded with Au nanoparticles during continuous selective excitation of the Au localized surface plasmon resonance with XAS and RIXS. Spectral variations strongly support the presence of long-lived charges localized on Ti states at the semiconductor surface, giving rise to new laser-induced low coordinated Ti sites.

Doping with transition metals is an effective method to enhance visible-light absorption in TiO_2 nanoparticles and to improve the efficiency of many photocatalytic processes under solar radiation. We have performed an in-depth XAS study of V dopants in TiO_2 nanoparticles deposited by gas-phase condensation with a local structure similar to anatase, rutile, or intermediate. The combination of K- and L-edge spectra in the pre-edge, edge, and extended energy regions with full potential ab initio spectral simulations shows that V ions occupy substitutional cationic sites in the TiO_2 structure, irrespective of whether it is similar to rutile, anatase, or mixed. Very recently we have also performed.

RIXS measurements which highlight changes in the occupation of electronic states localized on Ti and V induced by visible light absorption.

1. L. Amidani, A. Naldoni, M. Malvestuto, M. Marelli, P. Glatzel, V. Dal Santo, and F. Boscherini, *Angew. Chem. Internat.* Ed. 54, 5413 5416 (2015). DOI: 10.1002/anie.201412030.

2. G. Rossi, M. Calizzi, V. Di Cintio, S. Magkos, L. Amidani, L. Pasquini, and F. Boscherini, *Jour. Phys. Chem. C* **120**, 7457 (2015). DOI: 10.1021/acs.jpcc.5b12045.

C31

DYNAMIC X-RAY DIFFRACTION IN AMINO ACID CRYSTALS: A STEP TOWARDS IMPROVING STRUCTURAL RESOLUTION OF BIOLOGICAL MOLECULES VIA PHYSICAL PHASE MEASUREMENTS

Sérgio L. Morelhao[1], Cláudio M. R. Remédios[2], Guilherme Calligaris[3] ,Gareth Nisbet[4*]

[1]Institute of Physics, University of São Paulo, São Paulo, SP, Brazil
[2]Faculdade de Física, Universidade Federal do Pará, Belém, PA, Brazil
[3]Instituto de Física, Universidade Estadual de Campinas, Campinas, SP, Brazil
[4]Diamond Light Source, Harwell Science and Innovation Campus, OX11 0DE, UK
morelhao@if.usp.br

From inorganic crystals to protein crystals, structure determination with atomic resolution is mostly based on diffraction techniques (electrons, X-rays, and neutrons). However, since the coherent scattering cross-section for X-ray by atoms have intermediate values between those for electrons and neutrons, experimental measurements of structure factor phases have been successfully carried out with X-rays [1]. Dynamical diffraction taking place within perfect domains is another requirement for physical phase measurements via multi-beam diffraction experiments. In crystals with small unit cells, dynamical diffraction regime is achieved in much smaller domains than in crystals with large cells such as protein crystals. Fact that has allowed phase measurements to reveal structural details-inaccessi-

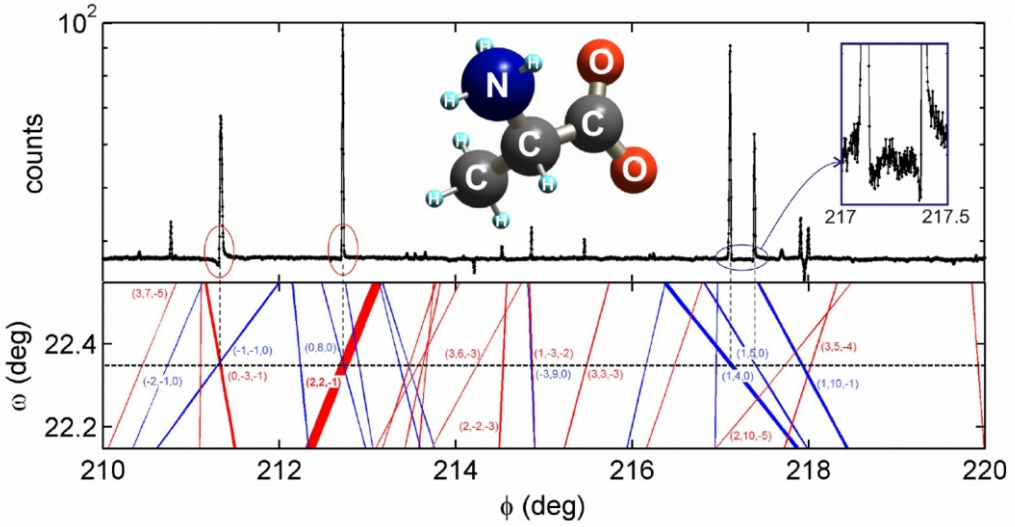

Figure 1. Dynamical diffraction in amino acid crystal giving rise to asymmetric peak profiles of multi-beam cases. Base line intensity (top panel) is from 26l reflection (dashed Bragg-cone line, bottom panel).

ble by other techniques-of optical crystals with dopant ions [1,2], as well as to solve chirality in crystals with no resonant atoms [3]. Differently from any other method in X-ray crystallography based on structure refinement of intensity data, phase measurements pinpoint a specific feature of the structure and directly prove its existence beyond of any reliability parameter or goodness-of-fitting values. In this work, we first present a simple approach to the graphic indexing of appropriate cases for phase measurements, e.g. Fig. 1 (bottom panel), which is also very useful for other diffraction techniques in semiconductor devices and single crystals in general [4,5]. Then, we present diffraction data in single crystals of D-alanine carried out at two synchrotron facilities and with different instrumentation (flux, optics, and goniometry). Model structures taking into account ionic charges of hydrogen atoms are proposed and compared to experimental data, leading to an ideal model to describe X-ray diffraction by this simple amino acid molecule in terms of invariant phase triplets. Moreover, dynamical diffraction calculation of critical domain size (perfect crystal lattice) for phase measurements in large molecule crystals, how to plan an experiment in non-perfect crystals, sensitivity to detect hydrogen atoms, and other applications are discussed.

1. Z. G. Amirkhanyan, C. M. R. Remédios, Y. P. Mascarenhas, S. L. Morelhão. *J. Appl. Cryst*. **47**, (2014), 160.

2. S. L. Morelhão, C. M. R. Remédios, R. O. Freitas, A. O. dos Santos. *J. Appl. Cryst*. **44**, (2011), 93.

3. S. L. Morelhão, Z. G. Amirkhanyan, C. M. R. Remédios. *Acta Cryst. A***71**, (2015), 291.

4. J. Z. Domagała, S. L. Morelhão, M. Sarzyński, M. Maździarz, P. Dłużewski, M. Leszczyński. *J. Appl. Cryst.* **49**, (2016).

5. A. G. A. Nisbet, G. Beutier, F. Fabrizi, B. Moser, S. P. Collins. *Acta Cryst. A***71**, (2015), 20.

Acknowledgments are due to the funding agency CNPq (projects 306982/2012-9 and 452031/20150), Diamond Light Source (proposal MT11922), and Brazilian Synchrotron Light Source (proposals 17063, 18011, and 19018).

C32

REVERSIBLE DISCRETE MONOLAYERS OF C8-BTBT-C8 MOLECULES ON SILICON OXIDE SURFACES AS A RESULT OF THERMODYNAMIC EQUILIBRIUM

M. Dohr[1], O. Werzer[2], H. Ehmann[2], C. Teichert[3], Y. Geerts[4], M. Sferrazza[4], I. Salzmann[5], A. O. F. Jones[1], R. Resel[1]

[1]Institute of Solid State Physics, Graz University of Technology, Austria
[2]Institute of Pharmaceutical Sciences, Graz University, Austria
[3]Institut für Physik, Montanuniversität Leoben, Austria
[4]Faculté des Sciences, Université Libre de Bruxelles, Belgium
[5]Department of Physics, Humboldt-Universität zu Berlin, Germany
roland.resel@tugraz.at

During the last years, the molecule dioctyl-benzothienobenrothiophene (C8-BTBT-C8) has attracted large attention, since thin film transistors based on this organic semiconductor show outstanding device performance. The high quality of C8-BTBT-C8 films may be one of the key features for this successful application. The presence of a liquid crystalline smectic state at elevated temperatures together with a crystalline state at low temperatures allows for special film preparation methods resulting in high structural perfectness. Films in the monolayer (thin films) and in the multilayer regime (thick films) are accessed by spin coating, a method known to work far from thermodynamic equilibrium. Heat treatment of such films results in strong islanding (for thick films). The structure of these or-

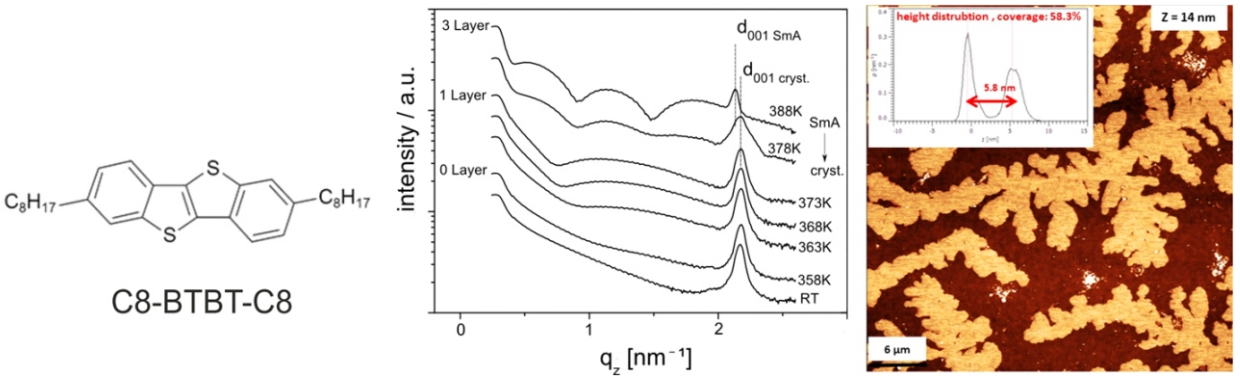

Figure 1. Chemical structure of the molecule C8-BTBT (left), in-situ X-ray reflectivity at decreasing temperature of a multilayer film crossing the phase transition temperature from the smectic A phase to the crystalline state (middle) and an atomic force microscopy image of a bilayer film with the height distribution image as an inset (right).

ganic films is investigated by temperature dependent in-situ methods using atomic force microscopy, X-ray reflectivity and grazing incidence X-ray diffraction. Already at temperatures few degrees below the phase transition from the crystalline state to the smectic A state (T = 381.5 K) the formation of a single monolayer is observed (for thin films). The molecular rearrangement is slow and it takes 30 minutes until the monolayer formation is completed. In case of thick films, an increase of the temperature induces discrete monolayer formation whereby bi-layer, triple-layer, … up to 5-monolayer structures form. The reversibility of the discrete layer formation strongly indicate that thermodynamic equilibrium states are the reason for this behaviour. Using rapid cooling, also non-equilibrium structures can be observed and are stabilised by the substrate surface. Explanation of these observations are given in terms of classical film formation models involving surface energy differences of the silicon oxide surfaces and the C8-BTBT-C8 molecules whereby the later changes concretely on temperature variation.

C33

UNCOVERING THREE-DIMENSIONAL GRADIENTS IN FIBRILLAR ORIENTATION IN AN IMPACT-RESISTANT BIOLOGICAL ARMOUR

Y. Zhang[1], O. Paris[2], N. J. Terrill[3]and H. S. Gupta[1,*]

[1]Queen Mary University of London, School of Engineering and Material Science, London, E1 4NS, UK
[2]Institute of Physics, Montauniversitaet Leoben, Leoben, Austria
[3]Diamond Light Source, Harwell Science and Innovation Campus, Harwell, UK

The architecture of the mineralized cuticle of arthropods like the mantis shrimp (stomatopod) may serve as examples of natural structural materials for bioinspired materials design [1-4]. The stomatopod telson is a defensive shield at the tail of the animal, used to resists blows during intra-species fights [2]. As such, it requires strong impact resistance, to resist the high loading rate blows inflicted by the dactyl club of other stomatopods [1, 4] without damage to structural integrity, and its architecture will provide insight into, for example, design of new armour materials. At the molecular- and supramolecular level, cuticle comprises a fibrous composite of chitin fibrils, calcium carbonate mineral and proteins [3, 5]. However the architecture and functional gradients in this composite at the meso- and microscale, including in fibril and mineral composition, are less investigated. The extraction of 3D orientation distributions of mineralized fibril as well as the quantitative information is technically challenging due to the anisotropic feature inside telson and the presence of both in-plane and out plane fibres. Here, we report the three-dimensional chitin-fibril orientation across the central carinae of the stomatopod telson and tergite, using a combination of microfocus synchrotron wide-angle X-ray diffraction (WAXD) together with a model for localized three-dimensional diffraction reconstruction. We identify two separate families of in-plane and out-plane fibrils, corresponding to the fibres in the lamellae and perpendicular pore-canals running through the cuticle. The 3D orientation of these two different fibril families and their quantitative ratios are mapped across the telson cuticle. We find gradients in fibril orientation in both groups and that the relative amounts of the two fibrils varies across the telson cross-section. Higher proportions of out-plane fibrils in the centre of the telson are identified, which may enable higher resistance to impact loads during natural use. We propose a simple two-phase fibre-buckling model to understand how the telson resists high-impact loading. Further, the 3D fibrillar orientation extraction methodology presented here can be applied to a range of other graded microtextured fibre composites to provide insights into structure-function correlations at multiple hierarchical levels.

1. J. C. Weaver et al, *Science* **336**:127-1279 (2012) .
2. J.R.A. Taylor and S.N. Patek, *J. Exp. Biol*, **213**: 3496-3504 (2010).
3. A. C. Neville, *Biology of the Arthropod Cuticle,* Berlin: Springer (1975).
4. S. Amini et al, *Nat Mater*, advance online publication (2015).
5. C. Sachs et al, *J Mater Res* **21** (8), 1987-1995 (2006)

Session XI

Thursday, September 8 - morning

I11

X-RAY NANO-FOCUSING FOR COHERENT IMAGING: MEET YOUR PROBE

Tim Salditt

Institut für Röntgenphysik, Universität Göttingen

Advanced X-ray optics and focusing opens us the potential of hard X-rays structure analysis, which is unique in terms of penetration, spatial resolution, contrast, and compatibility with environmental conditions was significantly. With the advent of highly brilliant radiation, coherent X-ray focusing, and lens-less diffractive imaging, we can now probe local structures selectively, even in hierarchical environment such as biological cells and tissues.

We illustrate central challenges and advances of hard X-ray nano focusing for coherent imaging, and present a compound optical system consisting of elliptical mirrors and X-ray waveguides. The setup enables full field projection imaging at high magnification down to 20 nm resolution [1], but can also cover a three-dimensional field of view, large enough to probe thick tissues with sensitivity to single cells and sub-cellular structures [2]. The required inversion of the coherent diffraction pattern can be mastered by different reconstruction algorithms in the optical far and near-field.

In this talk we focus on advanced waveguide x-ray optics [3] for coherent imaging, and on the characterisation of the illumination system (probe) by different ptychographic reconstruction schemes, both in the far- and near-field.

1. M. Bartels, M. Krenkel, J. Habe, R.N. Wilke, T. Salditt: X-Ray Holographic Imaging of Hydrated Biological Cells in Solution, *Phys. Rev. Lett.* **114**, 048103 (2015).
2. M. Krenkel, A. Markus, M. Bartels, C. Dullin, F. Alves, T. Salditt: Phase-contrast zoom tomography reveals precise locations of macrophages in mouse lungs, *Sci.Rep.* **5**, 09973 (2015).
3. T. Salditt, S. Hoffmann, M. Vassholz, J. Haber, M. Osterhoff, J. Hilhorst: X-Ray Optics on a Chip: Guiding X Rays in Curved Channels, *Phys. Rev. Lett.* (2015), 115, 203902.

C34

X-RAY WAVEGUIDE ARRAYS: TAILORED NEAR-FIELDS BY MULTI-BEAM INTERFERENCE

Q. Zhong[1], T. Salditt[1], M. W. Wen[2] , Z. S. Wang[2]

[1]Institut für Röntgenphysik, Universität Göttingen,Friedrich-Hund-Platz 1, 37077 Göttingen, Germany
[2]MOE Key Laboratory of Advanced Micro-Structured Materials, Institute of Precision Optical Engineering, Department of Physics, Tongji University, Shanghai 200092, China
tsalditt@gwdg.de

X-ray waveguides enable a variety of X-ray optical functions, from beam collimation to below 10 nm [1] and coherence filtering [2], as required for high resolution holographic X-ray imaging [3], to beam splitting [4] for interferometry, beam tapering [5] or angular redirections [6]. While the guided X-ray beams are well controlled in the waveguide device, the exit near-field distribution is governed by free-space propagation and diffraction broadening, and hence is always much wider than in the waveguide itself, which limits many interesting applications in imaging, diffraction or spectroscopy with nanometer sized X-ray beams.

In this work we show that by exploiting multi-waveguide interference, the near-field distribution behind the waveguide exit can be tailored for special properties, for example in view of creating a secondary focal spot. To this end we use an array of 7 planar waveguides, with precisely varied guiding layer thickness variation, as fabricated by

Table 1. The designed layer thickness values of the x-ray waveguide array (WGA).

Name	Ge sub	Mo	C	Mo	C	Mo	C	Mo	C	Mo	C	Mo	C	Mo	C	Mo
Layer/ nm		50.0	4.0	56.0	6.2	53.8	7.6	52.4	8.0	52.4	7.6	53.8	6.2	56.0	4.0	50.0

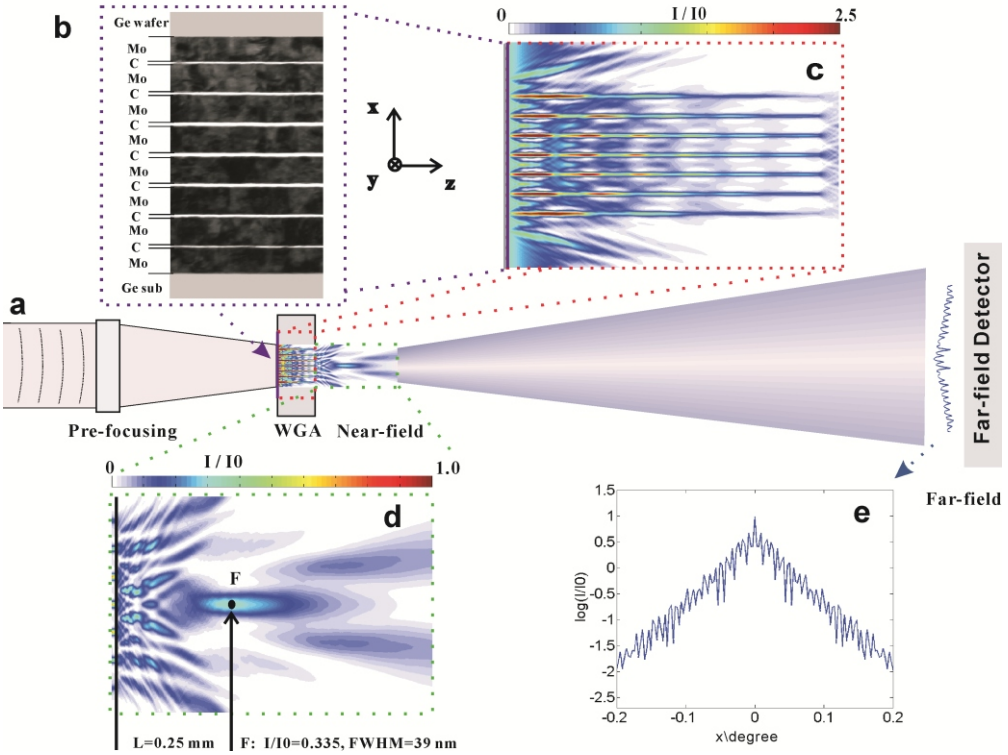

Figure 1. Setup and numerical simulations. (a) Schematic of experimental setup. The X-ray waveguide array (WGA) is positioned in at the focal plane of beamline optics. The incoming beam with 19.9 keV photo energy and primary intensity I0, is coupled into the X-ray waveguide array, which tailors the near-field to the desired shape. The far-field intensity distribution is recorded at a distance of 0.97m behind the WGA exit by a one-dimensional pixel detector (Mythen, Dectris) . (b) The structure of the WGA as visualized by its TEM cross section of WGA. The WGA shown has seven C layers (guiding layers) and eight Mo layers (cladding layers), as detailed in Table 1. The optical layers are sandwiched by Ge wafers; (c) Using finite-difference simulations, the simulated wave propagation in the WGA is shown (intensity values). A plane wave is coupled into the front side of WGA, with a length of 300 m from entrance to exit. (d) Simulations of the beam near the exit of the WGA, showing the multi-beam interference as tailored by the different phases. The focus point (F) is located at 0.25 mm behind the exit of WGA, with a normalized intensity I/I0 = 0.335 and a width (full width of half maximum , FWHM) of 39 nm). (e) The simulated far field pattern.

high precision magnetron sputtering of amorphous carbon and molybdenum. The controlled thickness variations in the range of 0.1 nanometers resulting in a desired phase shift of the different waveguide beams. In this way, special effects such as a single or a double focus or tilted emission of the beam can be achieved by multi-beam interference. In contrast to the previously used resonant beam coupling (RBC) for waveguides with multiple guiding layers [7], the present design based on front coupling of a pre-focused beam is much more versatile. Fig.1 visualizes the general concept of the X-ray waveguide arrays (WGA) with corresponding numerical simulations. The detailed layers thickness values of an example WGA structure are show in Tab. 1. This structure was simulated and measured using bending magnet radiation at the European Synchrotron Radiation Facility (ESRF) in Grenoble (data not shown).

Our study which includes numerical simulations, design, fabrication, and experimental results demonstrates that X-ray waveguide arrays can be used to tailor an X-ray near-field distribution. In particular, multi-beam interference with phase shifts controlled by variation of guiding layer thickness can lead to beam intensity maximum in free space behind the waveguide exit with a spot size (FWHM) in the sub-50nm range. The simulated near-field is compared to the reconstructed field based on the measured far-field (in progress).

1. S. P. Krueger, H. Neubauer, M. Bartels, S. Kalbfleisch, K. Giewekemeyer, P. J. Wilbrandt, M. Sprung, T. Salditt, *Journal of Synchrotron Radiation*, **19**, (2012), pp. 227-236.
2. M. Osterhoff, T. Salditt, *New Journal of Physics*, **13**, (2011), 103026.
3. M. Bartels, M. Krenkel, J. Haber, R.N. Wilke, T. Salditt, *Physical Review Letters*, **114**, (2015), 048103.
4. C. Fuhse, C. Ollinger, T. Salditt, *Physical Review Letters*, **97**, (2006), 254801.
5. H.-Y. Chen, S. Hoffmann, T. Salditt, *Applied Physics Letters*, **106**, (2015), 194105.
6. T. Salditt, S. Hoffmann, M. Vassholz, J. Haber, M. Osterhoff, J. Hilhorst, *Physical Review Letters*, **115**, (2015), 203902.
7. F. Pfeiffer, T. Salditt, P. Hřghřj, I. Anderson, N. Schell, *Physical Review B*, **62**, (2000), pp. 16939-16943.

We thank Mike Kanbach for help in waveguide processing, Markus Osterhoff and Sarah Hoffmann for help during the beamtime at the ROBL beamline of ESRF, and Hsin-Yi Chen and Lars Melchior for help the finite-difference simulations. We gratefully acknowledge the German Research Foundation (DFG) for funding through Grant No. SFB 755, the German Ministry of Research BMBF through Verbundforschung Großgeräte Synchrotronstrahlung, and the China Scholarship Council of P.R. China for financial support.

C35

SINGLE NANOWIRE X-RAY DIFFRACTION ANALYSIS IN ENSEMBLE MEASUREMENTS

J. Vogel[1], A. Davtyan[1], L. Feigl[2], J. Jakob[2], S. M. Mostafavi Kashani[1], P. Schroth[1,2], T. Baumbach[2,3,4] and U. Pietsch[1]

[1]Department of Physics, University of Siegen, Emmy- Noether Campus,Walter-Flex-Str. 3, 57072 Siegen, Germany
[2]Institute for Photon Science and Synchrotron Radiation, KIT - Karlsruhe Institute of Technology, Hermann-von-Helmholtz-Platz 1, 76344 Eggenstein-Leopoldshafen, Germany
[3]Laboratory for Applications of Synchrotron Radiation, KIT - Karlsruhe Institute of Technology, Kaiserstr. 12, 76131 Karlsruhe, Germany
[4]Synchrotron Radiation Facility ANKA, KIT - Karlsruhe Institute of Technology, Hermann-von-Helmholtz-Platz 1, 76344 Eggenstein-Leopoldshafen, Germany
jonas.vogel@student.uni-siegen.de

In a current project we are aiming to study the growth of a single semiconductor nanowire (NW) by in-situ X-ray diffraction. Here we report on recent experiments performed at beamline P09 of PETRA III using a portable MBE chamber. By time resolved reciprocal space mapping in the vicinity of the symmetric GaAs (111) and asymmetric (220) and (311) zinc-blende and (10.3) wurtzite Bragg reflections, the evolution of self-catalysed GaAs NWs on silicon substrates has been monitored. Single NWs were studied using pre-patterned substrates with a lateral spacing of five microns prepared by focused ion beam hole drilling.

Two different approaches were tested to investigate single NWs:

1) A set of Compound Refractive Lenses (CRL) with focal length of 0.75m mounted on a hexapod was used resulting in a beam size of at the centre of the growth chamber. With this approach we were able to select single NWs (see Fig. 1, 1)).

2) Another set of CRL equipped 13.5m upstream the sample focused the beam without major divergence to a size of. Although this setup illuminated simultaneous an ensemble of NWs, single objects could be separated because of the rather parallel beam and the small vertical misalignments of individual NWs with respect to the growth direction (see Fig.1, 2)).

In this work we report on X-ray diffraction data taken from single GaAs NWs using both methods. In particular, we recorded reciprocal space maps at symmetric and asymmetric Bragg peaks with settings 1) and 2) and compare the data in terms of resolution in reciprocal space and integrated intensity. In addition we compare both settings with respect to the capability of determining phase composition of a single NW [1]. Figure 1 shows separated X-ray diffraction signals in the vicinity of the (10.3) wurtzite reflection with focused beam using method 1) and ensemble measurements 2).

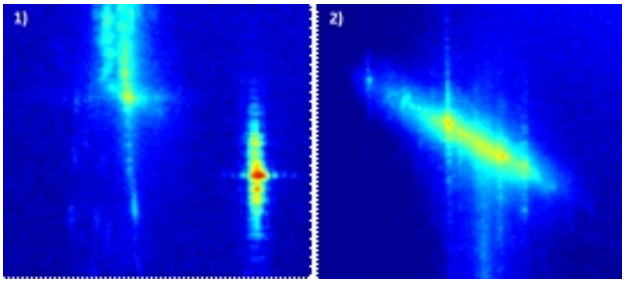

Figure 1. Comparison of X-ray diffraction in the vicinity of the GaAs (10.3) wurtzite reflection. Single objects are visible for both methods 1) (microfocus) and 2) (ensemble).

1. P. Schroth, M. Köhl, J.-W. Hornung, E. Dimakis, C. Somaschini, L. Geelhaar, A. Biermanns, S. Bauer, S. Lazarev, T. Baumbach and U. Pietsch, *Physical Review Letters,* **114,** (2015), 055504.

C36

DEFECT-ASSISTED X-RAY MICROSCOPY WITH POLYCAPILLARY OPTICS

P. Korecki, K. M. Sowa, B. R. Jany, F. Krok

Institute of Physics, Jagiellonian University, Lojasiewicza 11, 30-348 Krakow, Poland

Polycapillary X-ray focusing devices are built from hundreds of thousands of bent glass micro-capillaries that are stacked into hexagonal arrays. Defects were identified as to deteriorate the X-ray transmission of these devices. In this presentation, we demonstrate that natural point defects in the optics (missing, crushes, squeezed or larger capillaries) directly lead to the formation of multiple X-ray images of an object, which was positioned in the focal plane of the optics (see Fig 1) . These multiple images can be analysed using the so called coded aperture approach [1-3]. The resulting spatial resolution is limited by the defect size and not by the focal spot size, which has typically size of 10-100 μm. In a recent proof-of-principle experiment [4] of defect-assisted microscopy, using a commercially available optics, we obtained sub-micron resolution that has not been achieved with focusing polycapillary optics until now. Tailored optics with a controlled distribution of "defects'" (fabricated using procedures known from photonic crystal fibers [5]) could be used for multimodal nanoscale X-ray imaging with laboratory setups.

1. K. M. Dabrowski, D. T. Dul, and P. Korecki, *Opt. Express* **21**, (2013), 2920.
2. K. M. Dabrowski, D. T. Dul, A. Wrobel, and P. Korecki, *Appl. Phys. Lett.* **102**, (2013) 224104.
3. P. Korecki, T. P. Roszczynialski, and K. M. Sowa, *Opt. Express* **23**, (2015), 8749.
4. P. Korecki, K.M. Sowa, B. R. Jany, F. Krok, *Phys. Rev. Lett.* (2016), accepted for publication.
5. P. Russell, *Science* **299**, (2003) 358.

This work was supported by the Polish National Science Center (grant No. DEC-2013/11/B/ST2/04057).

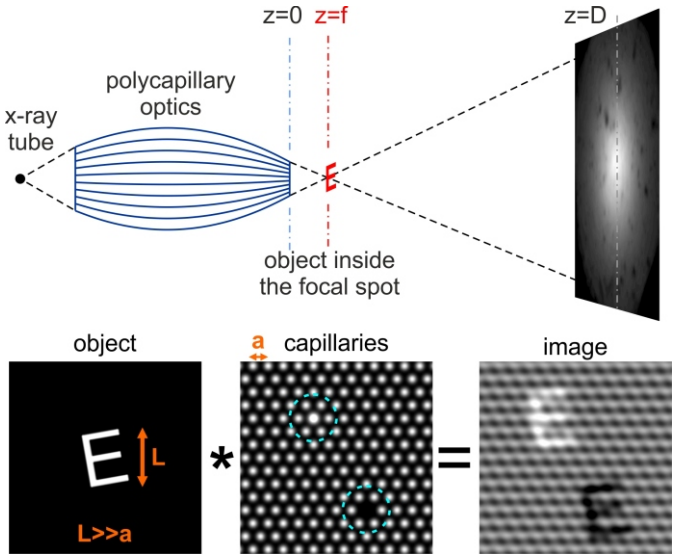

Figure 1. Idea of defect-assisted X-ray microscopy. Defects (missing or broken and larger capillaries - marked with dashed circles) break the periodicity and lead to the formation of distinct multiple x-ray images of the object.

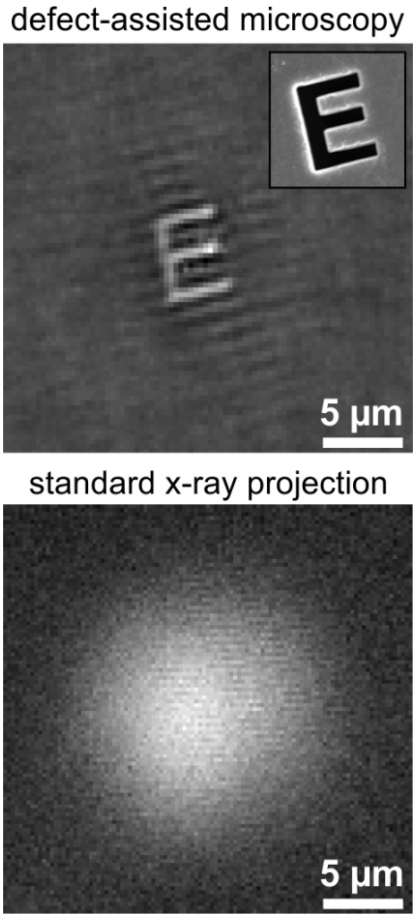

Figure 2. Comparison of defect-assisted imaging with standard X-ray projection imaging with the focal spot acting as a secondary source. Inset: SEM image of the object.

C37

SINGLE-SHOT-MULTIPROJECTION SETUP FOR ULTRAFAST AND ULTRAINTENSE IMAGING

P. Villanueva-Perez[1], B. Pedrini[1], R. Mokso[2], P. R. Willmott[1,3], V. Guzenko[1], C. David[1], and M. Stampanoni[1,4]

[1]Paul Scherrer Institut, Villigen, Switzerland
[2]MedMAX, Max IV Laboratory, Lund University, Sweden
[3]Experimenta Physics Institute, UZH Zurich, Zurich, Switzerland
[4]Institute for Biomedical Engineering, UZH/ETH Zurich, Zurich, Switzerland

The ultrashort and ultraintense pulses provided by X-ray free electron lasers enable to overcome the resolution limitations due to radiation damage for imaging biological materials [1]. Since each pulse destroys the sample, the accessible information in standard imaging approaches is limited to a single projection. We propose an experimental setup for the hard X-ray regime which permits the simultaneous acquisition of multiple projections from the same specimen, similar to that for soft X-rays in Ref. [2], exploiting the simultaneous illumination of the sample with multiple beams generated from the direct beam by a single crystal (see Figure). This technique thus allows acquisition of 3-D information from single-shot measurements.

We provide an experimental proof-of-principle of this concept at a synchrotron source in both coherent diffraction imaging and holographic geometries. For the former, implementation at X-ray free-electron laser is straightforward.

1. R. Neutze et al., *Nature* **406**, 752-757 (2000).
2. M. R. Howells and C.J. Jacobsen, Workshop on scientific applications of coherent X-rays SLAC-R-**437**, 159-162 (1994).

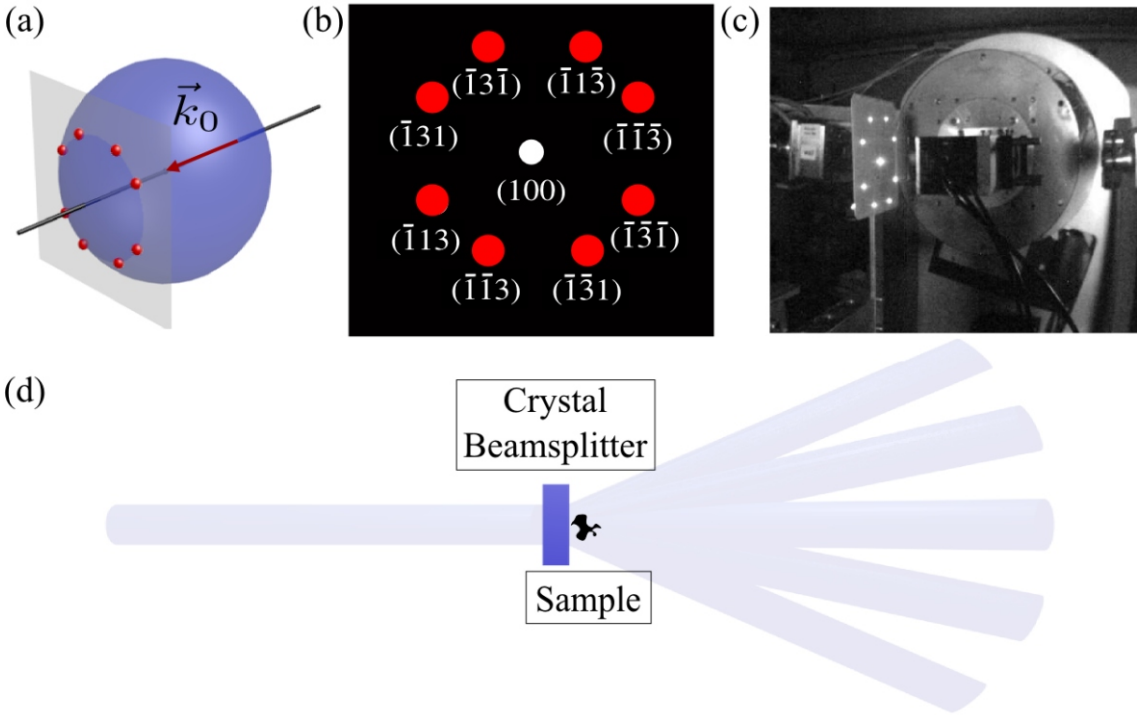

Figure 1: (a) Ewald sphere intersecting simultaneously a family of equivalent Bragg reflections, related by rotations around a symmetry axis of the silicon crystal. (b) Family of reflections in Bragg condition for a cubic lattice. (c) Picture of the experimental setup at the MS beamline of the Swiss Light Source, showing the direct beam and the eight diffracted beams on a phosphor screen. (d) Sketch of the concept of the sample being illuminated simultaneously by the direct and diffracted beams.

Session XI

Thursday, September 8 - morning

C38

EXPERIMENTAL ASSESSMENT OF THE SPATIAL TRANSVERSE DISPLACEMENT OF X-RAYS BY PERFECT CRYSTALS IN VIEW OF SELF-SEEDING APPLICATIONS

A. Rodriguez-Fernandez[1], S. Reiche[1], K. Finkelstein[2], B. Pedrini[1]

[1]Paul Scherrer Institut, CH-5232 Villigen PSI
[2]Cornell University (CHESS), Ithaca, New York
Angel.rodriguez@psi.ch

Free-electron laser (FEL) radiation arises from shot noise in the electron bunch, which is amplified along the undulator section and results in X-ray pulses consisting of many longitudinal modes [1]. The output bandwidth of FELs can be decreased by seeding the FEL process with longitudinally coherent radiation. In the hard X-ray region, there are no suitable external sources. This obstacle can be overcome by self-seeding. The X-ray beam is separated from the electrons using a magnetic chicane, and then monochromatized. The monochromatized X-rays serve as a narrowband seed, after recombination with the electron bunch, along the downstream undulators. This scheme generates longitudinally coherent FEL pulses.

Geloni et al. [2] have proposed monochromatization based on Forward Bragg Diffraction (FBD), which introduces a delay of the narrowband X-rays pulse (echoes) of the order of femtoseconds that can be matched to the delay of the electron bunch due to the chicane. Simulations based in the dynamical diffraction theory show a transverse displacement of the FBD X-ray beam, which can result in a loss of efficiency of the seeding process [3]. The delays and transverse displacements of the echoes are related by

$$x_0 \quad c \cos \qquad (1)$$

where is the Bragg angle of the crystal involved reflection for the average incoming photon energy. Fig. 1 presents the electric field amplitude E_H of the radiation transmitted in the forward direction as a function of transverse position and time on a section downstream a 600 m thick diamond crystal oriented in symmetric (4,0,0) Bragg geometry, and illuminated by a 10 keV beam of 10 m waist size. The two panels correspond to Bragg and Laue, respectively. In both panels, the dependence of the echo transverse displacement on the echo delay expressed in (1) is clearly visible.

To confirm the simulations, an experimental set-up was designed that fulfil the beam characteristics required for this type of studies (small energy bandwidth, beam size of about 10 m and small angular divergence are crucial). For this reason, after a Si (111) monochromator the beam is refined with a channel cut set of Si (531) crystals that reduce the angular width of incoming beam to 1.075'', which is slightly smaller than the expected Darwin acceptance for Diamond (400) Bragg reflection at 10 keV of 1.485''.

The layout of at Cornell High Energy Synchrotron Source (CHESS) C-line Beamline and Material Science (MS) beamline at Swiss Light Source (SLS) is shown in Fig. 2. The beam size was set to 12 ± 2 m by slits located upstream the channel cut set of crystals. A point detector

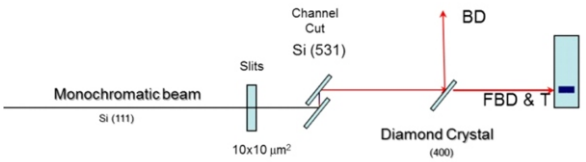

Figure 2. Experimental set-up for the experiment performed at C line at CHESS.

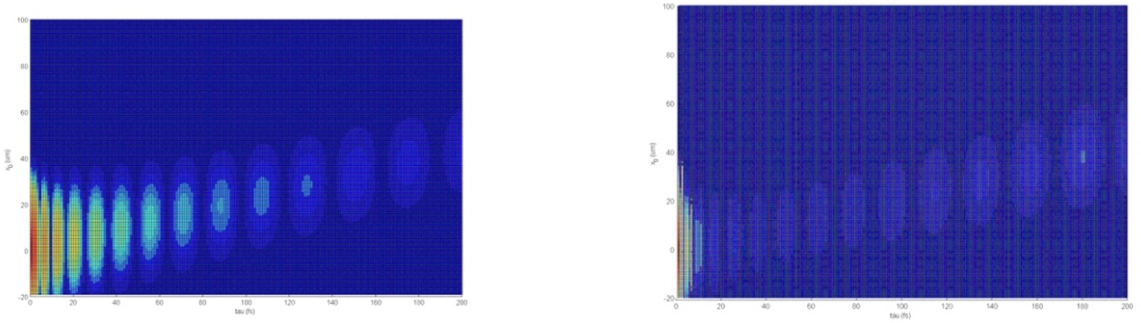

Figure 1. Forward diffracted field magnitude E_H from the (400) Bragg reflection at 10 keV for a 600 m thick Diamond crystal in the case of a 10 m size incident x-ray beam. Calculated following Lindberg and Shvyd ko approximation [3], (Left) Bragg and (right) Laue geometry.

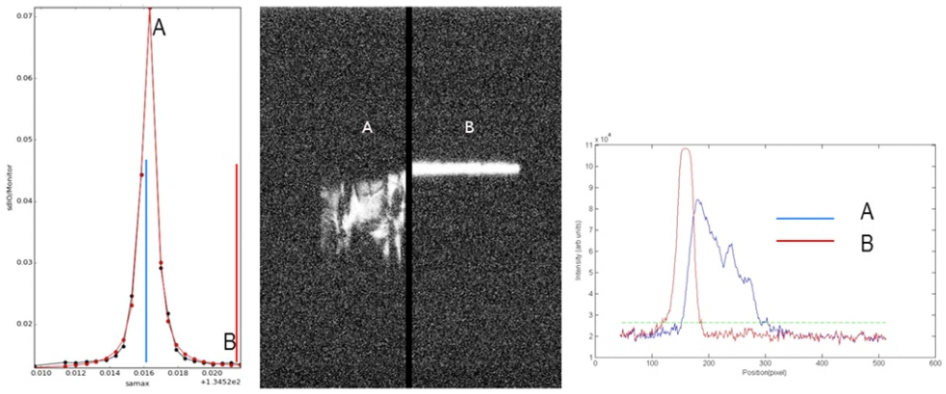

Figure 3. Forward Bragg diffraction signal of a 300 m thick diamond crystal at a 10 keV for the (400) reflection observed at Material Science Beamline of SLS. (Left) Bragg diffraction signal at the BD detector, (Center) signal at the FBD direction detector and (right) section of the FBD detector at two Bragg angles A (in the Bragg condition) and B (far from the Bragg condition).

was situated in the Bragg diffraction direction, 44.04°, which mission was record the width and intensity of the Bragg diffracted signal. The detector in the forward direction uses a GGG scintillator crystal to convert x-ray to visible photons, which are recorded with a high resolution camera with a resolution of less than 2 m/pixel. The samples under study were a series of diamond single crystal with thicknesses between 600 and 100 m. For each scan the sample was set up to the maximum Bragg diffraction signal of the NaI detector at 10 keV, one fixed the channel cut set was rotated allowing just a determined energy to go throw it with high resolution. Recording the signal transmitted thru the crystal in the forward camera.

An example of the data collection results is presented in Fig. 3. It is possible to observe how near the Bragg condition of diffraction, marc in the figure as A, the forward diffracted signal is displaced from the initial position, marc as B, and a series of maxima appear to be formed in the tail of the Bragg peak which are related to the echoes signal.

The results from the experiments performed at CHESS and SLS are beam compare with farther simulations of the beam properties at the synchrotron sources to be able to confirm the predicted transverse displacement, which in the case of a positive confirmation should be taken into account in the design of self-seeding infrastructure for optimizing the FEL performance. In a second step, beamtime at a FEL facility will be requested to correlate the different maxima shown in Fig. 3 with the actual delays.

1. J. S. Wark, et al., J. Apply. Crystallogr. **32**, (1999) 692.
2. G. Geloni, et al. DESY report 10-053 (2010).
3. Y. Shvyd'ko, et al. Phys. Rev. ST Accel. Beams 15, (2012) 100702

The authors acknowledge the staff of the Material Science beamline at Swiss Light Source and of the C-1beamline at Cornell High Energy Synchrotron Source, at which experiments related to this project were performed.

C39

X-RAY BEAM SPLITTING BY USE OF REFLECTION GRATINGS FOR PHOTON ENERGIES OF 4 – 12.4 kEV

W. Jark, D. Eichert

Elettra – Sincrotrone Trieste S.c.p.A., S.S. 14 km 163.5, I-34149 Basovizza (TS),Italy

Recently surprisingly high diffraction efficiencies were observed when a reflection grating was used in the conical diffraction scheme in combination with X-rays with photon energies between 4 and 12.4 keV [1]. As shown in figure 1 the conical diffraction is obtained when the trajectory of the incident beam is parallel to the grooves of the grating. In this case the incident intensity is diffracted into a cone symmetric around the plane of incidence. The highly efficient symmetric diffraction opens the possibility to use such gratings also as optical components for the X-ray range.

An interesting application is as an amplitude beam splitter. Beam splitting with equal intensity cannot only be achieved for two beams but also for more beams. The concept can thus be applied for interferometry experiments or simply for separating a high intensity beam for the use in different experimental stations. We will report related experimental data and compare them to predictions, which will allow us to discuss the optimum parameters for given applications.

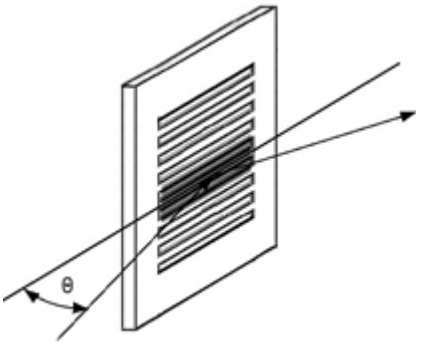

Figure 1. Principal beam trajectory parallel to the grooves when a reflection grating with rectangular groove profile produces conical diffraction in the extreme off-plane configuration for diffraction.

1. W. Jark and D. Eichert, *Opt. Express* **23**, 22753 (2015).

C40

DUAL DETECTOR SINGLE SHOT FAST QUANTITATIVE PHASE MICRO-TOMOGRAPHY

R. Mokso[1], M. Nyvlt[2,3], H. Kohr[4], P. Oberta[5], M. Skeren[2,3], M.Stampanoni[6,7]

[1]Max IV Laboratory, Lund University, SE-22100 Lund, Sweden
[2]FNSPE, Czech Technical University, Czech Republic
[3]Holoplus s.r.o., Prague, Czech Republic
[4]Dpt. Mathematics. KTH Stockholm 10044 Stockholm, Sweden
[5]Rigaku innovative Technologies, Czech Republic
[6]Swiss Light Source, Paul Scherrer Institut, 5232 Villigen PSI, Switzerland
[7]Institute for Biomedical Engineering, University and ETH Zurich, 8092 Zurich, Switzerland
rajmund.mokso@maxiv.lu.se

The first tomographic microscopy beamlines are currently proposed on the diffraction limited storage ring of Max IV. The main emphasis will be on micrometer resolution dynamic studies with high sensitivity to make optimal use of an intense X-ray beam with typically 20-50% coherent fraction and a spot size of 1 mm in diameter will scatter on the sample and give rise to interference fringes recorded in the near field - Fresnel regime. The state-of-the art indirect detector systems for micrometer resolution tomography employs a thin scintillator screen which typically converts about 50% of the X-rays at 20 keV to visible light that is then collected by a lens systems and reaches the detector sensor. We can improve this X-ray photons collection efficiency by using instead a semi transparent scintillator-mirror system and a second detector further downstream of the beam (see Fig. 1a). The added value of such optimization is the simultaneous recording of two distinct Fresnel diffraction patterns [1]. In respect to fast phase imaging the dual-detector principle favours the implementation of quantitative phase retrieval methods requiring data at a minimum of two defocus distances. They are of particular interest if the interaction of a transversely highly coherent X-ray beam scattered on the sample gives rise to multiple and well visible interference fringes in the Fresnel regime. Contrast transfer function based phasing methods [2] can under these conditions deliver optimal results and may therefore be considered for Max IV to complement the often used transport of intensity based phase retrieval [3].

Beside direct phasing methods from two simultaneous projections (Fig. 1b) we have implemented an iterative

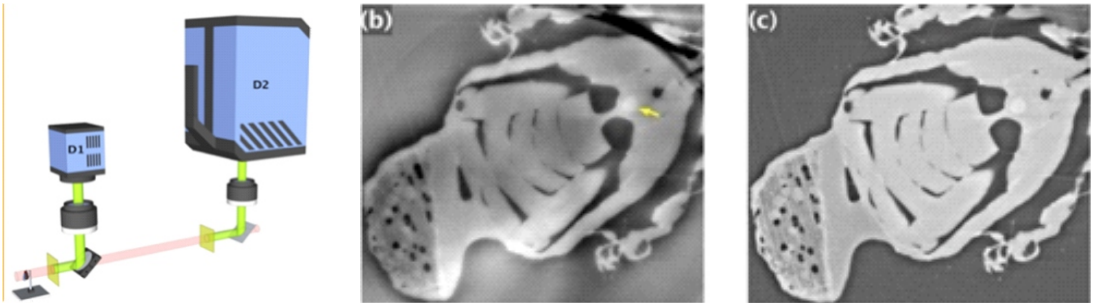

Figure 1. (a) The schematic representation of the dual detector system as implemented at the TOMCAT beamline at the Swiss Light Source. (b) Tomographic slice of a fly thorax reconstructed from the retrieved phase maps using CTF mixed approach based on simultaneously acquired two Fresnel diffraction patterns at sample-to-detector distances set to 4 and 377 mm. The effective pixel size on the first detector D_1 was 2.75 m and it was 2.9 m on the second detector D_2. In (c) a Paganin [3] type reconstruction is shown.

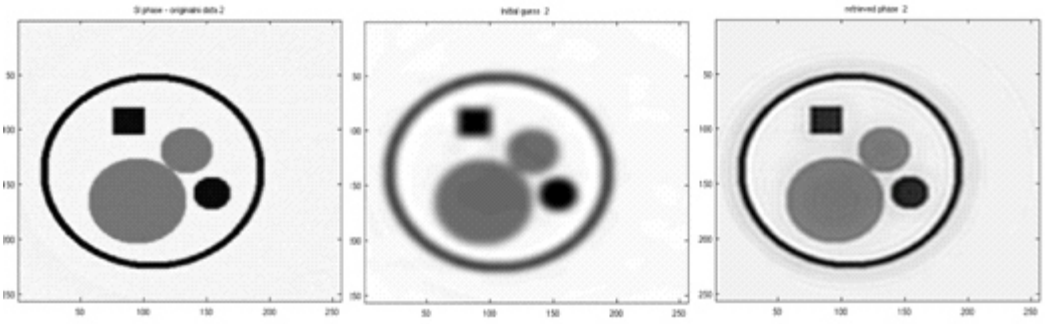

Figure 2. Phase retrieval performed on a phantom. The original tomographic slice of a phase map on the left a Paganin phase retrieval result in the middle and on the right a tomographic slice of resulting from the proposed iterative 3D phase retrieval based on two tomographic sets acquired at various defocus distances.

Fourier transform algorithm interlacing iterations at the phase retrieval and tomographic level. We propose to take advantage of the 3D structure of the recorded diffraction patterns to guide the phase retrieval by the naturally occurring constrains when the full 3D information about the sample is available in two imaging conditions. Furthermore with the proposed scheme we address the problem of background variations during the tomographic acquisition. The performance of this approach is illustrated on Fig 2.

The iterative 3D phase retrieval is being implemented in Operator Discretization Library (ODL) [4], a Python framework for rapid algorithm development in tomography. It offers the possibility to apply a variety of solver schemes to a particular reconstruction problem, for example the conjugate gradient method or TV regularization [5]. In particular, the full non-linear problem of phase tomography can be addressed without any linearization or model simplification. We will present the newest results based on the optimized iterative scheme and discuss the advantages of the small and highly coherent beam at Max IV to pursue high resolution phase tomographic studies in particular for bio-medical applications [6,7]. Some approaches will be built upon the experience gained from pilot studies performed at the TOMCAT beamline at the Swiss Light Source.

Simultaneous acquisition of two Fresnel diffraction patterns may be achieved also by using a crystal beam splitter as theoretically proposed in [8] and experimentally demonstrated in [9]. Of particular interest in this approach is that wavelength separation of the two beams is possible and therefore we can fine-tune the information content in each diffraction pattern independently.

1. R. Mokso, F. Marone, S. C. Irvine, M. Nyvlt, D. Schwyn, K. Mader, G. K. Taylor, H. G. Krapp, M. Skeren, M. Stampanoni, *J. Phys. D. Appl. Phys.* **46**, (2013), 494004.
2. P. Cloetens, W. Ludwig, J. Baruchel et al. *Appl. Phys. Lett.,* **75**, (1999), 2912-1914.
3. D. Paganin, S.C. Mayo, T.E. Gureyev et al. *J. Microscopy* **206**, (2002), 33-40.
4. https://www.github.com/odlgroup/odl
5. V. Caselles, A. Chambolle, M. Novaga. *Handbook of Mathematical Methods in Imaging* (2011), 1016–1057.
6. R. Mokso, D. A. Schwyn, S. M. Walker, M. Wicklein, T. Müller, M. Doube, M. Stampanoni, G. K. Taylor, H. G. Krapp, *Scientific Reports* **5**, (2015), 8727.
7. G. Lovric, S. F. Barré, J. C. Schittny, M. Roth-Kleiner, M. Stampanoni, R. Mokso, *J. Appl. Crystallogr*. **46**(4), (2013), 856.
8. P. Oberta & R. Mokso, A Laue-bragg monolithic beam splitter for efficient x-ray 2-beam imaging. *Nucl. Inst. Meth.* **703**, (2013), 59–63.
9. R. Mokso & P. Oberta, Simultaneous dual-energy X-ray stereo imaging. *J. Synch. Rad.* **22**(4), (2015), 1078-82.

C41

X-RAY IMAGING AT THE ADVANCED PHOTON SOURCE: OPPORTUNITIES WITH THE APS UPGRADE

Francesco De Carlo, Kamel Fezzaa, Vincent De Andrade, Tao Sun, Xianghui Xiao, Xiaogang Yang and Doga Gürsoy

Argonne National Laboratory, 9700 S. Cass Av. Argonne IL 60439
decarlo@aps.anl.gov

Full-field imaging is an extremely versatile technique that is broadly applicable to almost all scientific and engineering disciplines. Its versatility is reflected by the fact that every major synchrotron facility in the world has a dedicated full-field imaging facility. In many cases, full-field imaging is the keystone linking a sample to other X-ray techniques such as ptychography, μXRF, μXANES, and μXRD.

The current Advanced Photon Source (APS) allows for hierarchical 3D imaging of dynamic systems and materials with spatial resolution up to 1μm, without a major sacrifice in time resolution and 20 nm 3D imaging of static or slowly evolving systems.

In this talk we will present the latest nano and dynamic imaging results utilizing the current APS source and will describe the opportunities the new APS upgrade source will bring to this technique.

This research used resources of the Advanced Photon Source, a U.S. Department of Energy (DOE) Office of Science User Facility operated for the DOE Office of Science by Argonne National Laboratory under Contract No. DE-AC02-06CH11357.

1. J.W. Gibbs, K.A. Mohan, E.B. Gulsoy, A.J. Shahani, X. Xiao, C.A. Bouman, M. De Graef, P.W. Voorhees, "The Three-Dimensional Morphology of Growing Dendrites," *Sci. Rep.* **5**, 11824-1-11824-9 (2015). DOI: 10.1038/srep11824.

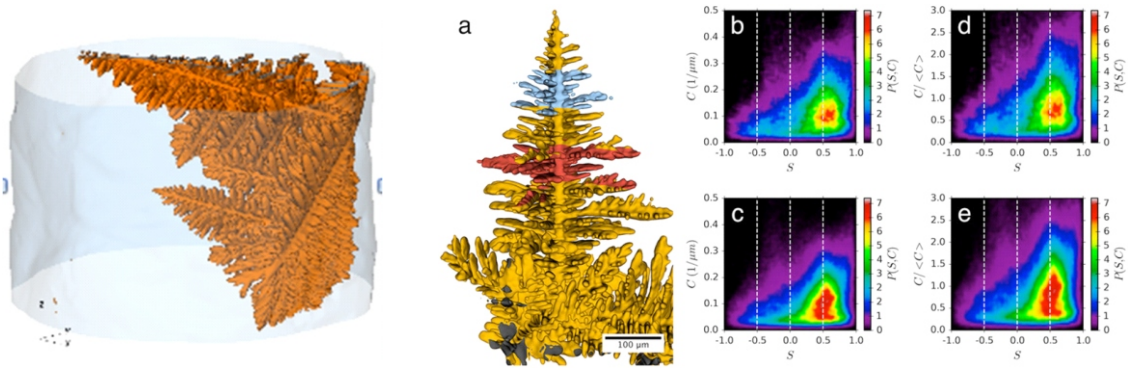

Figure 1. Left: animation at 1.6 3D-fps growth of Al-rich dendrite in Al-Cu alloy with a cooling rate 1 K/min from 550 K. Right: Interfacial shape distributions for two 75 m thick slices normal to the growth direction of the nearly free-growing dendrite at 9.0 seconds after nucleation [1].